

Summer 7-11-2018

# REGULATING MIRNA BIOGENESIS BY SMALL MOLECULES

Hao Yan

*University of New Mexico*

Follow this and additional works at: [https://digitalrepository.unm.edu/chem\\_etds](https://digitalrepository.unm.edu/chem_etds)



Part of the [Chemistry Commons](#)

---

## Recommended Citation

Yan, Hao. "REGULATING MIRNA BIOGENESIS BY SMALL MOLECULES." (2018). [https://digitalrepository.unm.edu/chem\\_etds/101](https://digitalrepository.unm.edu/chem_etds/101)

This Dissertation is brought to you for free and open access by the Electronic Theses and Dissertations at UNM Digital Repository. It has been accepted for inclusion in Chemistry ETDs by an authorized administrator of UNM Digital Repository. For more information, please contact [disc@unm.edu](mailto:disc@unm.edu).

Hao Yan

*Candidate*

---

Chemistry and Chemical Biology

*Department*

---

This dissertation is approved, and it is acceptable in quality and form for publication:

*Approved by the Dissertation Committee:*

Fu-Sen Liang, Chairperson

---

Lina Cui

---

Rebecca S. Hartley

---

Wei Wang

---

**REGULATING MIRNA BIOGENESIS BY SMALL MOLECULES**

**BY**

**HAO YAN**

B.Sc., Chemistry, Beijing Normal University, China, 2008

M.Sc., Chemistry, Beijing Normal University, China, 2011

DISSERTATION

Submitted in Partial Fulfillment of the

Requirements for the Degree of

**Doctor of Philosophy  
Chemistry**

The University of New Mexico

Albuquerque, New Mexico

July, 2018

## Acknowledgments

I would like to express my sincere gratitude to my advisor Prof. Dr. Fu-Sen Liang for giving me the opportunity to work in his lab and pursue my doctoral degree. His continuous support and guidance helped me in all the time of my PhD study and research. I was really impressed with his immense knowledge, patience and the free, relaxing atmosphere he created in the lab.

I would like to thank Dr. Lina Cui, Dr. Rebecca S. Hartley and Dr. Wei Wang for serving on my dissertation committee. I'm grateful for their insightful comments, encouragement, and help in revising this dissertation.

Completing this work would have been much more difficult, if not impossible, without the help from others. Umesh Bhattarai performed most of the radiation experiments. Dr. Zhi-Fo Guo synthesized some of the compounds. Dr. Jianfeng Cai, Dr. Mi Zhou and Dr. Mengmeng Zheng at University of South Florida screened the library in Chapter 4. Dr. Patrick S. Mariano revised the manuscripts for publication. I am indebted to them for the help.

I would also like to give my thanks to Dr. Zhi-Fo Guo, Ya-Wen Han, Dr. Jingli Xu, Dr. Lisa Whalen, Jan Harrington, Jacqueline Page and Priscilla Duncan. I can't imagine how hard my life in New Mexico would be without their generous help. My thanks go to my labmates: Zhi-Fo Guo, Tingjun Chen, Dan Gao, Yabin Song, Cat Wright, Guihua Zeng, Umesh Bhattarai, Roushu Zhang, Huong Nguyen, Weiye Zhao, Lin Zhou, Danielle Parsons, Eunju Lim, Larisa Breden, Annette Fernandez, and David Danielson, for the inspiring discussions and all the fun we had in the last four years.

Finally, I would like to express my gratitude to my parents and siblings for their continued support and encouraging. My wife gave up her career and followed me for my study. She experienced all of the ups and downs of my research. Research is stressful, but my kids make me happy every day. I have been extremely lucky to have all of them in my life. Thank myself, too.

# **Regulating miRNA biogenesis by small molecules**

by

**Hao Yan**

B.Sc., Chemistry, Beijing Normal University, China, 2008

M.Sc., Chemistry, Beijing Normal University, China, 2011

Ph.D., Chemistry, University of New Mexico, USA, 2018

## **Abstract**

MiRNAs are key cellular regulators and their dysregulation is associated with many human diseases. The development of miRNA inhibitors has significant implications for the therapy of diseases associated with aberrant miRNA expression. It also provides chemical tools for studying miRNA function. This dissertation focuses on the development of small-molecule based miRNA inhibitors targeting miRNA biogenesis.

The dissertation consists of four chapters. In Chapter 1, the biogenesis of miRNA was first introduced, followed by the explanation of miRNA function in health and disease. Then the approaches used for regulating miRNA were reviewed. Finally, the difficulties with miRNA regulation were summarized.

One of the key reactions in miRNA biogenesis is the processing of pre-miRNA by Dicer enzyme. In Chapter 2, we developed a general strategy for inhibiting miRNA biogenesis with bifunctional small molecules. By linking a pre-miRNA binder and a weak Dicer inhibiting unit, we obtained bifunctional conjugates that are able to block the Dicer processing of pre-miRNA and inhibit miRNA

production. This approach is expected to be applicable in generating more inhibitors for other miRNAs.

MiRNAs are usually produced locally in a spatiotemporally controlled manner to regulate gene expression. Thus, developing chemical tools for manipulating miRNA with spatiotemporal preciseness is critical for studying miRNA. In Chapter 3, we expanded the application of the strategy described in Chapter 2 in generating light controllable miRNA inhibitors. By conjugating the two functional units with a photocleavable linker, we made a new bifunctional miRNA inhibitor. Taking advantage of the photocleavage property of the linker, the bifunctional inhibitor can be fragmented into separate non-inhibiting units and therefore be deactivated by light. We expect that this strategy could be applied to generate chemical biological tools that allow light-mediated spatiotemporal control of miRNA maturation and contribute to the study of miRNA function.

In Chapter 4, we investigated the potential of targeting miRNA with macrocyclic peptidomimetics. By screening a combinatorial library of peptidomimetics against pre-miR-155, we identified a pre-miR-155 binder that is able to block the Dicer processing, thereby reduce oncogenic miR-155 level and induce apoptosis in cancer cells. This compound could be used as a lead for generating more potent miR-155 inhibitors. The results of this investigation also demonstrate that macrocyclic peptidomimetics could serve as new small molecule scaffolds for RNA targeting.

## Table of Contents

List of Figures .....	x
Chapter 1 Introduction.....	1
1.1 Biogenesis of miRNA .....	1
1.2 Function of miRNA.....	3
1.3 MiRNA dysregulation in disease.....	5
1.3.1 Cancer .....	5
1.3.2 Cardiovascular Disease.....	6
1.3.3 Neurodegeneration.....	6
1.3.4 Other diseases .....	7
1.4 miRNA regulation.....	7
1.4.1 Genetic knockout .....	7
1.4.2 MiRNA sponge .....	8
1.4.3 Antisense oligonucleotides.....	8
1.4.4 Small molecule inhibitors.....	11
1.5 Summary and outlook .....	19
Chapter 2 Regulating miRNA Biogenesis by Bifunctional Small Molecules.....	22
2.1 Introduction .....	22
2.2 Results and discussion .....	24
2.2.1 Identification of pre-miR-21 binder .....	24
2.2.2 Selection of Dicer inhibitor.....	29
2.2.3 Synthesis of bifunctional small molecules .....	29
2.2.5 MiRNA inhibition activity in cell.....	32
2.2.6 Downstream effect of miR-21 inhibition by 45A.....	33
2.2.7 Selectivity of bifunctional molecule .....	34
2.2.8 Effect of bifunctional molecule on translation.....	36
2.2.9 Cytotoxicity of bifunctional molecule.....	36
2.3 Summary.....	37
2.4 Experimental section.....	37
2.4.1 <i>In vitro</i> Transcription of pre-miR-21 .....	37

2.4.2 Fluorescence polarization binding assay .....	38
2.4.3 Dicer-mediated pre-miRNA cleavage assay .....	39
2.4.4 Cell culture and transfection.....	39
2.4.5 RNA extraction and RT-qPCR .....	40
2.4.6 Western Blotting .....	40
2.4.7 Cytotoxicity Assay.....	41
2.4.8 Translational Inhibition Assay .....	42
2.4.9 Chemical Synthesis .....	42
Chapter 3 Design, synthesis and activity of light deactivatable miRNA inhibitor.	61
3.1 Introduction .....	61
3.2 Results and discussion .....	63
3.2.1 Design and synthesis of light controllable miRNA inhibitor .....	63
3.2.2 Photolysis study by HPLC .....	64
3.2.3 <i>In vitro</i> Dicer inhibition activity .....	65
3.3 Summary .....	67
3.4 Experiment section .....	68
3.4.1 Chemistry .....	68
3.4.2 Photolysis study .....	74
3.4.3 Dicer enzyme expression .....	75
3.4.4 <i>In vitro</i> Dicer inhibition assay .....	75
Chapter 4 MiRNA inhibition by macrocyclic peptidomimetics.....	77
4.1 Introduction .....	77
4.2 Results and discussion .....	78
4.2.1 Screen for pre-miR-155 binder .....	78
4.2.2 Binding affinity of the hit to pre-miR-155.....	79
4.2.3 <i>In vitro</i> Dicer blocking activity.....	80
4.2.4 MiR-155 inhibition in cell.....	81
4.2.5 Selectivity of 58 to MiR-155 over other miRNAs.....	83
4.2.6 58 upregulates miR-155 target protein FOXO3A .....	84
4.2.7 58 induces cancer cell apoptosis .....	85
4.2.8 58 inhibits cancer cell growth.....	87

4.3 Summary .....	87
4.4 Experiment details .....	88
4.4.1 <i>In vitro</i> Transcription of pre-miR-155 .....	88
4.4.2 Fluorescence polarization binding assay .....	89
4.4.3 Electrophoretic mobility shift assay .....	89
4.4.4 Cell culture .....	89
4.4.5 Dicer enzyme expression .....	89
4.4.6 Dicer-mediated pre-miR-155 cleavage assay .....	89
4.4.7 Fluorescence microscope imaging .....	90
4.4.8 MiR-155 inhibition in cell .....	90
4.4.9 RNA extraction and RT-qPCR .....	91
4.4.10 Western Blotting .....	92
4.4.11 Flow Cytometry Assay .....	92
4.4.12 Cell viability assay .....	93
Statistical analysis .....	93
Reference .....	94

## List of Figures

<b>Figure 1.1</b> An illustration of miRNA biogenesis pathway .....	2
<b>Figure 1.2</b> (A) Structures of the most commonly used chemical modifications in anti-miR oligonucleotides. (B) Design of chemically modified anti-miR oligonucleotides. (C) Schematic overview of the miRNA inhibition approach using a fully complementary anti-miR and a seed-targeting tiny LNA .....	9
<b>Figure 2.1</b> A schematic illustration of the new approach to regulate miRNA biogenesis by using bi-functional small molecules that target pre-miRNA.....	23
<b>Figure 2.2</b> (a) Synthesis of Kanamycin building blocks. (b) Synthesis of KOF and KNF. ....	25
<b>Figure 2.3</b> Fluorescence polarization of <b>KOF</b> (a) and <b>KNF</b> (b) in the presence of different concentrations of pre-miR-21. ....	26
<b>Figure 2.4</b> Fluorescence polarization of <b>KOF</b> in the absence or presence of pre-miR-21 and different aminoglycosides.....	27
<b>Figure 2.5</b> Synthesis of neomycin building blocks (A) and <b>NF</b> (B) .....	27
<b>Figure 2.6</b> Fluorescence polarization of <b>NF</b> in the presence of different concentrations of pre-miR-21 .....	28
<b>Figure 2.7</b> Synthesis of bifunctional inhibitors.....	30
<b>Figure 2.8</b> (a) The representative image of the electrophoresis analysis of Dicer-mediated pre-miR-21 cleavage in the presence of tested compounds. (b) Densitometric quantitative analysis of miR-21 levels from three independent assays as in (a) .....	31
<b>Figure 2.9</b> RT-qPCR analyses of mature miR-21 expression levels in HEK293T cells .....	33
<b>Figure 2.10</b> (a) The representative image of western blotting analysis of PDCD4 levels in pre-miR-21 expressing HEK293T cells with or without <b>45A</b> treatment. (b) Densitometric quantitative analysis of PDCD4 levels from three independent assays as in (b) .....	34
<b>Figure 2.11</b> RT-qPCR analysis of mature miR-21 and miR-34a expression level in HEK293T cells expressing corresponding pre-miRNA with or without <b>45A</b> treatment .....	35
<b>Figure 2.12</b> The effects of <b>45A</b> on the expression of an EGFP reporter plasmid in HEK293T and CHO cells at 5 $\mu$ M concentration for 24 h treatment .....	35

<b>Figure 2.13</b> The cytotoxicity of <b>45A</b> (5 $\mu$ M) toward HEK293T and CHO cells was evaluated by the MTT assay.....	36
<b>Figure 3.1</b> Design of light controllable miR-21 inhibitor.....	62
<b>Figure 3.2</b> Synthetic scheme of light deactivable miR-21 inhibitor <b>46</b> .....	64
<b>Figure 3.3</b> (a) Time course HPLC analysis of the photolysis reactions of <b>46</b> . (b) Quantification of the relative amount of <b>46</b> left over in reactions as in panel (a). 65	65
<b>Figure 3.4</b> (a) Representative image from electrophoresis analysis of Dicer-mediated pre-miR-21 cleavage in the presence of varying concentrations of <b>46</b> with or without UV irradiation. (b) Densitometric quantitative analysis of miR-21 for images in panel a arising from three independent assays.....	66
<b>Figure 4.1</b> Fluorescence polarization of fluorescein (a) and <b>58-FI</b> (b) in the presence of different concentrations of pre-miR-155.....	79
<b>Figure 4.2</b> The electrophoretic mobility of pre-miR-155 in the presence of compound <b>58</b> .....	80
<b>Figure 4.3</b> (a) Representative image from electrophoresis analysis of Dicer-mediated pre-miR-155 cleavage in the presence of varying concentrations of <b>58</b> . (b) Densitometric quantitative analysis of miR-155 for images in panel a arising from three independent assays .....	81
<b>Figure 4.4</b> Fluorescence microscope imaging of HEK293T and MCF-7 cells treated with DMSO or <b>58-FI</b> .....	82
<b>Figure 4.5</b> (a) Inhibition of miR-155 production by <b>58</b> (24 h treatment) in HEK293T cells overexpressing miR-155. (b) <b>58</b> inhibits endogenous miR-155 formation after 96 h treatment of MCF-7 cells .....	82
<b>Figure 4.6</b> The selectivity of <b>58</b> in inhibiting miR-155 over other miRNAs in MCF-7 cells .....	83
<b>Figure 4.7</b> (a) RT-qPCR analysis of mRNA and (b) Western blotting analysis of protein levels of FOXO3A in MCF-7 cells either treated or not treated with <b>58</b> . (c) Densitometric quantitative analysis of FOXO3A as shown in panel b .....	84
<b>Figure 4.8</b> Flow cytometry analysis of MCF-7 cell apoptosis under different condition. (a) Control; (b) <b>58</b> (30 $\mu$ M); (c) anti-miR-155 (30 nM). (d) Quantitation of cell apoptosis rate as in panel a, b and c.....	85
<b>Figure 4.9</b> Morphological changes of MCF-7 cells after 4 day treatment of DMSO or <b>58</b> .....	86
<b>Figure 4.10</b> Viability analysis for MCF-7 cells treated with <b>58</b> .....	86

## Chapter 1 Introduction

MicroRNAs (miRNAs) are a class of genome-encoded, short (~22 nucleotides), single stranded, and non-coding RNAs. They regulate gene expression post-transcriptionally by targeting mRNA for translational repression or destabilization. A wide range of biological processes are under the control of miRNAs, including metabolism, proliferation, development, differentiation, apoptosis, et al.<sup>1-6</sup> Increasing evidence shows that dysregulation of individual or multiple miRNAs is associated with many human diseases, including cancer, viral infections, central nervous system disorders, metabolic and cardiovascular diseases.<sup>2, 7-10</sup> Thus, miRNAs are considered a novel type of therapeutic target. In this chapter, the biogenesis and function of miRNAs will be first introduced, followed by a discussion of roles played by miRNAs in diseases. Then the approaches currently used for miRNA regulation will be reviewed. Finally, an outlook on future directions will be provided.

### 1.1 Biogenesis of miRNA

Since the discovery of the first miRNA gene, *lin-4*,<sup>11, 12</sup> over 28,000 miRNAs have been found in animals, plants and viruses.<sup>13</sup> They are either independently transcribed from miRNA genes or produced from other transcripts, including introns of protein-coding genes, introns and exons of long non-coding RNAs.<sup>14</sup> The long primary transcript (pri-miRNA) of miRNA genes is transcribed by RNA polymerase II (Figure 1.1). The 5' end is capped by 7-methylguanosine (m7Gppp) and the 3' end is polyadenylated. Pri-miRNA is then processed into pre-miRNA by the RNase III enzyme Drosha in the nucleus (Figure 1.1).<sup>5</sup> Pre-miRNA is a

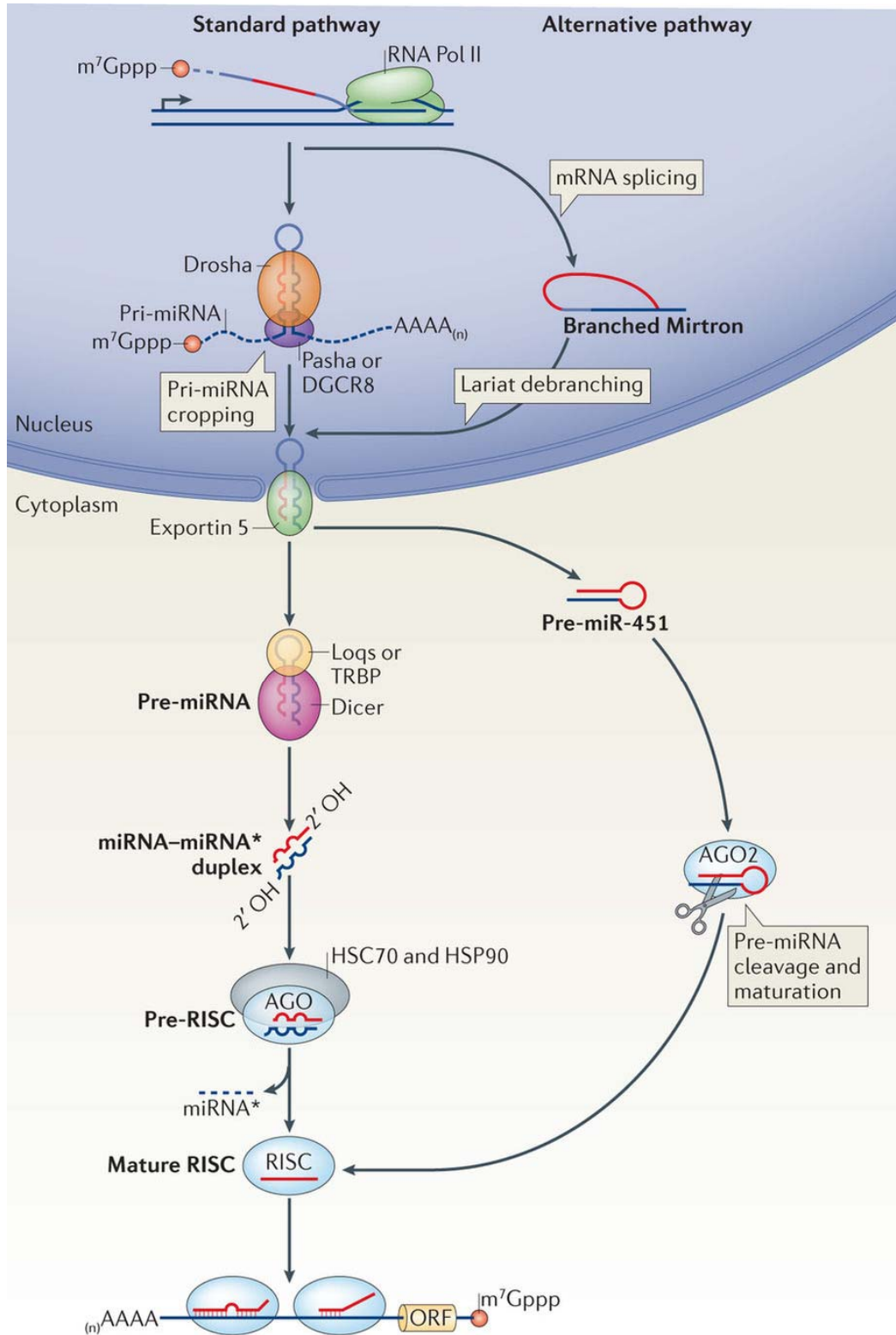


**Figure 1.1** An illustration of the miRNA biogenesis pathway. In the standard miRNA biogenesis pathway, the pri-miRNA, which is transcribed by RNA polymerase II (Pol II), begins with a 7-methylguanosine cap (m<sup>7</sup>Gppp) and ends

with a 3' poly(A) tail. The pri-miRNA contains a stem-loop structure that is cleaved in the nucleus by the endonuclease Drosha. The resulting pre-miRNA is exported from the nucleus by exportin 5 and then further cleaved by the endonuclease Dicer to liberate a miRNA-miRNA\* duplex, which is loaded into an AGO protein. Subsequent maturation steps expel the miRNA\*, producing a mature miRNA-induced silencing complex (miRISC). Alternative pathways typically replace individual steps of miRNA precursor processing. Adapted by permission from Springer Customer Service Centre GmbH,<sup>5</sup> COPYRIGHT (2014).

~60 nucleotide stem-loop structure. It can be recognized by nuclear transport receptor exportin 5, and exported to the cytoplasm through the nuclear pore. In the cytoplasm, another RNase III enzyme, Dicer, cleaves pre-miRNA to liberate a ~22 nucleotide miRNA-miRNA\* duplex. The duplex is then loaded into an Argonaute (AGO) protein and rapidly unwound. The mature miRNA is retained in the AGO protein to form a miRNA induced silencing complex (miRISC), and the complementary strand, miRNA star (miRNA\*), is released.<sup>5, 15</sup>

## **1.2 Function of miRNA**

The function of miRNA in miRISC is to guide the AGO protein to the complementary target mRNA sequence and promote its translational repression, deadenylation or degradation. The key determinant for miRNA target recognition is a short sequence at the 5' end of miRNA, called the seed region (mainly nucleotides 2 to 8).<sup>5</sup> The recognition is based on Watson-Crick pairing of the seed region to the match site (seed match) of the target mRNA. The seed match can be in any region of an mRNA, but it is usually more likely to repress the mRNA translation when the match site is in 3' UTR of the target. More than 60% of all mammalian protein coding-genes are regulated by miRNAs.<sup>16</sup> In addition to translational repression, miRNAs have also been found to activate target

mRNAs<sup>17, 18</sup> or act as molecular decoys that interfere with the function of regulatory proteins.<sup>19</sup> A recent study also showed that miRNA is capable of binding to cell surface receptors, thereby functioning as ligand for signal transduction.<sup>20</sup>

Through the regulation of target genes, miRNAs play important roles in diverse biological processes. Animals with defects in miRNA expression fail to survive or reproduce normally.<sup>8, 21, 22</sup> Cell differentiation is regulated by miRNAs.<sup>23, 24</sup> Depending on the cell type and environment, miRNAs can either inhibit or promote stem cell renewal.<sup>23</sup> A family of miRNAs from the miR-290 cluster were found to regulate the cell cycle of embryonic stem cells by targeting cell cycle inhibitors, thus facilitating the G1-S phase transition and promoting rapid proliferation.<sup>25</sup> MiR-125b was found to target multiple key proteins regulating hematopoietic proliferation, innate immunity, inflammation and apoptosis.<sup>26</sup> MiRNA-21 is another example of on miRNA that regulates apoptosis. One of its target proteins is programmed cell death protein 4 (PDCD4). Knockdown of miR-21 induces upregulation of PDCD4 and activates apoptotic pathways.<sup>27, 28</sup> MiRNAs are also important for development. The first two miRNAs, *lin-4* and *let-7*, both control the timing of larva development in *C. elegans*.<sup>11, 29</sup> The knockdown of miR-124 in vertebrates was found to prevent neural development.<sup>30</sup> The development of heart, blood and vasculature is modulated by miRNAs as well.<sup>31, 32</sup> In a mouse model, miR-122 acts as a key regulator of cholesterol and fatty acid metabolism,<sup>33</sup> and miR-33 was found to control cholesterol homeostasis,<sup>34</sup> implying a role of miRNAs in regulating metabolism. The function of miRNAs in

the immune system is also well documented.<sup>26, 35, 36</sup> All of these findings have unequivocally established the important roles of miRNAs in various biological processes.

### **1.3 MiRNA dysregulation in disease**

#### **1.3.1 Cancer**

The first evidence suggesting a role for miRNAs in cancer was reported in 2002.<sup>37</sup> Calin et al. found that miR-15 and miR-16 genes were deleted or downregulated in more than 60% of human chronic lymphocytic leukemias (CLL). Both miR-15 and miR-16 genes are located in a chromosomal region that is frequently deleted in CLL. Later, the same group found that a significant percentage of miRNA genes are located in the same region,<sup>38</sup> suggesting that miRNAs are genetically associated with cancer. MiR-15 and miR-16 were later found to induce apoptosis by targeting BCL2 mRNA.<sup>39</sup> In 2005, let-7 was found to regulate the expression of oncogenic RAS. The decreased expression of let-7 in lung cancer correlates with increased RAS protein level.<sup>40</sup> These findings clearly show that miRNAs can act as tumor suppressors in cancer. The role of miRNAs as oncogenes (oncomiRs) came to light in a study showing that lymphomagenesis can be accelerated by overexpressing the miR-17-22 cluster.<sup>41</sup> Soon afterwards, it was found that a single miRNA is sufficient to induce tumor development.<sup>42, 43</sup> To date, almost all types of cancer have been found to be associated with altered miRNA expression.<sup>44</sup> MiRNA deregulation in cancer can be caused by different mechanisms, including chromosomal abnormality, genomic mutation, epigenetic changes and alteration in miRNA

biogenesis.<sup>6, 44</sup> Different tumors share some common characteristics of miRNA deregulation, which creates opportunities for cancer treatment by miRNA regulation.<sup>6, 15</sup>

### **1.3.2 Cardiovascular Disease**

Cardiovascular disease is one of the leading causes of morbidity and mortality in industrialized countries.<sup>45</sup> Numerous recent studies support the role of miRNA in cardiovascular disease. MiR-1-1 and miR-1-2 are the first two miRNAs discovered to be relevant to cardiovascular diseases.<sup>45</sup> They are specifically expressed in cardiac and skeletal muscle precursor cells. The overexpression of miR-1 in developing heart was found to lead to a decreased pool of proliferating ventricular cardiomyocytes.<sup>46</sup> Together with miR-1, miR-133 was reported to stimulate myoblast proliferation.<sup>47</sup> These findings implied the possibility of miRNAs being involved in cardiovascular disease. This assumption was later verified by other research, in which more than 12 miRNAs were deregulated in cardiac tissue in mouse in response to stimuli that induce pathological cardiac remodeling. Cardiac overexpression of miR-195 caused pathological cardiac growth and heart failure in transgenic mice.<sup>48</sup> Some other miRNAs were also found to be deregulated in cardiac hypertrophy, including oncomiR-21.<sup>49</sup> All these studies clearly demonstrate the involvement of miRNAs in cardiovascular diseases.

### **1.3.3 Neurodegeneration**

As discussed above, miRNAs play important role in neuronal development, so it is not surprising that they participate in neurodegenerative diseases, such as

Alzheimer's disease, Huntington's disease and Parkinson's disease. In 2007, progressive neurodegeneration was observed in Purkinje cells in the absence of Dicer, one of the key proteins for miRNA biogenesis.<sup>50</sup> In the hippocampal region of Alzheimer's diseased brain, miR-9, miR-25b and miR-128 were found to be upregulated, while miR-124a was found to be downregulated.<sup>51</sup> An increasing number of studies indicate that miRNAs are involved in neurodegenerative diseases.

#### **1.3.4 Other diseases**

In addition to the diseases discussed above, the roles of miRNAs in many other pathological processes have also been studied.<sup>6, 22, 44</sup> For example, they are associated with autoimmune diseases,<sup>52</sup> diabetes,<sup>53</sup> metabolic disorders<sup>34, 54</sup> and infectious diseases.<sup>55, 56</sup>

#### **1.4 miRNA regulation**

As miRNAs are aberrantly expressed in many diseases, they are potential novel therapeutic targets.<sup>15</sup> For diseases associated with miRNA overexpression, inhibiting their function or biogenesis could serve as miRNA regulation approaches that might be potentially applied in disease therapy. These approaches also provide tools for the study of miRNA function. To this end, several methods have already been developed.

##### **1.4.1 Genetic knockout**

MiRNA biogenesis includes a series of enzyme catalyzed chemical reactions. Genetically knockout of the key processing enzymes, such as Drosha, Dicer and Ago, can stop the production of miRNAs.<sup>2, 21</sup> This method was used in studying

the bio-pathway and function of miRNA in early research. To study the function of individual miRNAs, generation of mice lacking a specific miRNA gene through knock out has been used. For example, the function of let-7 in developmental timing<sup>57</sup> and miR-1 in muscle growth<sup>58</sup> were both studied with this method.

#### **1.4.2 MiRNA sponge**

A miRNA sponge is a highly expressed transgene harboring multiple miRNA target sequences to sequester miRNA. This strategy can be applied to modulate miRNA activity for loss of function studies.<sup>15</sup> It makes both transient and long term inhibition possible. Virally delivered miRNA sponges have been used to study miRNA function in mouse models.<sup>59</sup>

#### **1.4.3 Antisense oligonucleotides**

Another approach for miRNA loss of function study is to use antisense oligonucleotides (ASO). By base pairing with the complementary sequence of mature miRNA, ASO is able to sequester mature miRNA and block its interaction with the target mRNA, thus resulting in an inhibition of the miRNA function.<sup>15</sup> The very first application of ASO was achieved by using antisense DNA in *Drosophila*.<sup>60</sup> But it was later proved to be not effective enough in other organisms. This is probably due to the fact that the antisense DNA is subject to degradation by nucleases even before it reaches the target region. Moreover, the poor binding affinity and lack of cell membrane permeability also limit its application in regulating miRNA.<sup>61</sup>

To overcome these problems, chemical modifications have been carried out, including modifications to the sugar and internucleotide linkage backbone

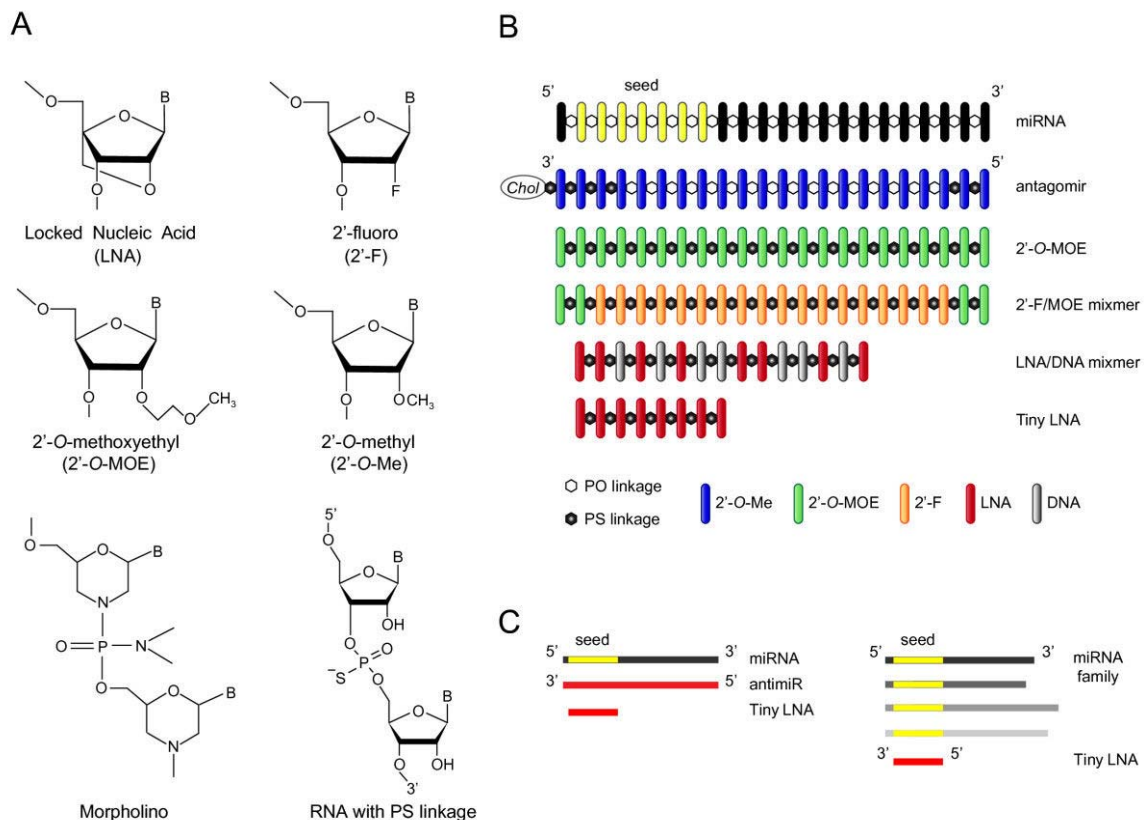


**Figure 1.2** (A) Structures of the most commonly used chemical modifications in anti-miR oligonucleotides. Locked nucleic acid (LNA) is a bicyclic RNA analogue in which the ribose is locked in a C3'-endo conformation by introduction of a 2'-O, 4'-C methylene bridge. The 2'-fluoro (2'-F), 2'-O-methoxyethyl (2'-MOE) and 2'-O-methyl (2'-O-Me) nucleotides are modified at the 2' position of the ribose moiety, whereas a six-membered morpholine ring replaces the sugar moiety in morpholino oligomers. In the phosphorothioate (PS) linkage, sulfur replaces one of the non-bridging oxygen atoms in the phosphate group. (B) Design of chemically modified anti-miR oligonucleotides. (C) Schematic overview of the miRNA inhibition approach using a fully complementary anti-miR and a seed-targeting tiny LNA. Adapted from reference.<sup>15</sup>

(Figure 1.2 A). The 2'-fluoro (2'-F), 2'-O-methoxyethyl (2'-MOE) and 2'-O-methyl (2'-O-Me) nucleotides are modified at the 2' position of the ribose moiety, while locked nucleic acid (LNA) contains a 2'-O, 4'-C methylene bridge resulting in 3'-endo conformation (Figure 1.2 A). All these modifications greatly improve the binding affinity of ASO to the cognate miRNAs. LNA possess the highest affinity.

To improve the stability, the phosphodiester linkage can be modified into a phosphorothioate (PS) linkage, in which one oxygen atom in the phosphate is replaced with sulfur atom. The modification improves the nuclease resistance of ASO significantly. Other modifications include the incorporation of a non-charged morpholine ring (morpholino) or *N*-(2-aminoethyl)-glycine (PNA) into the internucleotide linkage backbone. They are completely nuclease resistant. To improve the cellular uptake efficiency, ASO can be conjugated to cell permeable lipids (Figure 1.2 B). Cell penetrating peptides, nanoparticles and aptamers were also reported to be able to deliver ASO.<sup>62-64</sup> The seed targeting tiny 8-mer LNA ASO (Figure 1.2 C) was found to be able to silence target miRNA *in vivo* without additional conjugation.<sup>65</sup> With these research progresses, ASO has made their way into clinical trial.<sup>66, 67</sup>

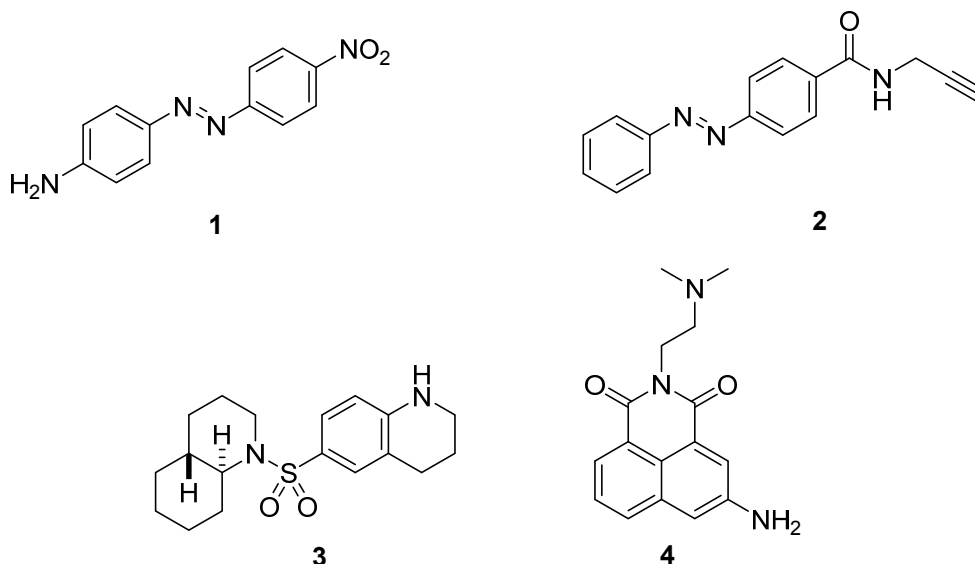
Despite the great success in the design and application of chemically modified ASOs, the *in vivo* delivery efficiency is still very low. With current technology, most of the ASO delivered into cells are trapped inside the endosomes, only a few are exported into the cytosol to scan for the target miRNA.<sup>68</sup> Another limitation for their use *in vivo* is the off target effects. The short ASO carries the inherent risk of binding RNAs other than the intended miRNAs. Imperfect base pairing could also contribute to off target binding. Thus, an understanding of the off target effects resulting from undesired binding is important for the development of ASO based therapeutics.<sup>15</sup> ASO also suffers from poor pharmacokinetic and bio-distribution profiles.<sup>69, 70</sup>

#### 1.4.4 Small molecule inhibitors

MiRNA biogenesis is a multiple-step enzyme catalyzed process, including transcription, Drosha processing, Dicer processing and AGO loading. Small molecules, capable of inhibiting any of these processes by binding the enzymes, factors or RNA substrates, may serve as potential miRNA regulators.

##### 1.4.4.1 Targeting miRNA transcription

One of the first studies on small-molecule inhibitors of the miRNA pathway was reported by Deiters and co-workers.<sup>71</sup> They designed constructs expressing luciferase under the control of miRNA binding sequences in the 3'-untranslated region (3'-UTR). These constructs served as sensors to detect the presence of specific mature miRNAs. With this assay, they screened more than 1000 compounds and identified compound **1**, which was further optimized to compound **2**, as an inhibitor of miR-21 production. Mechanistic studies showed that compound **2** blocks the transcription of the miR-21 gene into pri-miR-21.



A similar assay was used for screening inhibitors of miR-122,<sup>72</sup> which is the most abundant miRNA in liver and is involved in hepatocellular carcinoma development and hepatitis C virus (HCV) infection. Compound **3** was identified to inhibit miR-122 transcription and HCV replication in liver cells, representing a new approach to the treatment of HCV infections. In addition, compound **4** was found to activate pro-apoptotic miR-122 expression, leading to increased caspase expression and reduced cell viability, having implications in cancer therapy.<sup>72</sup>

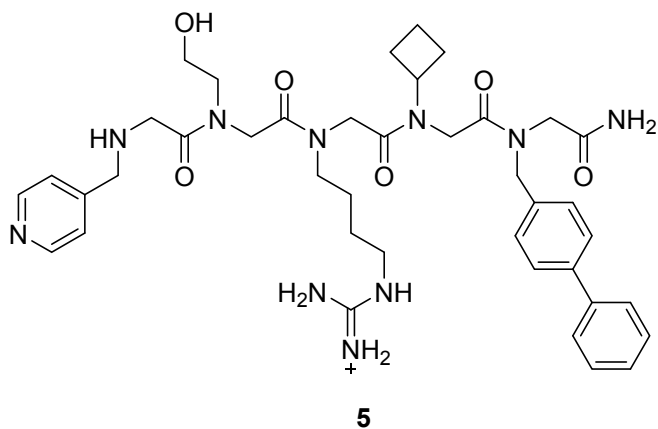
#### **1.4.4.2 Targeting Drosha/Dicer processing**

RNA consists of different types of secondary structures, including duplex, internal loop, bulge and hairpin loop. These structures can serve as binding pockets for small molecules,<sup>73</sup> which may disrupt the interaction between targeted RNA and related protein, thus inducing the desired biological effects. Many different types of RNA including rRNA, tRNA, mRNA, et al. have been shown targetable by small molecules.<sup>73</sup> Within pri-miRNA and pre-miRNA, secondary structures play important roles for proper recognition and processing by Drosha or Dicer. They provide great opportunity for identifying pri/pre-miRNA binders, which could interrupt the Drosha/Dicer processing and serve as miRNA inhibitors.<sup>61</sup>

##### **1.4.4.2.1 Drosha inhibitor**

Diaz et al. screened a library of 14,024 peptoids for pri-miR-21 binders.<sup>74</sup> Compound **5** was identified to bind the apical loop of pri-miR-21. Further study

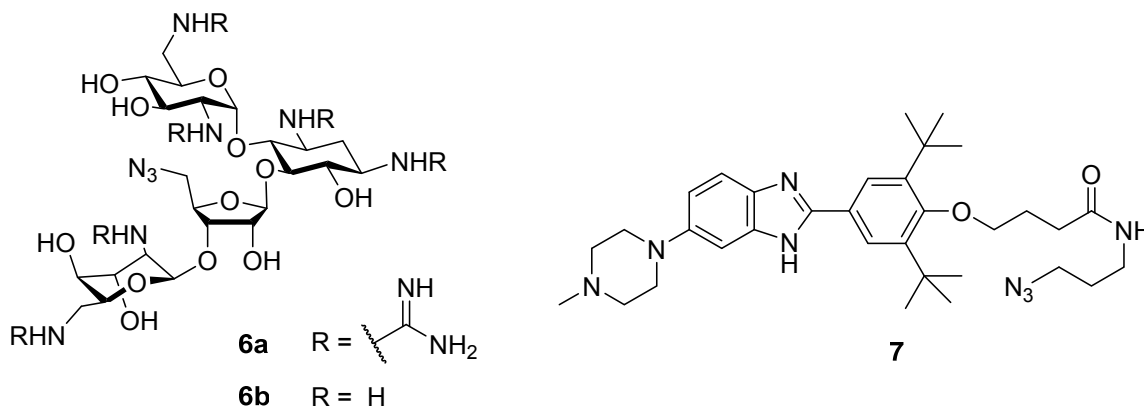
showed that it inhibits the cleavage of pri-miR-21 by Drosha with a clear specificity over pri-miR-16.<sup>74</sup>



The Disney group developed a rational design approach, named Inforna, to target miRNAs in a transcriptome-wide and target agnostic manner.<sup>75</sup> They first designed a two dimensional combinatorial screening (2-DCS) strategy, in which a library of random RNA secondary structures is titrated against a small molecule microarray.<sup>76</sup> The subsequent RNA sequencing reveals the RNA motifs that bind small molecules. The data is then subject to a statistical approach, called Structure-Activity Relationships Through Sequencing (StARTS), which predicts the fitness of RNA motif and small molecule interaction based on affinity and selectivity.<sup>77</sup> The information is then cross referenced to the motifs found in pri/pre-miRNAs as reported in miRBase,<sup>13</sup> thereby identifying the ideal RNA target for a given small molecule.

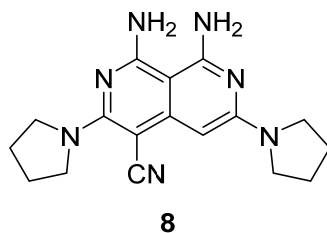
Using this approach, compound **6a** was identified to be an effective inhibitor for miR-10b.<sup>78</sup> It increases the amount of pri-miR-10b while decreasing the amount of precursor and mature miR-10b in cells, suggesting an inhibition of Drosha processing. Recently, they found that compound **6b** inhibits the Drosha

processing of pri-miR-525.<sup>79</sup> Compound **7** was identified as a Drosha site inhibitor for miR-96. It increases the level of pri-miR-96 while reducing those of pre- and mature miR-96 in cells. Further study showed that compound **7** is even more selective than a LNA oligonucleotide that is complementary to the seed region of miR-96.<sup>75</sup>



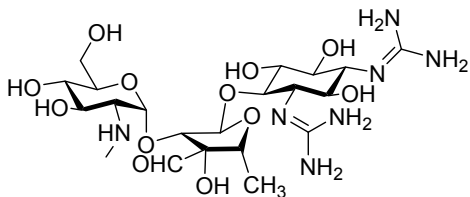
#### 1.4.4.2.2 Dicer inhibitor

Inforna can also be used to identify Dicer processing inhibitors. Compound **8** is one example. The Disney group found that it impedes the biogenesis of miR-544 by inhibiting the Dicer processing. They also probed the role of miR-544 using compound **8**. It turns out that inhibition of miR-544 biogenesis disrupts adaptive responses to hypoxia by modulating ATM-mTOR signaling.<sup>80</sup>

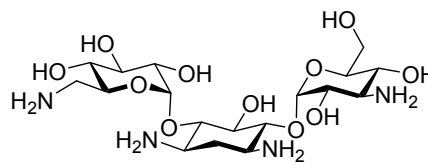


Aminoglycosides are a category of widely used anti-bacterial agents. They disrupt protein elongation by targeting the 30S ribosomal subunit.<sup>81</sup> Because of

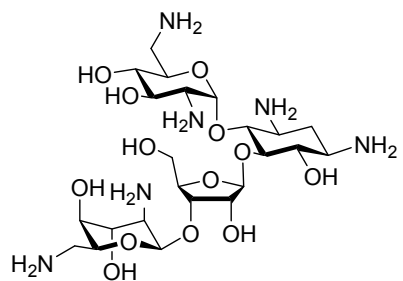
their great affinity to RNA, they are frequently used for probing various RNA



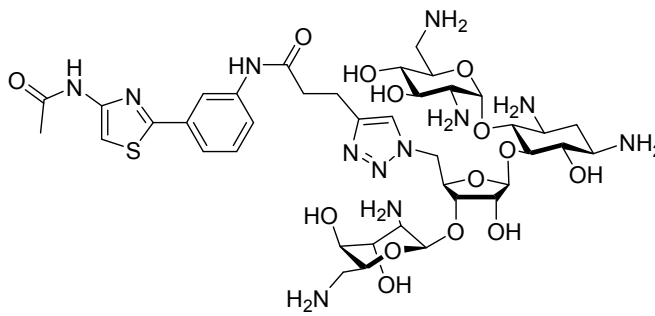
**Streptomycin**



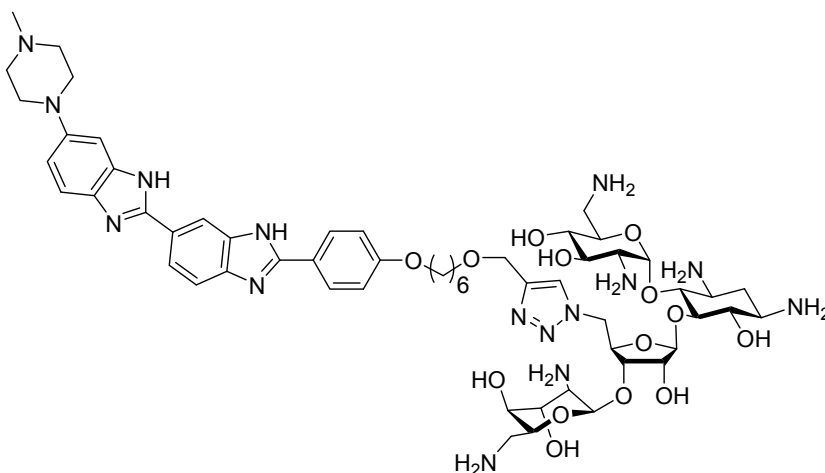
**Kanamycin**



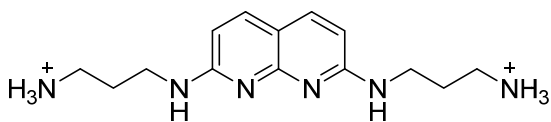
**Neomycin**



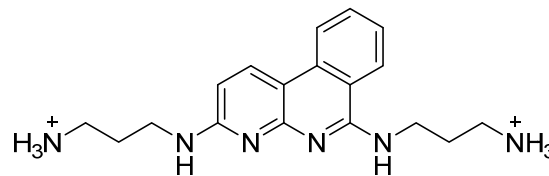
**10**



**9**



**11**



**12**

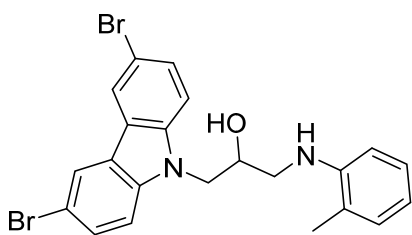
targets.<sup>73, 82-84</sup> The Maiti group first reported the study of aminoglycosides in miRNA inhibition.<sup>85</sup> They screened a library of aminoglycosides in cells

expressing luciferase under the control of miR-21 target sequence within the 3' UTR. Streptomycin, which is used as a tuberculosis drug, was found to decrease the expression of luciferase. *In vitro* assays showed that it was able to block Dicer cleavage of pre-miR-21 significantly and induce downstream effects. In another study, several aminoglycosides (including neomycin and kanamycin) were found to bind pre-miR-155 but not inhibit the Dicer cleavage *in vitro*.<sup>86</sup> Meanwhile, the Duca group found that neomycin was able to inhibit Dicer cleavage of several other miRNAs *in vitro*, including pre-miR-17, pre-miR-21, pre-miR-372 and pre-miR-373.<sup>87</sup> The Maiti group also reported that neomycin inhibits the biogenesis of pre-miR-27 in MCF-7 breast cancer cells.<sup>88</sup> These results showed the possibility of using aminoglycosides as leads for generating miRNA inhibitors.

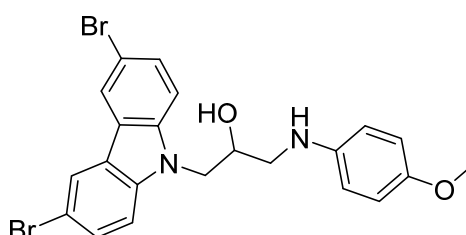
Therefore, rationally designed modification of RNA binders, like aminoglycosides, emerges as a new way for targeting pre-miRNAs. To improve the cell permeability, affinity and selectivity of neomycin toward pre-miRNAs, Maiti et al. designed a synergistic approach in which a bisbenzimidazole moiety was linked to neomycin, a pre-miR-27 binder.<sup>89</sup> The bisbenzimidazole scaffold is cell permeable and also known to bind various RNA structures. The dual binding conjugate **9** was found to penetrate easily into cells and inhibit miR-27 production significantly. Similarly, the Duca group conjugated artificial nucleobases to neomycin. They found that the incorporation of the nucleobases increased the binding affinity and selectivity of the conjugate **10** towards miR-372 and miR-373.<sup>90</sup> To improve the binding affinity of **11** to the cytosine bulge in RNA duplexes,

the Nakatani group designed an expanded three ring system (**12**), which improved the stacking interaction with neighboring base pairs in RNA duplex.<sup>91</sup> **12** shows strong binding affinity to pre-miR-29a and inhibits miR-29a maturation *in vitro*.

In an effort to search for new RNA binding scaffolds, Schneekloth and coworkers screened a microarray based small molecule library for new motifs binding to pre-miR-21. Hit compounds **13** and **14** were found to bind to pre-miR-21 and disrupt the processing by Dicer.



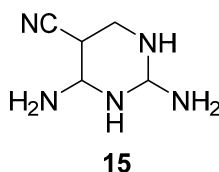
**13**



**14**

Peptides serve as an important source for discovering small molecules targeting various biological molecules. To discover peptides targeting pre-miR-155, the Shin group performed microarray based screening.<sup>92</sup> A few peptides were identified to bind pre-miR-155, inhibit miR-155 production and induce cancer cell apoptosis. By using electrophoresis mobility shift assay, the Varani group screened a library of cyclic peptides for binding pre-miR-21. **Cyclo(RVRTRGKRRIRRpP)** was found to bind to the pre-miR-21 hairpin with an apparent  $K_d$  of 200 nM. It is also active in blocking pre-miR-21 processing *in vitro* and in cells. Phage display technology has been widely used for studying protein-protein, protein-peptide, protein-DNA and protein-RNA interactions.<sup>93, 94</sup> Recently, the Maiti group used this technology to discover peptides that bind pre-miR-21 by

screening a peptide library of around  $10^9$  or more complexity.<sup>95</sup> One peptide, **ALWPPNLHAWVP**, was identified to selectively downregulate miR-21 expression in cells by blocking Dicer processing. They also found that this peptide inhibitor induces apoptosis and suppresses cell invasion and migration. The results of these studies demonstrate the potential of targeting pre-miRNAs with peptides.

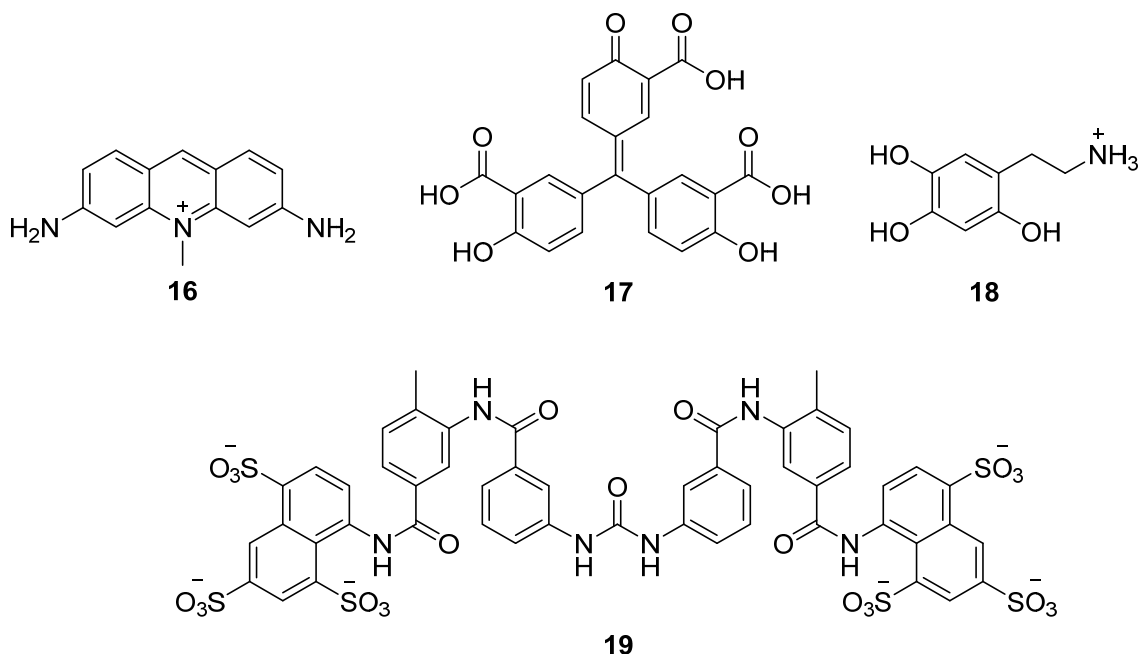


Computer-aided drug discovery or design methods have played a major role in the development of therapeutically important small molecules for over three decades.<sup>96</sup> Shi et al. first used high-throughput docking to screen for ligands that target miR-21. Compound **15** was identified to bind the Dicer site of pre-miR-21. In cell assays showed that **15** inhibits the biogenesis of miR-21 in a dose-dependent manner, resulting in suppression of tumor growth and progression.<sup>97</sup>

#### 1.4.4.3 Targeting AGO loading

Another approach used for the inhibition of miRNA function is to block the loading of mature miRNA onto the AGO2 protein, thus preventing the formation of miRISC complex. In a cell based generic screening, Watashi et al. found that tryptaflavine (**16**) interrupts the miRNA pathway by blocking the AGO2 loading process.<sup>98</sup> Tan et al. developed an assay for large scale screening of miRNA/RISC loading modulators. The assay is based on the fluorescence

polarization of TAMRA-labeled RNAs loaded onto AGO2. Using this method they identified compound **17**, **18** and **19** as RISC loading inhibitors.<sup>99</sup>



#### 1.4.4.4 Other inhibitors

The Deiters group recently screened a library of more than 300,000 compounds for miR-21 inhibitors with a luciferase-based reporter assay.<sup>100</sup> A set of aryl amide small-molecule inhibitors were identified to inhibit miR-21 specifically. Estradiol was also reported to downregulate miR-21 expression and increase miR-21 target expression in MCF-7 cells.<sup>101</sup> However, the inhibition modes of both remain unclear.

#### 1.5 Summary and outlook

When the first small non-coding RNA was identified two decades ago, the existence of miRNAs was completely unknown, not to mention the importance. Since then, our knowledge of miRNAs has grown exponentially. A great amount of success has been achieved in disclosing the mechanism of the miRNA bio-

pathway. Efforts for exploring the detailed role of miRNA in various biological activities and developing miRNA as a new therapeutic target are still desired. This research field will benefit from the development of miRNA regulators.

Although it is extremely difficult to target RNA,<sup>73</sup> promising progress has been achieved in miRNA regulation. ASO based miRNA inhibition has recently made its way to clinical trials, despite the constraints of delivery, pharmacokinetics, pharmacodynamics and off-target effects. Within a very short time span, many small-molecule based miRNA inhibitors have been reported for targeting different processes of the miRNA biogenesis pathway, especially pre-miRNA processing by Dicer. However, challenges remain for small-molecule based miRNA inhibition. Some pri/pre-miRNA binders identified from affinity based screening were not active in blocking Drosha/Dicer processing due to different reasons. Rational designed modification of those pre-miRNA binders may create new opportunities for regulating miRNA. Moreover, the understanding of pri/pre-miRNA motifs that are targetable is very poor so far, and the knowledge of chemical structures with high binding affinity to pri/pre-miRNAs is also very limited. Finally, the diversity of the currently used RNA targeting scaffolds is very low. Most of them are polycationic compounds, such as aminoglycosides and multiply charged peptides. They usually suffer from poor selectivity and cell permeability. Thus, the development of novel RNA targeting scaffolds with good cellular uptake efficiency and specificity is highly desired.

In this dissertation, a general strategy was first developed for inhibiting miRNA biogenesis with bifunctional small molecules made from pre-miRNA binder

(Chapter 2). The potential of using this strategy for spatiotemporal miRNA regulation was also studied (Chapter 3). Finally, a novel type of miRNA targeting scaffold was developed (Chapter 4). The results of these studies have significant implications for not only the therapy of diseases associated with miRNA dysregulation, but also the study of miRNA function.

## Chapter 2 Regulating miRNA Biogenesis by Bifunctional Small Molecules

Adapted with permission from *J. Am. Chem. Soc.*, 2017, 139 (14), 4987–4990.  
Copyright © 2017, American Chemical Society

### 2.1 Introduction

One common way used for developing miRNA inhibitors is to screen chemical libraries against pre-miRNAs. The hits are expected to bind pre-miRNAs and disrupt the interactions between pre-miRNAs and Dicer, thus inhibiting miRNA maturation. However, it is not uncommon that small molecules, which are selected using binding-based screening against miRNA precursors, are unable to block miRNA maturation.<sup>86, 87</sup> This phenomenon might be a consequence of promiscuous targeting and/or poor cell permeability of these small molecules. In addition, these small molecules might possess binding affinities that are insufficiently low to compete with the extensive macromolecule interactions occurring between RNAs and other binding partners. To enhance binding between small molecules and targeted miRNA precursors, rationally designed bifunctional molecules have been developed in which additional binding moieties are conjugated to the original RNA-recognizing molecules. For example, Duca and co-workers designed neomycin-nucleobase conjugates that have additional base pairing driven affinities against pre-miRNAs to give new inhibitors that block maturation of miR-372 and -373.<sup>90, 102</sup> Maiti and co-workers developed dual binding neomycin-bisbenzimidazole conjugates, which contain an intercalating unit to enhance binding of neomycin, and showed that the conjugates serve as inhibitors for oncogenic miR-27a.<sup>89</sup>

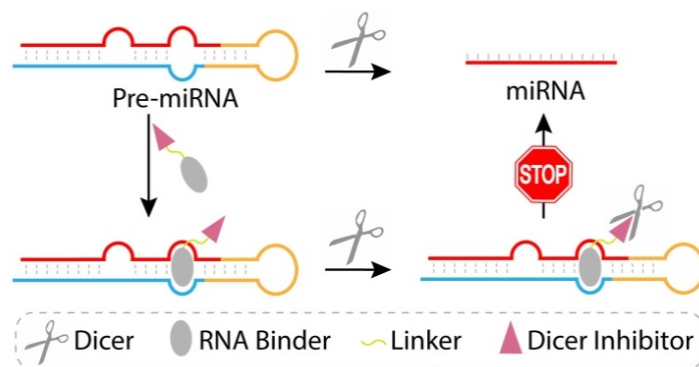


**Figure 2.1** A schematic illustration of the new approach to regulate miRNA biogenesis by using bi-functional small molecules that target pre-miRNA.

In this chapter, we devised and tested a new strategy to regulate miRNA biogenesis that relies on the use of newly designed bifunctional small molecules (Figure 2.1). The purpose of previously developed bifunctional molecules is to target two closely located binding sites and utilize bi-valent recognition to enhance binding affinity. In contrast, our bifunctional molecules are designed to deliver a specific Dicer inhibitor to the Dicer-catalyzed cleavage site in the target pre-miRNA/Dicer complex. The new conjugates consist of a high affinity pre-miRNA binding unit linked to a low affinity Dicer inhibition unit. The Dicer inhibitor in the conjugate is selected so that it alone does not inhibit Dicer to a significant extent. As a result, the pan-cellular function of Dicer will not be disrupted by the bifunctional molecule. However, recognition of a target pre-miRNA by the RNA binding unit in the conjugate brings the Dicer inhibitor unit into close proximity with the pre-miRNA cleavage site of bound Dicer, thus causing blockage of the activity of Dicer. Importantly, by functioning in this manner, the inhibition unit will promote inhibition of the production of the target miRNA.

Oncogenic miR-21 is upregulated in many cancers.<sup>49</sup> As a result, small molecules that inhibit the production of miR-21 can serve as useful tools to study the roles played by miR-21 in cancers and as potential cancer therapeutic agents. To demonstrate the feasibility of the new strategy described above, we designed, prepared and tested bifunctional inhibitors that block the biogenesis of human miR-21.

## 2.2 Results and discussion

### 2.2.1 Identification of pre-miR-21 binder

The first stage of assembling the newly designed bifunctional miR-21 inhibitors involves identification of a pre-miR-21 targeting small molecule. Fluorescence polarization (FP), a powerful tool for studying molecular interactions, was utilized for this purpose.<sup>103, 104</sup> In this assay, the degree of FP from a fluorophore-labeled small molecule increases when it forms a complex with a macromolecule owing to a reduction in the rate of fluorophore tumbling.

To identify small molecules that bind pre-miR-21, we used the FP-based competitive binding assay to screen ligands that can compete with a moderate affinity ligand for binding to pre-miR-21. Because kanamycin (Figure 2.2) binds to several RNAs,<sup>73, 83, 105, 106</sup> we expected that it would bind pre-miR-21 and, as a result, serve as the standard ligand in the FP-based screening protocol. To verify this assumption, kanamycin derivatives, containing a 1,8-naphthalimide fluorophore at either the primary hydroxyl (**KOF**) or the primary amine group (**KNF**) were prepared (Figure 2.2). The binding affinity of **KOF** and **KNF** to pre-

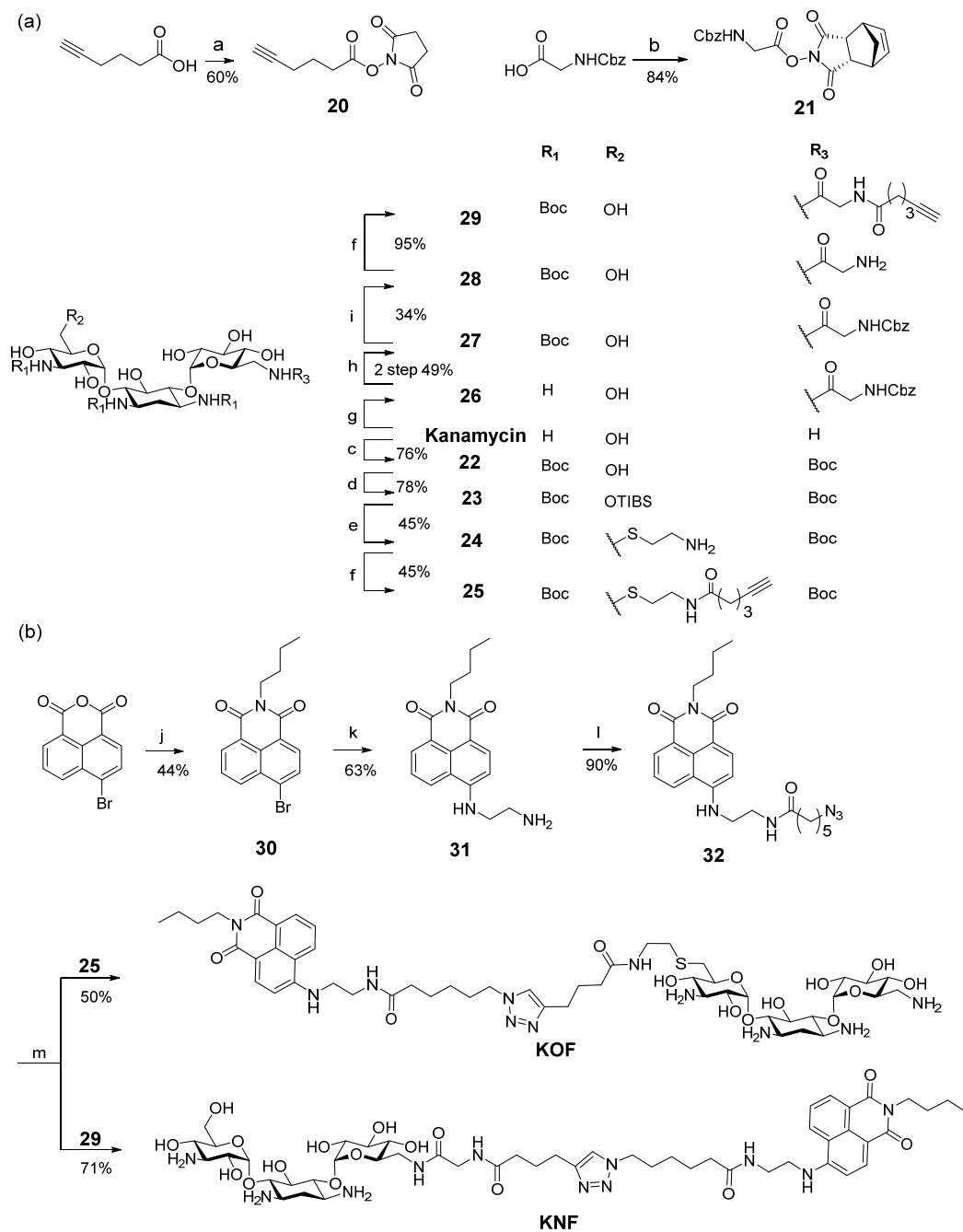


**Figure 2.2** (a) Synthesis of kanamycin building blocks. (b) Synthesis of KOF and KNF. *Reagents and conditions:* (a) DCC, HOSu, DCM; (b) DCC, endo-N-hydroxy-5-norbornene-2,3-dicarboximide, DCM; (c) Boc<sub>2</sub>O, TEA, DMF/H<sub>2</sub>O, 60 °C; (d) 2,4,6-Triisopropylbenzenesulfonyl chloride, pyridine, R.T., 16 h; (e) Cysteamine hydrochloride, Cs<sub>2</sub>CO<sub>3</sub>, DMF, 16 h; (f) Compound 20, TEA, DCM; (g) Compound 21, H<sub>2</sub>O/acetone; (h) Boc<sub>2</sub>O, H<sub>2</sub>O/acetone; (i) H<sub>2</sub>, Pd/C, MeOH; (j) n-Butylamine, EtOH, reflux; (k) Ethylenediamine, dioxane, reflux; (l) 6-Azidohexanoic, EDCI, HOBT, DMF; (m) i) CuSO<sub>4</sub>, Sodium ascorbate, DMSO/H<sub>2</sub>O; ii) TFA, DCM.

miR-21 was determined using the FP assay. Based on the saturation binding curve of **KOF** versus pre-miR-21 from the FP assay, a binding affinity ( $K_d$ ) of  $419 \pm 83$  nM was obtained (Figure 2.3 a). On the other hand, the binding affinity of **KNF** to pre-miR-21 was found to be too small to be determined (Figure 2.3 b). Based on these results, **KOF** was employed as the standard pre-miR-21 binding ligand in the FP-based screening protocol.

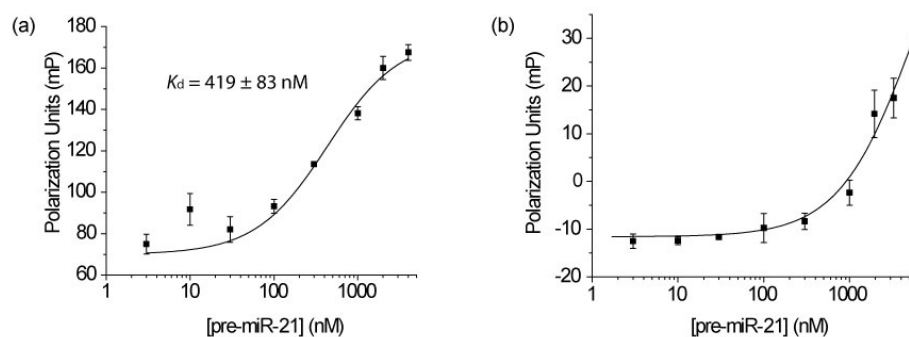


**Figure 2.3** Fluorescence polarization of **KOF** (a) and **KNF** (b) in the presence of different concentrations of pre-miR-21. The results were the average from 3 independent experiments. The error bars represent the standard error of mean (N = 3).

Screening was carried out by incubating the pre-formed **KOF**/pre-miR-21 complex with 13 commercially available aminoglycosides, which are one of the best studied classes of molecules that target RNAs.<sup>73, 83, 103-107</sup> Displacement of **KOF** from pre-miR-21 by an aminoglycoside with higher affinity against pre-miR-21 is reflected in a decrease of the FP value. Among the tested substances, neomycin was found to reduce the FP of **KOF**/pre-miR-21 to a value that matches that of free **KOF**, indicating a complete displacement (Figure 2.4).

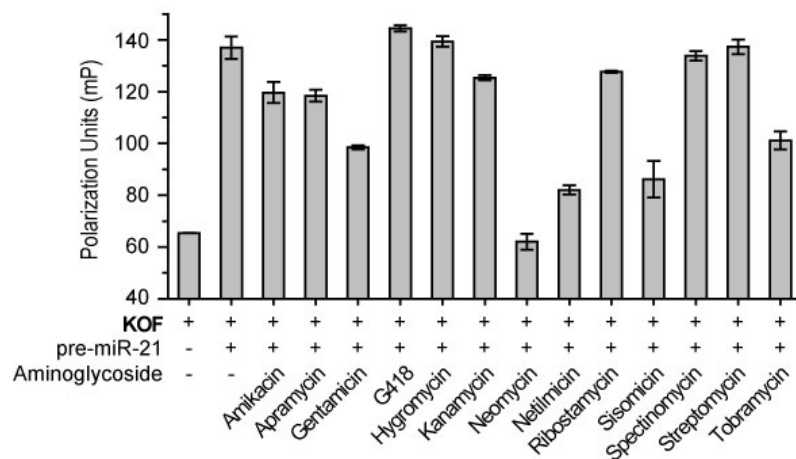


**Figure 2.4** Fluorescence polarization of **KOF** in the absence or presence of pre-miR-21 and different aminoglycosides. The error bars represent the standard error of the mean (N = 3).

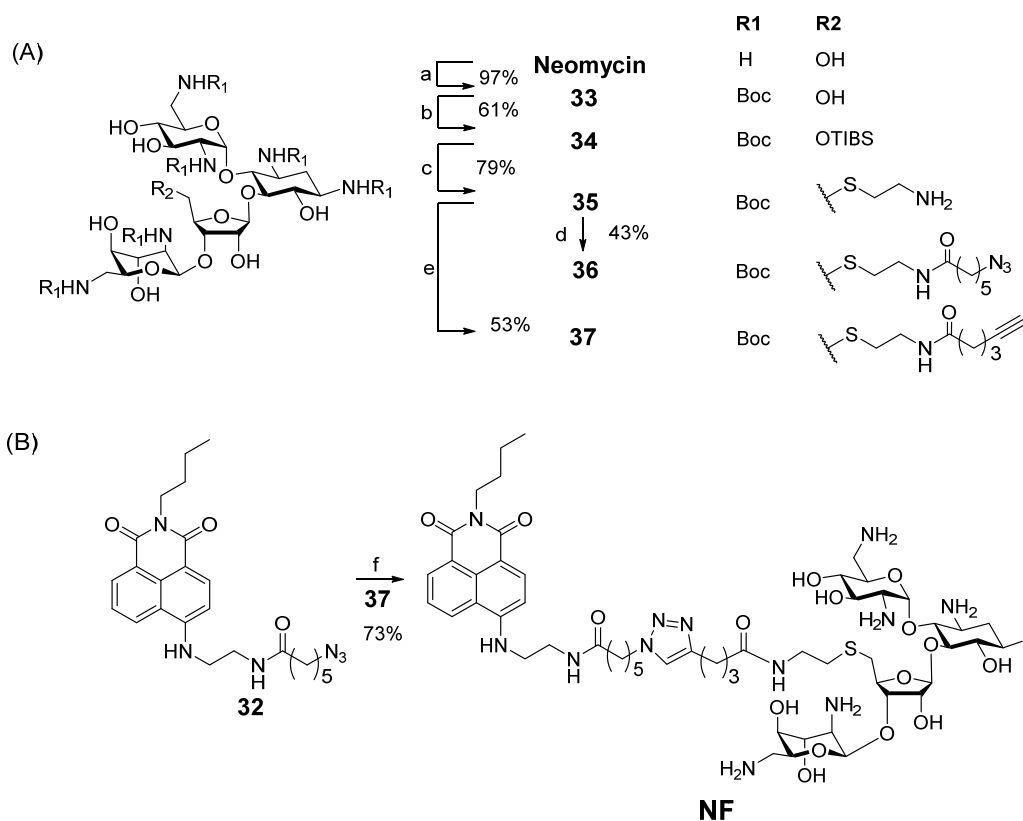


**Figure 2.5** Synthesis of neomycin building blocks (A) and **NF** (B). *Reagents and conditions:* (a)  $\text{Boc}_2\text{O}$ , TEA, DMF/ $\text{H}_2\text{O}$ , 60 °C; (b) 2,4,6-Triisopropylbenzenesulfonyl chloride, pyridine, R.T., 16 h; (c) Cysteamine hydrochloride,  $\text{Cs}_2\text{CO}_3$ , DMF, 16 h; (d) 6-Azidohexanoic, EDCI, DIPEA, DCM; (e) 6-hexynoic, EDCI, DIPEA, DCM; (f) i)  $\text{CuSO}_4$ , Sodium ascorbate, DMSO/ $\text{H}_2\text{O}$ ; ii) TFA, DCM.

To validate the binding of neomycin to pre-miR-21, the hydroxyl fluorophore-tagged derivative of neomycin, **NF**, was prepared (Figure 2.5). Employing the reported method,<sup>103, 104</sup> the amino groups in neomycin were protected and the primary hydroxyl group was transformed to an amino group to give **35**. Reaction of **35** with 6-hexynoic gave the alkyne **37**, which was later coupled with **32**. The subsequent deprotection of the amino groups produced **NF**.

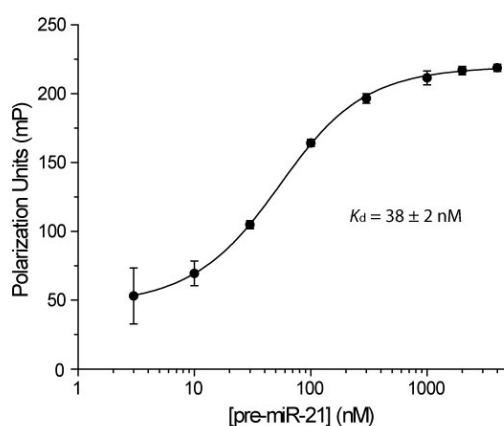
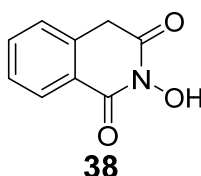


**Figure 2.6** Fluorescence polarization of **NF** in the presence of different concentrations of pre-miR-21. The error bars represent the standard error of the mean (N = 3).

Using the FP assay, we determined that the  $K_d$  of **NF** to pre-miR-21 is  $38 \pm 2$  nM (Figure 2.6), which is 10 fold smaller than that of **KOF**. This result confirms that neomycin strongly binds to pre-miR-21 and led to the selection of neomycin as the pre-miR-21 binding unit in the new bifunctional molecules. Importantly, the above result indicates that modification of the primary hydroxyl group on neomycin does not disrupt the binding, therefore, this hydroxyl group can be a suitable position to conjugate the Dicer inhibition unit.

### 2.2.2 Selection of Dicer inhibitor

The active site of Dicer is located within the RNase III domain, which cleaves pre-miRNAs through a mechanism in which two metal ions ( $Mg^{2+}$ ) catalyze the phosphoryl transfer reaction.<sup>108</sup> The distance between the two  $Mg^{2+}$  is around 4 Å, similar to those in active sites of other mechanistically similar RNases. Many RNase inhibitors with metal chelating properties have been developed,<sup>109, 110</sup> including the N-hydroxyimide **38** that inhibits influenza endo-nuclease at micromolar concentrations.<sup>110</sup> As a result, **38** was used as the Dicer inhibiting unit in the new bifunctional molecules.



### 2.2.3 Synthesis of bifunctional small molecules

The route to synthesize bifunctional inhibitors began with preparation of a series of homophthalic acids (**42A-D**) possessing alkynyl polyethylene glycol tails of different lengths (Figure 2.7). Reactions of **42A-D** with *para*-methoxybenzyl (PMB) oxyamine produced O-PMB-oxyimides **43A-D** that were later coupled to neomycin. The free imide **44**, used as a control in activity assays, was produced by removing the PMB group in **43A** with trifluoroacetic acid. An azide modified neomycin derivative **36** was synthesized as shown in Figure 2.5. **36** and **43A-D** were then coupled using click chemistry. Subsequent removal of the Boc and PMB protecting groups from the click products by using trifluoroacetic acid

generated bifunctional molecules **45A-D** containing tethers of different length linking the two functional units.

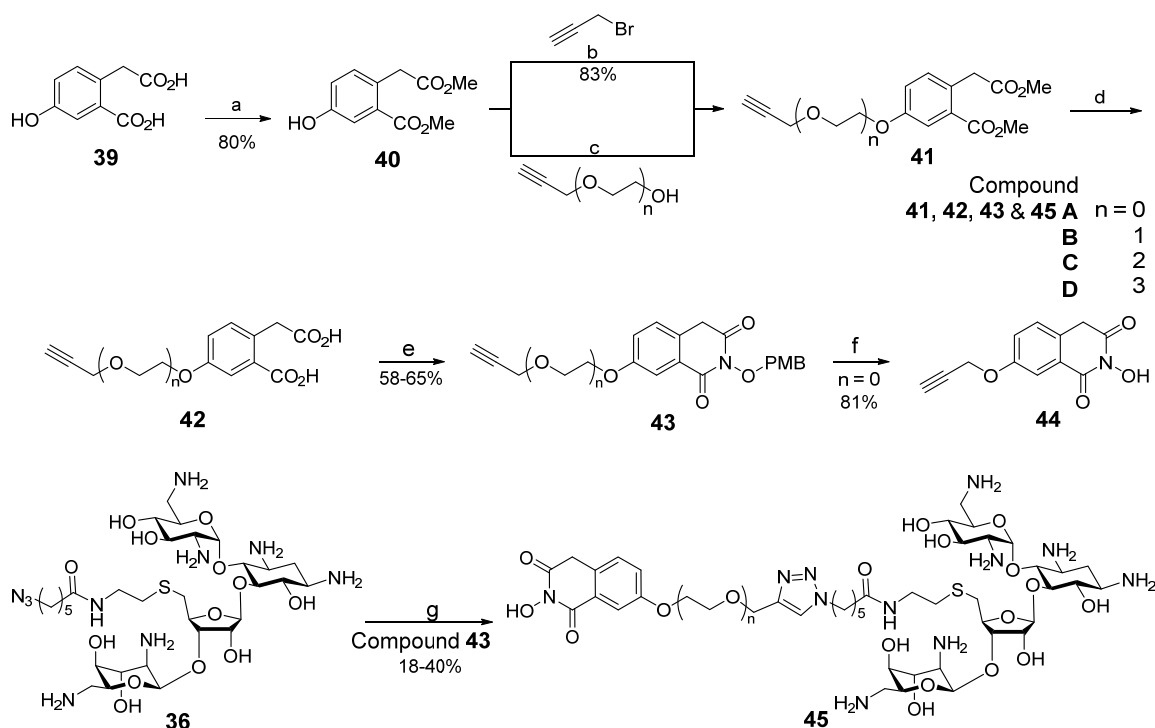


**Figure 2.7** Synthesis of bifunctional inhibitors. *Reagents and conditions:* (a)  $\text{H}_2\text{SO}_4$ , MeOH, reflux; (b) Propargyl bromide,  $\text{K}_2\text{CO}_3$ , DMF; (c) DIAD,  $\text{Ph}_3\text{P}$ , THF; (d) i) LiOH, MeOH/ $\text{H}_2\text{O}$ ; ii) HCl; (e) O-(4-Methoxybenzyl)-hydroxylamine, toluene, reflux; (f) TFA, DCM; (g) i)  $\text{CuSO}_4$ , Sodium ascorbate, DMSO/ $\text{H}_2\text{O}$ ; ii) TFA, DCM.

### 2.2.4 *In vitro* Dicer blocking activity

The ability of **45A-D** to inhibit Dicer-mediated pre-miR-21 cleavage *in vitro* was determined (Credit to Umesh Bhattarai). For this purpose,  $^{32}\text{P}$ -labeled pre-miR-21 was prepared by *in vitro* transcription,<sup>111</sup> and then incubated (37 °C, 2.5 h) with recombinant human Dicer in the absence or presence of **45A-D**, or one of the following, the Dicer inhibition unit alone (i.e. compound **44**), the pre-miR-21 binding unit alone (i.e., neomycin), or a commercial morpholino-based anti-miR-21 ASO designed to block miR-21 maturation (anti-miR-21 A). The extent of

cleavage of pre-miR-21 (72 nt) into mature miR-21 (22 nt) was then determined

u t i l i z i n g a

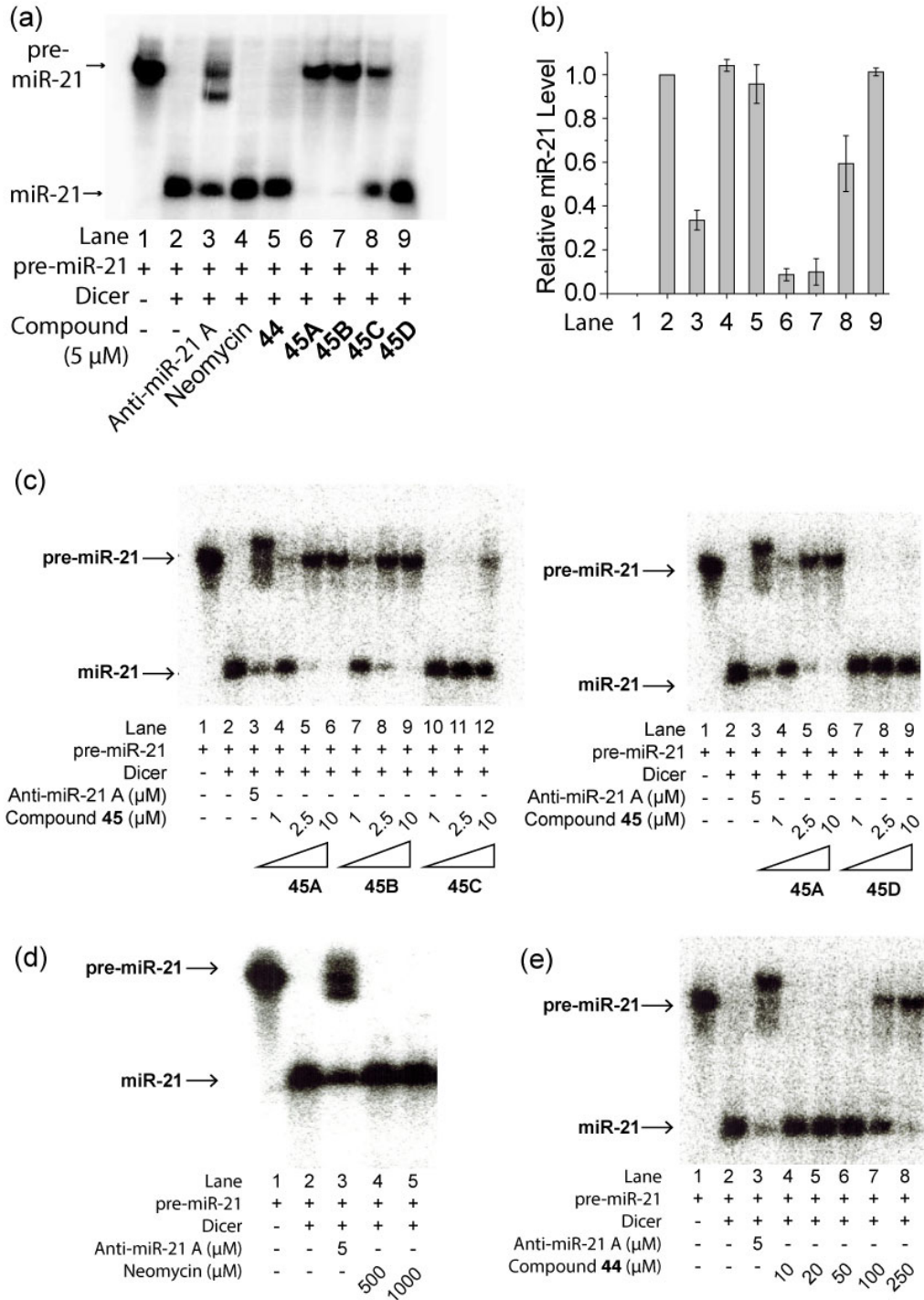


**Figure 2.8** (a) The representative image of the electrophoresis analysis of Dicer-mediated pre-miR-21 cleavage in the presence of tested compounds. (b)

Densitometric quantitative analysis of miR-21 levels from three independent assays as in (a). The error bars represent the standard error of mean (N = 3). (c, d & e) Dose dependent inhibition of Dicer by different compounds. Figure courtesy of Umesh Bhattarai.

15% denaturing polyacrylamide gel and phosphor-imaging. As shown in Figure 2.8 a, Dicer cleaves pre-miR-21 completely to form mature miR-21. In addition, anti-miR-21 A, as a positive control, inhibits cleavage by 70% at 5  $\mu$ M, indicating that the assay performs correctly. Importantly, bifunctional molecule **45A** inhibits Dicer promoted cleavage in a dose dependent manner, reducing the level of miR-21 formation by 90% at 5  $\mu$ M (Figure 2.8 a-c). A comparison of the results coming from studies with **45A-D** shows that Dicer catalyzed miR-21 formation increases as the length of the linker between the two functional units increases, demonstrating that the inhibitory activity is critically altered by the distance between the two functional units. In contrast to the bifunctional molecules, unmodified neomycin, at concentrations up to 1 mM, does not inhibit Dicer activity (Figure 2.8 a & d). Furthermore, the inhibitor unit alone (i.e., **44**) displays no inhibition at concentrations up to 50  $\mu$ M (Figure 2.8 a & e). The combined results clearly show that conjugation of neomycin, the pre-miR-21 recognition unit, to the Dicer inhibitory unit **38** significantly enhances the Dicer inhibition potency (>200 fold comparing **45A** to neomycin) and that the presence of a linker of proper length between the two units is essential for the activity.

### 2.2.5 MiRNA inhibition activity in cell

Because **45A** is the most potent Dicer inhibitor in the *in vitro* assay, it was used for in cell investigations. To study the in cell inhibitory activity of **45A**, mature miR-21 expression levels were determined by utilizing the RT-qPCR

assay. HEK293T cells were transfected with pCMV-miR21 plasmid expressing pre-miR-21 and treated at the time of transfection with neomycin, a commercial phosphorothioate-based anti-miR-21 ASO (anti-miR-21 B), or various concentrations of **45A**. As shown in Figure 2.9, **45A** inhibits the expression of miR-21 in a dose-dependent manner (76% reduction at 5  $\mu$ M when compared to non-treated cells). The activity of **45A** is similar to that of anti-miR-21 B. In contrast, neomycin does not cause a significant decrease in miR-21 level at 100  $\mu$ M. When **45A** was added 4 h after transfection, no inhibitory activity was observed, which suggests the transfection procedure may assist cellular delivery of **45A**.

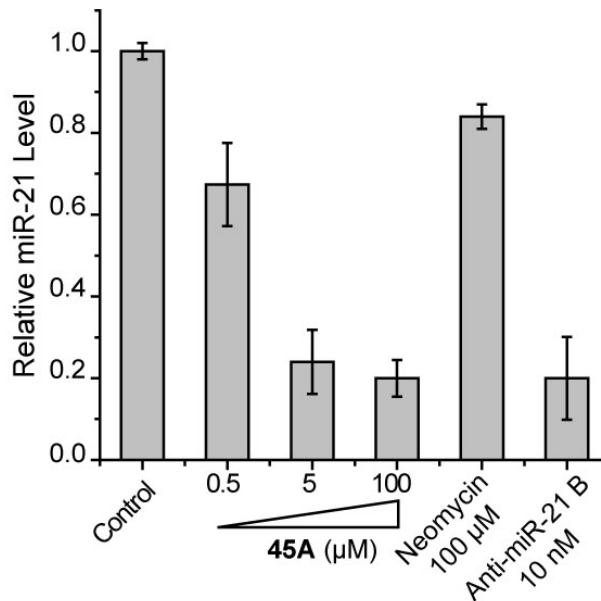


**Figure 2.9** RT-qPCR analyses of mature miR-21 expression levels in HEK293T cells. The error bars represent the standard error of the mean (N = 3).

### 2.2.6 Downstream effect of miR-21 inhibition by 45A

Programmed cell death protein 4 (PDCD4) is a tumor suppressor protein, whose mRNA is a direct target of miR-21.<sup>112</sup> Expression of miR-21 represses

PDCD4 expression in HEK293T cells and repression of miR-21 should de-repress PDCD4 production. As expected, the expression level of PDCD4 protein, determined by using western blotting and compared to non-treated cells, increases by 90% when cells are treated with **45A** (Figure 2.10). The cellular assay results demonstrate that **45A** is highly active in repressing miR-21 formation in cells.

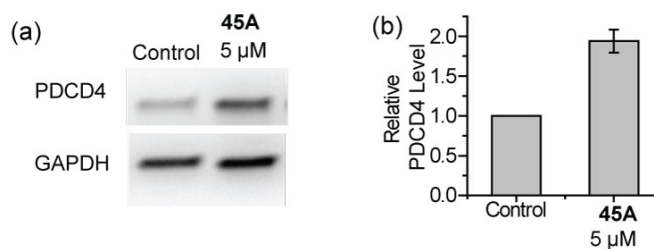


**Figure 2.10** (a) The representative image of western blotting analysis of PDCD4 levels in pre-miR-21 expressing HEK293T cells with or without **45A** treatment. (b) Densitometric quantitative analysis of PDCD4 levels from three independent assays as in (b). The error bars represent the standard error of the mean (N = 3).

## 2.2.7 Selectivity of bifunctional molecule

In the design of bi-functional molecules employed in this study, we utilized aminoglycosides as the pre-miRNA binding unit because they are well-known RNA binders. However, aminoglycosides, including neomycin, are known to target a number of RNA sequences and, as a result, the new bifunctional substances could suffer from selectivity issues.<sup>73, 83, 89, 90, 102-107</sup>

To investigate the miRNA regulation selectivity of the neomycin-based bi-functional molecule **45A**, its ability to inhibit another randomly chosen miRNA, miR-34a, in HEK293T cells was determined using RT-qPCR. The results show that **45A** indeed reduces the production of miR-34a (40% reduction at 5 μM when

compared to non-treated cells), but not at the same level of potency as it does against miR-21 at the same concentration (Figure 2.11). Thus, although **45A** displays some degree of selectivity, the incorporation of more selective pre-miRNA recognition moieties other than aminoglycosides in the bifunctional design may lead to improved RNA selectivity.

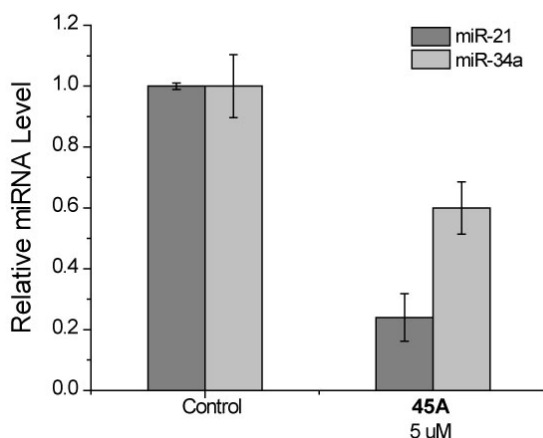


**Figure 2.11** RT-qPCR analysis of mature miR-21 and miR-34a expression level in HEK293T cells expressing corresponding pre-miRNA with or without **45A** treatment. The results were the average from 3 independent experiments. The error bars represent the standard errors of the mean (N = 3).

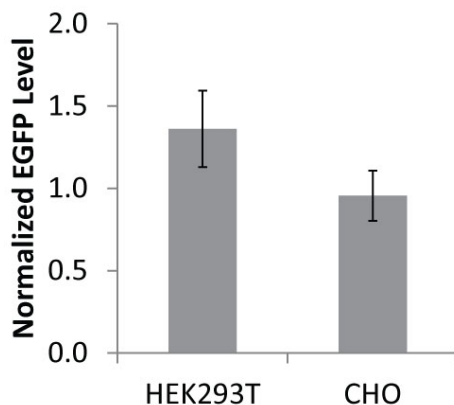


**Figure 2.12** The effects of **45A** on the expression of an EGFP reporter plasmid in HEK293T and CHO cells at 5  $\mu$ M concentration for 24 h treatment. The results were the average from 3 independent experiments. The error bars represent the standard deviations (N = 3).

### 2.2.8 Effect of bifunctional molecule on translation

Because neomycin is known to target ribosomal RNA and interfere with translation, effects of **45A** on translation were tested by transfecting HEK293T and CHO cells with an EGFP reporter followed by **45A** treatment.<sup>75, 113, 114b</sup> No significant change in EGFP expression was observed at the concentration that inhibits miR-21 maturation (Figure 2.12), indicating that the bifunctional small molecule does not interfere with the function of ribosomal RNA.

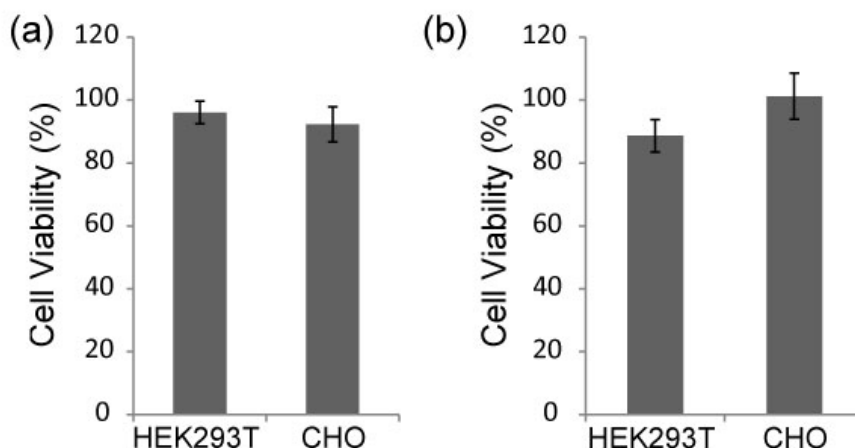


**Figure 2.13** The cytotoxicity of **45A** (5  $\mu$ M) toward HEK293T and CHO cells was evaluated by the MTT assay. (a) Cells were directly treated with **45A**. (b) Cells were transfected with an EGFP reporter plasmid and treated with **45A** at the same time. The cell viability percentages were calculated by comparing treated cells to non-treated ones. The results were the average from 3 independent experiments. The error bars represent the standard deviations (N = 3).

### 2.2.9 Cytotoxicity of bifunctional molecule

The effect of **45A** on the viability of HEK293T and CHO cells was also studied by MTT (3-(4,5-Dimethylthiazol-2-yl)-2,5-diphenyltetrazolium bromide) assay. As shown in Figure 2.13 a, no significant change in cell viability was observed when cells were directly treated with **45A** (5  $\mu$ M). Considering the improved cellular uptake of **45A** by the transfection procedure (discussed in 2.2.5), we also tested

the viability of cells transfected with the EGFP reporter plasmid and treated with **45A** at the same time. Compared to the control without **45A** treatment, cells treated with **45A** showed the same level of viability (Figure 2.13 b). These results show that under the condition of miR-21 inhibition, **45A** does not cause cell toxicity.

### 2.3 Summary

In summary, a new approach to regulate miRNA maturation was developed that relies on the use of a Dicer-inhibiting bifunctional small molecule. The study showed that **45A**, which contains neomycin as a pre-miR-21 binding unit and the N-hydroxyimide **38** as the Dicer inhibitory unit, inhibits miR-21 maturation *in vitro* and in cells. Together, these observations demonstrate that the new bifunctional strategy is applicable to the design of active miR-21 inhibitors based on an otherwise non-active pre-miR-21 binder. We expect that the strategy will be effective in generating new bifunctional regulators for miRNAs.

### 2.4 Experimental section

#### 2.4.1 *In vitro* Transcription of pre-miR-21

The pre-miR-21 RNA was *in vitro* transcribed<sup>111</sup> from template oligonucleotides using transcription kit (Ambion). Briefly, forward primer:

5'-GAAATTAATACGACTCACTATAGGTGTCGGGTAGCTTATCAGACTGATGTT  
GACTGTTGAATCTCATGGC-3'

and reverse primer:

5'-TGTCAGACAGCCCATCGACTGGTGTGGCCATGAGATTCAACAGTCAAC-3'

2  $\mu\text{M}$  of each were subjected to primer extension using Taq polymerase per the manufacturer's protocol. The hybrid template with T7 promoter was used for *in vitro* transcription following manufacturer's instructions (Ambion). Right before use, the RNA prepared was refolded as follows: RNA was heated to 94  $^{\circ}\text{C}$  for 2 min and then cooled to 4  $^{\circ}\text{C}$  at a rate of 1  $^{\circ}\text{C}/\text{s}$ .

#### 2.4.2 Fluorescence polarization binding assay

The affinity of fluorophore tagged aminoglycosides to pre-miR-21 was determined following a literature method.<sup>103</sup> 30 nM of fluorophore tagged aminoglycoside was incubated with various concentrations of pre-miR-21 (3 nM to 4  $\mu\text{M}$ ) in cacodylate buffer (10 mM, pH 7.4, 0.01% Triton X-100) at room temperature for 1 hour. The polarization values were obtained with a microplate reader (SpectraMax i3X, Molecular Devices) equipped with a fluorescence polarization detection cartridge. Polarization units (mP) were plotted against pre-miR-21 concentration and fit in the following equation to determine  $K_d$ :

$$P = P_0 + \Delta P \frac{[\text{RNA}]_{\text{total}} + [\text{F}]_{\text{total}} + K_d - \sqrt{([\text{RNA}]_{\text{total}} + [\text{F}]_{\text{total}} + K_d)^2 - 4[\text{RNA}]_{\text{total}}[\text{F}]_{\text{total}}}}{2[\text{F}]_{\text{total}}}$$

Where  $P_0$  is the polarization of free fluorescent small molecule,  $P$  is the measured polarization at each pre-miR-21 concentration  $[\text{RNA}]_{\text{total}}$ ,  $\Delta P$  is the total change of polarization upon saturation,  $[\text{F}]_{\text{total}}$  is the total concentration of fluorescent compound. For the competition binding experiments, various competitors (3  $\mu\text{M}$ ) were incubated with fluorophore tagged aminoglycosides (30 nM) and pre-miR-21 (1  $\mu\text{M}$ ) for 1 h before reading. The experiment was performed in triplicate.

### **2.4.3 Dicer-mediated pre-miRNA cleavage assay**

The Dicer-mediated pre-miR-21 cleavage assay was performed at 37 °C for 2.5 h using Dicer buffer (Genlantis). Each reaction mixture contained 1 µL of <sup>32</sup>P labeled pre-miR-21 (~20 ng, prepared by *in vitro* transcription), 0.5 unit of Dicer (1 µL, Genlantis) and indicated compounds with a final volume of 10 µL. A morpholino anti-miR-21 nucleotide (Anti-miR-21 A, Sequence: 5'-AGTCAACATCAGTCTGATAAGCTAC-3') was used as a positive control. The reaction was stopped by boiling with equal volume of 95% formamide with dyes (Thermo Fisher Scientific) and then separated in 15% denaturing polyacrylamide gel. The gel was imaged with phosphorimager and analyzed by Quantity one software (Bio-rad).

### **2.4.4 Cell culture and transfection**

pCMV-miR21 (Addgene plasmid # 20381) and MSCV-miR-34a (Addgene plasmid # 63932) were obtained from Addgene. HEK293T and Chinese hamster ovary (CHO) cells were cultured in DMEM medium (Gibco) without antibiotics, supplemented with 10% FBS and 2 mM GlutaMAX (Life Technologies) at 37 °C in a humidified atmosphere containing 5% CO<sub>2</sub>. HEK293T cells were plated 1 day before transfection in 24-well plates at  $2.0 \times 10^5$  cells/well. Transfections with DNA plasmid mixtures were carried out at ~70% cell confluency using Lipo2000 transfection reagent (Invitrogen). Briefly, DNA 200 ng, Lipofectamine 2000 (Thermo Fisher Scientific) 1 µL and indicated amount of tested compounds were incubated in Opti-MEM reduced serum medium (50 µL) at room temperature for

5 min before transfection. A phosphorothioate-based anti-miR-21 ASO (Anti-miR-21 B, Integrated DNA Technologies, Sequence: 5'-CAACATCAGTCTGATAAGC TAC-3') was used as a positive control. Cells were harvested for RNA extraction after 22 h or for western blot analysis after 84 h.

#### **2.4.5 RNA extraction and RT-qPCR**

Total RNA was extracted using miRNeasy Mini Kit (Qiagen) per the manufacturer's protocol. Approximately 10 ng of total RNA was used in reverse transcription reactions, which were completed using a Taqman MicroRNA RT Kit (Applied Biosystems) per the manufacturer's protocol. RT-qPCR was performed on CFX96 Real Time PCR System (Bio-Rad) using Taqman Universal PCR Master Mix (Applied Biosystems) with 1  $\mu$ L of the RT product. All primer sets for mature miRNAs were purchased from Applied Biosystems. The triplicate threshold cycles (*Ct*) obtained for each treatment were used to determine the relative levels of miRNA normalized to U6 small nuclear RNA using the  $2^{-\Delta\Delta C_t}$  method.<sup>115</sup> The result presented was based on three independent assays.

#### **2.4.6 Western Blotting**

Total protein was extracted using RIPA buffer and quantified using a Bio-Rad Protein Assay. Approximately 20  $\mu$ g of total protein was resolved on a 4-15% SDS-polyacrylamide gel, and then transferred to a PVDF membrane. The membrane was briefly washed with 1 $\times$  Tris-buffered saline (TBS), and then blocked in 5% milk dissolved in 1 $\times$  TBST (1 $\times$  TBS containing 0.1% Tween-20) for 1 h at room temperature. The membrane was then incubated in 1:1000 PDCD4 (Cell Signaling Technology, PDCD4 (D29C6) XP<sup>®</sup> Rabbit mAb) or GAPDH

primary antibody (Cell Signaling Technology, GAPDH (D16H11) XP® Rabbit mAb) in 1 × TBST containing 3% (w/v) BSA overnight at 4 °C. The membrane was washed with 1 × TBST and incubated with 1:10000 anti-rabbit IgG horseradish-peroxidase conjugate in 1 × TBS for 1 h at room temperature. After washing with 1× TBST, protein expression was quantified using Clarity Western ECL Substrate (Bio-Rad) per the manufacturer's protocol. The image was quantified with Image lab software. The quantification data provided were based on three independent assays.

#### **2.4.7 Cytotoxicity Assay**

The cytotoxicity of **45A** toward HEK293T and CHO cells were tested by MTT assays (MTT = 3-(4, 5-dimethylthiazol-2-yl)-2, 5-diphenyltetrazolium bromide). HEK293T (50,000 cells/well) and CHO (25,000 cells/well) cells were seeded in 96-well plates and grown overnight to around 70% confluency. For the cell viability under non-transfected condition, the cells were treated with or without **45A** (5 µM) for 24 h. For the cell viability under transfection condition, the cells were transfected with 100 ng of EGFP reporter plasmid (Actin-IRES-eGFP)<sup>116</sup> following the method mentioned above and treated with or without **45A** (5 µM) for 24 h. Subsequently, the medium was removed and 10 µL of MTT stock solution (12 mM) was added to wells along with 100 µL of phenol free DMEM. The cells were incubated at 37 °C for 4 h. The MTT containing medium was replaced with 50 µL of DMSO. The solution was mixed thoroughly with the pipette and incubated 37 °C for 10 min. The absorbance at 540 nm was recorded with a plate reader (SpectraMax i3X, Molecular Devices). The relative viability of the cells

was calculated based on 6 parallel tests by comparing to the controls. The results presented were based on three independent assays.

#### **2.4.8 Translational Inhibition Assay**

Translational inhibition was studied following a method modified from the literature.<sup>113</sup> HEK293T ( $2 \times 10^5$  cells/well) and CHO cells ( $1 \times 10^5$  cells/well) were plated into 24-well plates and grown overnight to around 70% confluency. The cells were then transfected with 400 ng of eGFP reporter plasmid (Actin-IRES-eGFP)<sup>116</sup> following the method mentioned above and treated with or without **45A** (5  $\mu$ M). After 24 h, the cells were collected by trypsinizing and centrifugation. The GFP expression was quantified with a microplate reader (SpectraMax i3X, Molecular Devices). The relative cell viability obtained from the cytotoxicity assay was used for normalizing the EGFP level. The assay was performed in triplicate. The results presented were based on three independent assays.

#### **2.4.9 Chemical Synthesis**

*Chemicals and instrumentation.* Neomycin tri-sulfate was purchased from Sigma Aldrich (Neomycin B > 85%). Kanamycin A was purchased from Amresco. All other reagents and solvents were purchased from BroadPharm, Aldrich or Alfa Aesar and used without further purification. Reactions involving air- or moisture-sensitive reagents were performed under an argon atmosphere. Analytical thin-layer chromatography (TLC) was conducted on silica gel plates with fluorescent indicator 254 nm, and compounds were visualized by irradiation (254 nm) or by staining with ninhydrin stain or cerium ammonium molybdate stain. Column chromatography was carried out on silica gel (pore size 60 Å, 200-425 mesh

particle size, Sigma Aldrich). HPLC was performed using a Thermo Scientific UltiMate 3000 semi-preparative system coupled with a Thermo Scientific Acclaim 120 C18 column (100 mm × 4.6 mm, 3 μm). All HPLC analyses were run at RT and monitored at 260 nm. A gradient of CH<sub>3</sub>CN containing 0.1% TFA in water containing 0.1% TFA was used at a flow rate of 1 mL/min. For analytical HPLC, acetonitrile was increased from 5% to 90% in 25 min. For Prep-HPLC, acetonitrile was increased from 5% to 19% in 10 min, 19% to 90% in 1 min and then kept constant for 3 min. <sup>1</sup>H and <sup>13</sup>C NMR spectra were recorded on a Bruker Avance III 300 spectrometer. Chemical shifts are reported in parts per million (ppm, δ) referenced to the residual <sup>1</sup>H resonance of the solvent.<sup>117</sup> Splitting patterns are designated as follows: s (singlet), d (doublet), t (triplet), m (multiplet), br (broad). Coupling constants (J values) are listed in hertz (Hz). High resolution mass spectra (HRMS) were obtained with a Waters Micromass mass spectrometer with electrospray ionization probe.

#### *Synthesis of **KOF** and **KNF**.*

Compound **20**<sup>118</sup> To a solution of 5-hexynoic acid (2.0 g, 17.8 mmol) in anhydrous THF (50 mL) was added N-hydroxysuccinimide (2.05 g, 17.8 mmol) and DCC (3.68 g, 17.8 mmol). The reaction was stirred at room temperature for overnight. The DCU solid was filtered out and the product was purified by column chromatography (EA: Hexane = 1:2) to give **20** as a colorless oil (2.2 g, 60%). <sup>1</sup>H NMR (300MHz, CDCl<sub>3</sub>, δ) 2.84 (br, 4H), 2.78 (t, *J* = 7.5 Hz, 2H), 2.46 (m, 2H), 2.02 (t, *J* = 2.7 Hz, 1H), 1.97 (t, *J* = 7.2 Hz, 2H).

Compound **22**<sup>104</sup>

A solution of kanamycin (2.0 g, 3.43 mmol) in a mixture of DMF (40 mL), water (8 mL) and triethylamine (1 mL) was treated with di-*tert*-butyldicarbonate (3.1 g, 14.1 mmol). The reaction solution was heated to 60 °C for 6 h, then cooled to room temperature. The volatiles were removed in vacuo. The residue was partitioned between water (300mL) and ethyl acetate (600 mL). The aqueous layer was separated and extracted with ethyl acetate (2 × 150 mL). The combined organic layer was washed with brine, dried over Na<sub>2</sub>SO<sub>4</sub>, and concentrated in vacuo. The residue was purified by column chromatography (MeOH: DCM = 1:10) to give **22** as a white solid (2.3 g, 76%). R<sub>f</sub> = 0.2 (10% methanol in dichloromethane). <sup>1</sup>H NMR(300 MHz, MeOD, δ): 5.10 (br, 1H), 5.07 (d, *J* = 3.3 Hz, 1H), 4.07 (d, *J* = 8.7 Hz, 1H), 3.80-3.52 (m, 10H), 3.47-3.35 (m, 5H), 3.19(t, *J* = 9.3 Hz, 1H), 2.09 (d, *J* = 12.6 Hz, 1H), 1.45 (m, 37H).

#### Compound **23**<sup>104</sup>

A solution of **22** (0.45 g, 0.51 mmol) in pyridine (10 mL) was treated with 2,4,6-triisopropylbenzenesulfonyl chloride (2.5 g, 8.3 mmol). The reaction mixture was stirred at room temperature for overnight and then neutralized by adding hydrochloric acid (1.0 N). The mixture was partitioned between water (100 mL) and ethyl acetate (200 mL). The aqueous layer was separated and extracted with ethyl acetate (2 × 100 mL). The combined organic layer was washed with brine, dried over Na<sub>2</sub>SO<sub>4</sub>, and concentrated in vacuo. The residue was purified by column chromatography (50% to 100% EA in hexane) to give **23** a white solid (0.46 g, 78%). R<sub>f</sub> = 0.35 (Methanol: DCM = 1:10). <sup>1</sup>H NMR (300 MHz, MeOD, δ) 7.28 (s, 2H), 5.04 (br, 2H), 4.38 (t, *J* = 10.2 Hz, 2H), 4.15 (m, 3H), 3.69 (br, 2H),

3.61-3.35 (m, 11H), 3.16 (m, 1H), 2.95 (m, 1H), 2.01 (m, 1H), 1.45 (m, 36H), 1.25 (m, 19H).

#### Compound **24**<sup>104</sup>

A solution of **23** (328 mg, 0.285 mmol) and cesium carbonate (1.10 g, 3.42 mmol) in DMF (5 mL) was treated with cysteamine hydrochloride (0.65 g, 5.7 mmol). The reaction mixture was stirred at 80 °C for 4 h and then partitioned between water (100 mL) and ethyl acetate (200 mL). The aqueous layer was separated and extracted with ethyl acetate (2 × 150 mL). The combined organic layer was washed with brine, dried over Na<sub>2</sub>SO<sub>4</sub>, and concentrated in vacuo. The residue was purified by column chromatography (MeOH: DCM = 1:1) to give **24** as a white solid (120 mg, 45%). R<sub>f</sub> = 0.15 (15% methanol in dichloromethane). <sup>1</sup>H NMR (300 MHz, MeOD, δ) 5.09 (br, 1H), 5.03 (br, 1H), 4.15 (br, 1H), 3.67 (m, 2H), 3.59 (m, 3H), 3.53 (br, 2H), 3.52-3.32 (m, 5H), 3.17 (m, 1H), 3.02 (m, 2H), 2.97 (d, *J* = 7.8 Hz, 1H), 2.80 (m, 3H), 2.67 (m, 1H), 2.05 (m, 1H), 1.42 (m, 36H), 1.25 (m, 1H).

#### Compound **25**

To a solution of **24** (100 mg, 0.106 mmol) in DCM (2 mL) was added TEA (50 μL) and **20** (22.2 mg, 0.106 mmol). The reaction was stirred at 40 °C for 10 h. After removal of the solvents, the residue was purified by column chromatography (MeOH: DCM = 1:20) to give **25** as a white solid (50 mg, 45%). R<sub>f</sub> = 0.55 (15% MeOH in DCM). <sup>1</sup>H NMR (300 MHz, MeOD, δ) 5.11 (br, 1H), 5.05 (br, 1H), 4.20 (br, 1H), 3.65 (m, 3H), 3.59 (m, 2H), 3.47 (m, 4H), 3.38 (m, 4H), 3.29 (m, 2H), 2.95 (m, 1H), 2.61 (m, 4H), 2.30 (m, 5H), 2.08 (br, 1H), 1.79 (m, 2H), 1.42 (m,

36H), 1.26 (m, 1H).  $^{13}\text{C}$  NMR (75 MHz, MeOD,  $\delta$ ): 175.44, 174.90, 159.41, 157.94, 157.72, 102.69, 99.91, 85.15, 84.25, 80.57, 80.38, 80.12, 77.02, 74.60, 74.05, 73.48, 72.33, 72.18, 71.76, 70.31, 57.13, 52.21, 50.89, 41.87, 40.21, 35.88, 34.57, 33.24, 29.95, 28.81, 28.40, 26.27, 25.92, 18.68. HRMS (ESI): calculated for  $\text{C}_{46}\text{H}_{79}\text{N}_5\text{O}_{19}\text{S}$   $[\text{M} + \text{H}]^+$  1038.5168, found 1038.5146.

Compound **27**<sup>119, 120</sup>

Compound **21** was first synthesized with a similar procedure as compound **20**. To a solution of kanamycin (free base, 0.243g, 0.5 mmol) in  $\text{H}_2\text{O}$  (25 mL) was added a solution of **21** (0.185 g, 0.5 mmol) in acetone (25 mL) dropwise at 15 °C. The reaction was stirred at room temperature for 1 h to produce compound **26** (not isolated).  $\text{Boc}_2\text{O}$  (0.437 g, 2 mmol) was then added and the reaction was stirred for 48 h. The precipitate was collected by filtration and purified by column chromatography (MeOH:  $\text{CHCl}_3$ :  $\text{NH}_3 \cdot \text{H}_2\text{O}$  = 1:4:0.1) to give **27** as a white solid (0.240 g, 49%).  $R_f$  = 0.4 (MeOH: DCM:  $\text{NH}_3 \cdot \text{H}_2\text{O}$  = 1:5:0.1).  $^1\text{H}$  NMR (300 MHz, DMSO and  $\text{D}_2\text{O}$ ,  $\delta$ ) 7.54 (br, 1H), 7.48 (br, 1H), 7.36 (m, 5H), 6.90 (br, 1), 6.54 (d,  $J$  = 4.8 Hz, 1H), 6.50 (d,  $J$  = 5.4 Hz, 1H), 5.03 (s, 2H), 4.94 (s, 1H), 4.91 (s, 1H), 3.80 (br, 1H), 3.67 (m, 2H), 3.60 (m, 1H), 3.50 (m, 2H), 3.47-3.21 (m, 12H), 3.04 (m, 1H), 1.79 (br, 1H), 1.35 (m, 27H), 1.23 (m, 1H).  $^{13}\text{C}$  NMR (75 MHz, DMSO and  $\text{D}_2\text{O}$ ,  $\delta$ ): 170.11, 156.85, 156.75, 155.71, 155.29, 137.19, 128.68, 128.15, 127.99, 101.19, 98.07, 84.04, 80.48, 78.35, 78.31, 77.71, 75.25, 73.15, 72.77, 72.27, 70.44, 70.34, 70.19, 67.57, 65.86, 60.49, 56.03, 50.31, 49.26, 43.59, 40.94, 29.29, 28.59, 28.48, 28.42. HRMS (ESI): calculated for  $\text{C}_{43}\text{H}_{69}\text{N}_5\text{O}_{20}$   $[\text{M} + \text{H}]^+$  976.4614, found 976.4660.

### Compound **28**

To a suspension of **27** (0.2g, 0.2 mmol) in MeOH (20 mL) was added Pd/C (10%, 0.05g). The mixture was stirred under H<sub>2</sub> atmosphere (30 psi) for 4 h. The Pd/C was filtered away and the solvents were evaporated in vacuum. The residue was purified by column chromatography (MeOH: CHCl<sub>3</sub>: NH<sub>3</sub>·H<sub>2</sub>O = 1:1:0.1) to give the product as a white solid (56 mg, 34%). R<sub>f</sub> = 0.2 (MeOH: DCM: NH<sub>3</sub>·H<sub>2</sub>O = 1:1:0.1). <sup>1</sup>H NMR (300 MHz, DMSO, δ) 7.77 (br, 1H), 6.92 (br, 1H), 6.61 (br, 1H), 6.51 (br, 1H), 4.91 (br, 2H), 4.23 (br, 1H), 3.80 (br, 1H), 3.63 (br, 1H), 3.50 (m, 6H), 3.35 (m, 5H), 3.24 (m, 3H), 3.03 (m, 2H), 1.79 (br, 1H), 1.38 (m, 27H), 1.23 (br, 1H). <sup>13</sup>C NMR (75 MHz, DMSO, δ): 172.45, 156.38, 155.37, 154.94, 101.16, 97.75, 84.16, 80.22, 77.87, 77.24, 74.99, 72.95, 72.78, 72.29, 70.34, 70.24, 70.10, 70.00, 67.35, 60.25, 55.90, 50.04, 49.02, 43.83, 34.79, 28.36, 28.25, 28.19. HRMS (ESI): calculated for C<sub>35</sub>H<sub>63</sub>N<sub>5</sub>O<sub>18</sub> [M + H]<sup>+</sup> 842.4246, found 842.4245.

### Compound **29**

Following the procedure for the synthesis of **25**, Compound **28** (56 mg, 0.067 mmol), TEA (60 μL) and compound **20** (50 mg, 0.24 mmol), were used to give **29** (61 mg, 95%) as a white solid. R<sub>f</sub> = 0.2 (DCM: MeOH: NH<sub>3</sub>·H<sub>2</sub>O = 5:1:0.1). <sup>1</sup>H NMR (300 MHz, DMSO, δ) 8.14 (br, 1H), 7.53 (br, 1H), 6.92 (br, 1H), 6.58 (br, 1H), 6.52 (br, 1H), 4.97 (br, 1H), 4.92 (br, 1H), 4.23 (br, 1H), 3.80 (m, 2H), 3.62 (m, 1H), 3.50 (m, 1H), 3.35-3.22 (m, 13H), 3.05 (br, 1H), 2.78 (s, 1H), 2.23 (br, 2H), 2.16 (br, 2H), 1.78 (br, 1H), 1.67 (br, 2H), 1.38 (m, 27H), 1.09 (br, 1H). <sup>13</sup>C NMR (75 MHz, DMSO, δ): 172.09, 169.67, 156.39, 155.407, 154.95, 101.11,

97.79, 84.12, 80.26, 77.92, 77.26, 75.07, 72.96, 72.69, 72.19, 71.50, 70.36, 70.12, 67.37, 64.96, 60.29, 55.93, 50.09, 48.98, 45.67, 42.04, 34.82, 33.97, 28.37, 28.25, 28.20, 24.28, 17.39, 15.21. HRMS (ESI): calculated for  $C_{41}H_{69}N_5O_{19}$   $[M + Na]^+$  958.4484, found 958.4487.

### Compound **32**

To a solution of **31** (0.15 g, 0.48 mmol) (synthesized following a reported method<sup>121</sup> and characterized by  $^1H$  NMR) in DMF (5 mL) was added 6-azidohexanoic (0.076g, 0.48 mmol), EDCI·HCl (0.10g, 0.528 mmol), HOBt (0.072 g, 0.528 mmol) and TEA (0.097 mg, 0.96 mmol). The reaction was stirred at room temperature for overnight. The mixture was partitioned between water (20 mL) and EA (20 mL). The aqueous phase was separated and extracted with EA (2 × 20 mL). The combined organic phase was dried with  $Na_2SO_4$  and filtered. After removing the solvents, the residue was purified by column chromatography (MeOH: DCM = 1:25) to give **32** as a yellow solid (0.20 g, 90%).  $R_f$  = 0.4 (5% MeOH in DCM).  $^1H$  NMR (300 MHz,  $CDCl_3$ ,  $\delta$ ) 8.57 (d,  $J$  = 7.5 Hz, 1H), 8.42 (d,  $J$  = 8.4 Hz, 1H), 8.22 (d,  $J$  = 8.4 Hz, 1H), 7.65 (t,  $J$  = 7.5 Hz, 1H), 7.15 (s, 1H), 6.54 (d,  $J$  = 8.4 Hz, 1H), 6.17 (t,  $J$  = 6.0 Hz, 1H), 4.16 (t,  $J$  = 7.5 Hz, 2H), 3.77 (m, 2H), 3.48 (m, 2H), 3.13 (t,  $J$  = 6.6 Hz, 2H), 2.30 (t,  $J$  = 7.5 Hz, 2H), 1.73 (m, 4H), 1.55 (m, 2H), 1.48 (m, 2H), 1.42 (m, 2H), 0.95 (t,  $J$  = 7.5 Hz, 3H).  $^{13}C$  NMR (75 MHz,  $CDCl_3$ ,  $\delta$ ): 176.15, 164.55, 164.12, 150.12, 134.21, 130.87, 129.45, 127.20, 124.55, 122.28, 120.04, 109.05, 103.06, 50.98, 46.21, 39.83, 38.60, 36.08, 30.23, 28.43, 26.18, 25.17, 20.34, 13.81. HRMS (ESI): calculated for  $C_{24}H_{30}N_6O_3$   $[M + H]^+$  451.2458, found 451.2464.

*General procedure for the synthesis of **KOF** and **KNF***

*Procedure A.* To a solution of kanamycin alkyne (1 equiv) in DMSO (280  $\mu$ L) and H<sub>2</sub>O (40  $\mu$ L) was added **32** (1 equiv), CuSO<sub>4</sub> (0.1 equiv) and sodium ascorbate (0.2 equiv). The reaction was stirred at room temperature for overnight. The crude product was extracted with ethyl acetate and purified by chromatography on a silica gel column using a DCM/MeOH mixture to give the Boc protected conjugates.

*Procedure B.* The Boc protected conjugates was treated with TFA (1 mL) and DCM (1 mL) for 24 h. The solvent and TFA were removed under reduced pressure. The residue was purified by precipitation from a solution in MeOH by Et<sub>2</sub>O (repeat 5 times), leading to the final product as solids (TFA salts).

**KOF.** General procedure A was employed for the reaction between **25** (10 mg, 0.01 mmol) and compound **32** (4.3 mg, 0.01 mmol), leading to the Boc protected **KOF** as a yellow solid (8 mg, 52%). <sup>1</sup>H NMR (300 MHz, DMSO,  $\delta$ ) 8.61 (d,  $J$  = 8.7 Hz, 1H), 8.44 (d,  $J$  = 7.2 Hz, 1H), 8.26 (d,  $J$  = 8.7 Hz, 1H), 8.10 (br, 1H), 7.90 (br, 1H), 7.85 (br, 1H), 7.81 (s, 1H), 7.70 (t,  $J$  = 7.5 Hz, 1H), 6.93 (br, 1H), 6.83 (d,  $J$  = 8.7 Hz, 1H), 6.62 (br, 1H), 6.53 (d,  $J$  = 8.7 Hz, 1H), 6.37 (br, 1H), 5.48 (s, 1H), 5.26 (s, 1H), 4.22 (t,  $J$  = 7.5 Hz, 2H), 4.14 (m, 1H), 4.01 (t,  $J$  = 7.5 Hz, 2H), 3.60-3.10 (m, 13H), 2.57 (m, 4H), 2.08 (m, 4H), 1.77 (m, 5H), 1.55 (m, 4H), 1.37 (m, 36H), 1.25 (m, 5H), 0.93 (t,  $J$  = 7.5 Hz, 3H). HRMS (ESI): calculated for C<sub>70</sub>H<sub>109</sub>N<sub>11</sub>O<sub>22</sub>S [M + Na]<sup>+</sup> 1510.7367, found 1510.7410. General procedure B was further applied to remove Boc and give **KOF** as a yellow solid (8.2 mg, 97%). <sup>1</sup>H NMR (300 MHz, D<sub>2</sub>O,  $\delta$ ) 7.98 (d,  $J$  = 7.5 Hz, 1H), 7.82 (d,  $J$  = 7.8 Hz, 1H),

7.77 (d,  $J = 8.7$  Hz, 1H), 7.31 (t,  $J = 7.8$  Hz, 1H), 7.21 (s, 1H), 6.41 (d,  $J = 8.7$  Hz, 1H), 5.51 (d,  $J = 3.6$  Hz, 1H), 5.01 (d,  $J = 3.3$  Hz, 1H), 3.92 (m, 2H), 3.85 (m, 2H), 3.69 (m, 4H), 3.61-3.32 (m, 9H), 3.27 (m, 2H), 3.17 (m, 2H), 2.95 (m, 1H), 2.63 (m, 2H), 2.47 (m, 2H), 2.11 (m, 4H), 1.84 (m, 1H), 1.71 (br, 2H), 1.26 (br, 7H), 0.85 (t,  $J = 7.5$  Hz, 3H). HRMS (ESI): calculated for  $C_{50}H_{77}N_{11}O_{14}S$   $[M + H]^+$  1088.5450, found 1088.5485.

**KNF** General procedure A was employed for the reaction between **29** (10 mg, 0.01 mmol) and compound **32** (4.3 mg, 0.01 mmol), leading to the Boc protected **KNF** as a yellow solid (10 mg, 72%).  $^1H$  NMR (300 MHz, DMSO,  $\delta$ ) 8.58 (d,  $J = 5.4$  Hz, 1H), 8.44 (d,  $J = 5.1$  Hz, 1H), 8.26 (d,  $J = 8.4$  Hz, 1H), 8.10 (br, 2H), 7.85 (s, 1H), 7.81 (s, 1H), 7.70 (m, 1H), 7.58 (s, 1H), 6.92 (m, 1H), 6.84 (d,  $J = 8.1$  Hz, 1H), 6.59 (m, 2H), 5.39 (s, 1H), 5.22 (s, 1H), 5.0-2.3 (very poor resolution), 2.17 (m, 2H), 2.08 (m, 2H), 1.77 (m, 5H), 1.55 (m, 4H), 1.35 (m, 28H), 0.91 (t,  $J = 7.5$  Hz, 3H). HRMS (ESI): calculated for  $C_{65}H_{99}N_{11}O_{22}$   $[M + Na]^+$  1408.6864, found 1408.6891. General procedure B was applied to remove Boc and give **KNF** as a yellow solid (9.9 mg, 98%).  $^1H$  NMR (300 MHz,  $D_2O$ ,  $\delta$ ) 7.88 (d,  $J = 6.0$  Hz, 1H), 7.72 (d,  $J = 6.9$  Hz, 1H), 7.68 (d,  $J = 7.5$  Hz, 1H), 7.27 (s, 1H), 7.24 (d,  $J = 8.7$  Hz, 1H), 6.33 (d,  $J = 6.0$  Hz, 1H), 5.40 (d,  $J = 3.6$  Hz, 1H), 5.05 (d,  $J = 3.6$  Hz, 1H), 3.93 (m, 3H), 3.75 (m, 7H), 3.68 (m, 7H), 3.55 (m, 7H), 3.46 (m, 3H), 3.25 (t,  $J = 9.3$  Hz, 1H), 2.48 (br, 3H), 2.20 (m, 2H), 2.18 (m, 2H), 1.92 (m, 1H), 1.76 (br, 2H), 1.41 (br, 5H), 1.32 (m, 4H), 0.91 (t,  $J = 7.2$  Hz, 3H). HRMS (ESI): calculated for  $C_{50}H_{75}N_{11}O_{16}$   $[M + H]^+$  1086.5472, found 1086.5488.

### *Synthesis of NF*

Compound **35** was prepared according to a reference method.<sup>104</sup>

#### Compound **36**

To a solution of **35** (200 mg, 0.157 mmol) in DCM (2 mL) was added 6-azidohexanoic (30 mg, 0.188 mmol), *N*-(3-Dimethylaminopropyl)-*N*-ethylcarbodiimide hydrochloride (36 mg, 0.188 mmol) and *N,N*-diisopropylethylamine (49 mg, 0.377 mmol). The reaction was stirred at room temperature for overnight. The mixture was partitioned between water (50 mL) and ethyl acetate (50 mL). The aqueous phase was separated and extracted with ethyl acetate (2 × 50 mL). The combined organic phase was washed with brine (3 X 50 mL) and dried over Na<sub>2</sub>SO<sub>4</sub>. After removing the solvents, the residue was purified by column chromatography (4.5% MeOH in DCM) to give **36** as a white solid (96 mg, 43%). R<sub>f</sub> = 0.5 (10% MeOH in DCM). <sup>1</sup>H NMR (300 MHz, CD<sub>3</sub>OD, δ) 5.38 (s, 1H), 5.15 (s, 1H), 4.94 (s, 1H), 4.61 (s, 1H), 4.25 (br, 2H), 4.09 (m, 1H), 3.90 (m, 2H), 3.77 (s, 1H), 3.71 (m, 1H), 3.59 (m, 3H), 3.48 (m, 4H), 3.43 (m, 3H), 3.21 (m, 2H), 2.89 (d, *J* = 5.4 Hz, 2H), 2.76 (t, *J* = 6.6 Hz, 2H), 2.24 (t, *J* = 7.5 Hz, 2H), 1.94 (m, 1H), 1.66 (m, 4H), 1.45 (m, 61H). <sup>13</sup>C NMR (75 MHz, CD<sub>3</sub>OD, δ): 176.05, 159.08, 158.87, 158.49, 158.19, 158.15, 157.87, 111.09, 100.52, 99.14, 87.03, 82.71, 81.54, 80.74, 80.67, 80.58, 80.38, 80.22, 79.93, 75.63, 75.29, 74.47, 73.28, 72.86, 71.58, 68.86, 56.85, 53.60, 52.33, 51.45, 42.57, 41.75, 40.14, 36.94, 35.92, 35.56, 32.83, 29.65, 29.01, 28.88, 28.85, 28.77, 27.40, 26.52. HRMS (ESI): calculated for C<sub>61</sub>H<sub>109</sub>N<sub>10</sub>O<sub>25</sub>S [M + H]<sup>+</sup> 1413.7286, found 1413.7264.

Compound **37** was prepared according to a reference method.<sup>122</sup>

**NF**. A similar procedure as the synthesis of **KOF** was employed for the reaction between **37** (10 mg, 7.3  $\mu$ mol) and compound **32** (4.0 mg, 7.3  $\mu$ mol), leading to the Boc protected **NF** as a yellow solid (12 mg, 90%).  $^1\text{H}$  NMR (300 MHz, MeOD,  $\delta$ ) 8.48 (d,  $J = 7.2$  Hz, 1H), 8.42 (d,  $J = 8.4$  Hz, 1H), 8.33 (d,  $J = 8.4$  Hz, 1H), 7.70 (s, 1H), 7.65 (t,  $J = 8.1$  Hz, 1H), 6.82 (d,  $J = 8.7$  Hz, 1H), 5.37 (s, 1H), 5.15 (s, 1H), 4.93 (s, 1H), 4.24 (m, 4H), 4.12 (m, 3H), 3.90 (br, 2H), 3.76 (br, 2H), 3.59 (m, 8H), 3.48 (m, 4H), 3.39 (m, 4H), 3.31 (m, 1H), 2.90 (m, 2H), 2.74 (m, 4H), 2.22 (m, 4H), 1.95 (m, 3H), 1.85 (m, 2H), 1.63 (m, 6H), 1.45 (m, 54H), 1.28 (m, 5H), 0.96 (t,  $J = 7.5$  Hz, 3H). HRMS (ESI): calculated for  $\text{C}_{85}\text{H}_{135}\text{N}_{13}\text{O}_{28}\text{S}$  [ $\text{M} + \text{Na}$ ] $^+$  1840.9158, found 1840.9204. The Boc was then removed by TFA to give **NF** as a yellow solid (11 mg, 82%).  $^1\text{H}$  NMR (300 MHz,  $\text{D}_2\text{O}$ ,  $\delta$ ) 7.98 (d,  $J = 7.5$  Hz, 1H), 7.82 (d,  $J = 8.1$  Hz, 1H), 7.79 (d,  $J = 8.7$  Hz, 1H), 7.30 (t,  $J = 8.1$  Hz, 1H), 7.28 (s, 1H), 6.40 (d,  $J = 8.7$  Hz, 1H), 6.04 (d,  $J = 3.9$  Hz, 1H), 5.39 (s, 1H), 5.28 (s, 1H), 4.39 (s, 2H), 4.31 (m, 2H), 4.23 (m, 1H), 4.01 (m, 2H), 3.90 (m, 3H), 3.77 (m, 3H), 3.65 (m, 3H), 3.55 (m, 5H), 3.49-3.29 (m, 12H), 3.12 (m, 1H), 2.71 (m, 1H), 2.49 (m, 3H), 2.14 (m, 4H), 1.91 (m, 1H), 1.78 (m, 2H), 1.42 (m, 4H), 1.39 (m, 5H), 0.92 (t,  $J = 7.2$  Hz, 3H). HRMS (ESI): calculated for  $\text{C}_{55}\text{H}_{87}\text{N}_{13}\text{O}_{16}\text{S}$  [ $\text{M} + 2\text{H}$ ] $^{2+}$  1219.6271, found 1219.6224.

### *Synthesis of bifunctional inhibitors*

#### Compound **40**

To a stirred solution of 2-(carboxymethyl)-5-hydroxybenzoic acid (**39**) (1.00 g) in MeOH (50 mL) was added sulfuric acid (200  $\mu$ L) dropwise. The mixture was refluxed for 4 h. The solvents were removed by vacuum and the residue was partitioned between water (50 mL) and ethyl acetate (50 mL). The organic phase

was washed with water (2 X 50 mL) and dried over Na<sub>2</sub>SO<sub>4</sub>. The solid was removed by filtration. The filtrate was vacuumed to remove the solvent. The crude product was purified by chromatography (Hexane/Ethyl Acetate: 1/1) to give **40** as a yellow oil (0.98 g, 86%). <sup>1</sup>H NMR (300 MHz, DMSO): δ (ppm) 9.76 (s, 1H), 7.31 (d, *J* = 2.7 Hz, 1H), 7.16 (d, *J* = 8.4 Hz, 1H), 6.92 (dd, *J* = 8.4 Hz, 2.7 Hz, 1H), 3.84 (s, 2H), 3.75 (s, 3H), 3.57 (s, 3H).

#### Compound **41A**

To a stirred solution of **40** (200 mg, 0.89 mmol) in DMF (5 mL) was added K<sub>2</sub>CO<sub>3</sub> (370 mg) and propargyl bromide (400 mg, 80% in toluene, 2.68 mmol). The reaction was stirred overnight at 70 °C. Water (50 mL) was added. The mixture was extracted with ethyl acetate (2 X 50 mL). The combined organic phase was washed with brine (3 X 50 mL) and dried over Na<sub>2</sub>SO<sub>4</sub>. The solid was filtered off. The filtrate was vacuumed to remove the solvent. The residue was further purified by chromatography (Hexane/Ethyl Acetate: 5/1) to give **41A** as a yellow oil (0.195 g, yield 83%). <sup>1</sup>H NMR (300 MHz, MeOD): δ (ppm) 7.59 (d, *J* = 2.7 Hz, 1H), 7.24 (d, *J* = 8.4 Hz, 1H), 7.15 (dd, *J* = 8.4 Hz, 2.7 Hz, 1H), 4.77 (d, *J* = 2.4 Hz, 2H), 3.94 (s, 2H), 3.84 (s, 3H), 3.66 (s, 3H), 2.97 (t, *J* = 2.4 Hz, 1H). <sup>13</sup>C NMR (75 MHz, MeOD): δ (ppm) 174.2, 168.6, 158.1, 134.6, 131.8, 130.1, 120.0, 118.1, 79.4, 77.2, 56.8, 52.5, 52.3, 40.3. HRMS (ESI) *m/z* [M + Na]<sup>+</sup> 285.0731, calculated for C<sub>14</sub>H<sub>14</sub>O<sub>5</sub>Na 285.0739.

#### General method for compound **41B-D**

To a stirred solution of **40** (1.1 eq) in THF was added appropriate alcohol (1 eq) and triphenylphosphine (1.1 eq). The mixture was cooled to 5 °C with ice bath. Diisopropyl azodicarboxylate (1.1 eq) was then added dropwise to maintain the

temperature below 5 °C. The reaction was allowed to warm to room temperature and stirred overnight. The solvents were removed by vacuum. The resulting residue was dissolved in ethyl acetate (50 mL) and washed with saturated sodium carbonate solution (3 X 50 mL). The organic phase was then dried, concentrated and purified by chromatography (hexane/ethyl acetate). The crude product (containing diisopropyl-1, 2-hydrazinedicarboxylate) was used for next step reaction without further purification and characterization.

*General method for compound **42A-C***

To a solution of **41** (1 eq) in methanol (5 mL) was added water (5 mL) and LiOH·H<sub>2</sub>O (4 eq). The reaction was stirred overnight at room temperature. The solvents were removed by vacuum. The residue was dissolved in water (10 mL). Concentrated HCl (2 mL) was added to adjust the pH to 1, resulting in white precipitation. The solid was collected by filtration and dried to give the product as a white solid.

**Compound 42A**

290 mg of **41A** was used to produce 187 mg of **42A** (white solid, yield 72%). <sup>1</sup>H NMR (300 MHz, MeOD): δ (ppm) 7.63 (d, *J* = 2.7 Hz, 1H), 7.23 (d, *J* = 8.4 Hz, 1H), 7.14 (dd, *J* = 8.4 Hz, 3.0 Hz, 1H), 4.77 (d, *J* = 2.4 Hz, 2H), 3.95 (s, 2H), 2.96 (t, *J* = 2.4 Hz, 1H). <sup>13</sup>C NMR (75 MHz, MeOD): δ (ppm) 175.8, 170.0, 157.9, 134.5, 132.4, 130.7, 119.8, 118.4, 79.5, 77.1, 56.8, 40.4. HRMS (ESI) *m/z* [M - H]<sup>-</sup> 233.0451, calculated for C<sub>12</sub>H<sub>9</sub>O<sub>5</sub> 233.0450.

**Compound 42B**

340 mg of **41B** was used to produce 111 mg of **42B** (off white solid, 40% total yield from **40**). <sup>1</sup>H NMR (300 MHz, MeOD): δ (ppm) 7.58 (d, *J* = 2.7 Hz, 1H), 7.22

(d,  $J = 8.4$  Hz, 1H), 7.10 (dd,  $J = 8.7$  Hz, 2.7 Hz, 1H), 4.25 (d,  $J = 2.4$  Hz, 2H), 4.18 (m, 2H), 3.94 (s, 2H), 3.89 (m, 2H), 2.88 (t,  $J = 2.4$  Hz, 1H).  $^{13}\text{C}$  NMR (75 MHz, MeOD):  $\delta$  (ppm) 175.9, 170.2, 159.1, 134.6, 132.5, 130.2, 119.6, 117.9, 80.4, 76.1, 69.3, 68.6, 59.2, 40.4. HRMS (ESI)  $m/z$   $[\text{M} - \text{H}]^-$  277.0705, calculated for  $\text{C}_{14}\text{H}_{13}\text{O}_6$  277.0712.

#### Compound **42C**

330 mg of **41C** was used to produce 160 mg of **42C** (white solid, 50% total yield from **40**).  $^1\text{H}$  NMR (300 MHz, MeOD):  $\delta$  (ppm) 7.58 (d,  $J = 3.0$  Hz, 1H), 7.21 (d,  $J = 8.4$  Hz, 1H), 7.10 (dd,  $J = 8.4$  Hz, 2.7 Hz, 1H), 4.19 (m, 4H), 3.94 (s, 2H), 3.86 (m, 2H), 3.70 (m, 4H), 2.84 (t,  $J = 2.4$  Hz, 1H).  $^{13}\text{C}$  NMR (75 MHz, MeOD):  $\delta$  (ppm) 175.9, 170.2, 159.2, 134.6, 132.4, 130.1, 119.6, 118.0, 80.5, 75.9, 71.5, 70.7, 70.1, 68.8, 59.0, 40.4. HRMS (ESI)  $m/z$   $[\text{M} - \text{H}]^-$  321.0969, calculated for  $\text{C}_{16}\text{H}_{17}\text{O}_7$  321.0974.

#### Compound **42D**

To a solution of **41D** (330 mg) in methanol (5 mL) was added  $\text{LiOH}\cdot\text{H}_2\text{O}$  (233 mg) and water (3 mL). The reaction was stirred overnight at room temperature. The solvents were removed by vacuum. The residue was dissolved in water (10 mL). Concentrated HCl (2 mL) was added to adjust the pH to 1. The mixture was then extracted with ethyl acetate (2 X 10 mL). The combined organic phase was washed with brine (2 X 10 mL), dried and concentrated to give **42D** as colorless oil (244 mg, 67% total yield from **40**).  $^1\text{H}$  NMR (300 MHz, MeOD):  $\delta$  (ppm) 7.58 (d,  $J = 2.7$  Hz, 1H), 7.22 (d,  $J = 8.4$  Hz, 1H), 7.10 (dd,  $J = 8.4$  Hz, 2.7 Hz, 1H), 4.17 (m, 4H), 3.94 (s, 2H), 3.86 (m, 2H), 3.71 (m, 2H), 3.65 (m, 6H), 2.83 (t,  $J = 2.4$  Hz, 1H).  $^{13}\text{C}$  NMR (75 MHz, MeOD):  $\delta$  (ppm) 175.9, 170.1, 159.2, 134.6, 132.4,

130.1, 119.6, 118.0, 80.6, 75.9, 71.7, 71.5, 71.4, 70.8, 70.1, 68.8, 59.0, 40.4.

HRMS (ESI)  $m/z$   $[M - H]^-$  365.1232, calculated for  $C_{18}H_{21}O_8$  365.1236.

#### *General method for Compound 43*

A solution of **42** (1 eq) and *O*-(4-Methoxybenzyl)-hydroxylamine (1.2 eq) in toluene (180 mL) was refluxed using a Dean-Stark apparatus overnight. The solvent was removed by vacuum and the residue was purified by column chromatography.

#### Compound **43A**

**42A** (187 mg) was used to give **43A** (174 mg) as a white solid. Elution solvent: Hexane/Ethyl acetate 2/1; yield 62%.  $^1H$  NMR (300 MHz,  $CDCl_3$ ):  $\delta$  (ppm) 7.76 (d,  $J = 2.1$  Hz, 1H), 7.52 (d,  $J = 8.7$  Hz, 2H), 7.22 (m, 2H), 6.90 (d,  $J = 8.7$  Hz, 2H), 5.08 (s, 2H), 4.77 (d,  $J = 2.1$  Hz, 2H), 4.07 (s, 2H), 3.81 (s, 3H), 2.56 (t,  $J = 2.4$  Hz, 1H).  $^{13}C$  NMR (75 MHz,  $CDCl_3$ ):  $\delta$  (ppm) 166.0, 161.5, 160.4, 157.2, 131.8, 128.9, 126.4, 126.2, 122.9, 114.0, 112.8, 78.1, 77.8, 76.4, 56.3, 55.4, 37.0. HRMS (ESI)  $m/z$   $[M + Na]^+$  374.1008, calculated for  $C_{20}H_{17}NNaO_5$  374.1004.

#### Compound **43B**

**42B** (111 mg) was used to give **43B** (92 mg) as a white solid. Elution solvent: Hexane/Ethyl acetate 2/1; yield 58%.  $^1H$  NMR (300 MHz,  $CDCl_3$ ):  $\delta$  (ppm) 7.67 (d,  $J = 2.4$  Hz, 1H), 7.51 (d,  $J = 8.7$  Hz, 2H), 7.20 (m, 2H), 6.90 (d,  $J = 8.4$  Hz, 2H), 5.07 (s, 2H), 4.28 (d,  $J = 2.1$  Hz, 2H), 4.23 (t,  $J = 4.5$  Hz, 2H), 4.05 (s, 2H), 3.93 (t,  $J = 4.5$  Hz, 2H), 3.81 (s, 3H), 2.48 (t,  $J = 2.1$  Hz, 1H).  $^{13}C$  NMR (75 MHz,  $CDCl_3$ ):  $\delta$  (ppm) 166.1, 161.6, 160.4, 158.5, 131.8, 128.8, 126.4, 126.2, 125.9, 123.0, 114.0, 112.0, 79.4, 78.2, 75.1, 68.1, 67.8, 58.8, 55.4, 37.1. HRMS (ESI)  $m/z$   $[M + Na]^+$  418.1259, calculated for  $C_{22}H_{21}NNaO_6$  418.1267.

### Compound **43C**

**42C** (160 mg) was used to give **43C** (141 mg) as a white solid. Elution solvent: Hexane/Ethyl acetate 1/1; yield 65%.  $^1\text{H}$  NMR (300 MHz,  $\text{CDCl}_3$ ):  $\delta$  (ppm) 7.67 (d,  $J = 2.4$  Hz, 1H), 7.52 (d,  $J = 8.4$  Hz, 2H), 7.21 (m, 2H), 6.90 (d,  $J = 8.7$  Hz, 2H), 5.07 (s, 2H), 4.21 (m, 4H), 4.05 (s, 2H), 3.90 (t,  $J = 4.5$  Hz, 2H), 3.81 (s, 3H), 3.75 (m, 4H), 2.44 (t,  $J = 2.4$  Hz, 1H).  $^{13}\text{C}$  NMR (75 MHz,  $\text{CDCl}_3$ ):  $\delta$  (ppm) 166.1, 161.6, 160.4, 158.5, 131.8, 128.7, 126.3, 126.2, 125.7, 122.9, 113.9, 112.1, 79.7, 78.1, 74.8, 70.8, 69.7, 69.2, 68.0, 58.6, 55.4, 37.0. HRMS (ESI)  $m/z$   $[\text{M} + \text{Na}]^+$  462.1531, calculated for  $\text{C}_{24}\text{H}_{25}\text{NNaO}_7$  462.1529.

### Compound **43D**

**42D** (244 mg) was used to give **43D** (210 mg) as a white solid. Elution solvent: Hexane/Ethyl acetate 3/4; yield 65%.  $^1\text{H}$  NMR (300 MHz,  $\text{CDCl}_3$ ):  $\delta$  (ppm) 7.67 (d,  $J = 2.4$  Hz, 1H), 7.53 (dd,  $J = 6.6$  Hz, 2.1 Hz, 2H), 7.19 (m, 2H), 6.90 (dd,  $J = 6.6$  Hz, 2.1 Hz, 2H), 5.07 (s, 2H), 4.21 (m, 4H), 4.05 (s, 2H), 3.90 (t,  $J = 4.8$  Hz, 2H), 3.81 (s, 3H), 3.76 (m, 2H), 3.68 (m, 6H), 2.43 (t,  $J = 2.1$  Hz, 1H).  $^{13}\text{C}$  NMR (75 MHz,  $\text{CDCl}_3$ ):  $\delta$  (ppm) 166.1, 161.6, 160.4, 158.6, 131.8, 128.7, 126.3, 126.2, 125.7, 122.9, 113.9, 112.1, 79.8, 78.1, 74.7, 71.0, 70.8, 70.6, 69.7, 69.2, 68.0, 58.5, 55.4, 37.0. HRMS (ESI)  $m/z$   $[\text{M} + \text{Na}]^+$  506.1773, calculated for  $\text{C}_{26}\text{H}_{29}\text{NNaO}_8$  506.1791.

### Compound **44**

To a stirred solution of **43A** (27 mg, 0.077 mmol) in DCM (1.5 mL) was added TFA (1.5 mL). The reaction turned to dark red after 4 h. The solvents were removed by vacuum. The residue was washed with ether (3 X 1.5 mL) to give **44** as a white solid (15 mg, yield 81%).  $^1\text{H}$  NMR (300 MHz, DMSO):  $\delta$  (ppm) 10.39

(s, 1H), 7.57 (d,  $J = 2.4$  Hz, 1H), 7.31 (m, 2H), 4.90 (d,  $J = 2.1$  Hz, 2H), 4.18 (s, 2H), 3.60 (t,  $J = 2.1$  Hz, 1H).  $^{13}\text{C}$  NMR (75 MHz, DMSO):  $\delta$  (ppm) 166.4, 161.5, 156.2, 129.1, 127.5, 126.0, 121.7, 111.9, 78.8, 78.7, 55.7, 36.2. HRMS (ESI)  $m/z$   $[\text{M} + \text{H}]^+$  232.0616, calculated for  $\text{C}_{12}\text{H}_{10}\text{NO}_4$  232.0610.

#### *General method for compound 45*

To a solution of **36** (1 eq) in DMSO/ $\text{H}_2\text{O}$  (400  $\mu\text{L}$ /40  $\mu\text{L}$ ) was added **43** (1.2 eq), sodium ascorbate (0.4 eq) and  $\text{CuSO}_4$  (0.2 eq). The reaction was stirred at room temperature for 1 h. Water (5 mL) was added and the mixture was extracted with ethyl acetate (3 X 10 mL). The combined organic phase was washed with brine (3 X 10 mL), dried and concentrated. The residue was purified by preparative thin layer chromatography (Prep-TLC), leading to a white solid. The solid was then dissolved in a mixture of TFA and DCM (1 mL/1 mL). After being stirred overnight, the reaction was vacuumed to remove the solvents. The residue was purified by HPLC to give the final product.

#### Compound **45A**

Solvent for Prep-TLC: 6% methanol in DCM. **36** (25 mg) was used to give **45A** (12 mg) as a white solid, yield 40%, keto form (100%),  $t_{\text{R}}$  6.2 min (analytical HPLC method).  $^1\text{H}$  NMR (300 MHz,  $\text{D}_2\text{O}$ ):  $\delta$  (ppm) 8.09 (s, 1H), 7.68 (d,  $J = 1.5$  Hz, 1H), 7.36 (m, 2H), 6.04 (d,  $J = 3.6$  Hz, 1H), 5.37 (d,  $J = 3.3$  Hz, 1H), 5.33 (s, 2H), 5.27 (s, 1H), 4.42 (t,  $J = 6.0$  Hz, 2H), 4.37 (d,  $J = 5.4$  Hz, 1H), 4.33 (m, 3H), 4.21 (s, 1H), 4.10 (m, 1H), 4.00 (m, 1H), 3.92 (m, 2H), 3.82 (s, 1H), 3.75 (m, 2H), 3.58 (s, 2H), 3.48-3.55 (m, 4H), 3.38 (m, 3H), 3.27 (m, 3H), 3.09 (m, 1H), 2.75 (m, 1H), 2.62 (m, 2H), 2.49 (m, 1H), 2.11 (t,  $J = 7.2$  Hz, 2H), 1.87 (m, 3H), 1.49 (m,

2H), 1.10 (m, 2H). HRMS (ESI)  $m/z$   $[M + H]^+$  1044.4653, calculated for  $C_{43}H_{70}N_{11}O_{17}S$  1044.4672.

#### Compound **45B**

Solvent for Prep-TLC: 6% methanol in DCM. **36** (50 mg) was used to give **45B** (23 mg) as a white solid, yield 37%, keto form (100%),  $t_R$  6.7 min (analytical HPLC method).  $^1H$  NMR (300 MHz,  $D_2O$ ):  $\delta$  (ppm) 7.97 (s, 1H), 7.55 (d,  $J = 2.7$  Hz, 1H), 7.31 (d,  $J = 8.4$  Hz, 1H), 7.25 (dd,  $J = 8.4$  Hz, 2.7 Hz, 1H), 6.03 (d,  $J = 4.2$  Hz, 1H), 5.37 (d,  $J = 3.0$  Hz, 1H), 5.27 (s, 1H), 4.71 (m, 3H), 4.35 (m, 4H), 4.27 (m, 2H), 4.23 (m, 2H), 4.19 (m, 1H), 4.08 (m, 1H), 3.99 (m, 1H), 3.89 (m, 4H), 3.80 (s, 1H), 3.67 (m, 1H), 3.28-3.57 (m, 12H), 3.10 (m, 1H), 2.70 (m, 1H), 2.64 (m, 2H), 2.48 (m, 1H), 2.12 (t,  $J = 7.2$  Hz, 2H), 1.82 (m, 3H), 1.49 (m, 2H), 1.13 (m, 2H). HRMS (ESI)  $m/z$   $[M + H]^+$  1088.4969, calculated for  $C_{45}H_{74}N_{11}O_{18}S$  1088.4934.

#### Compound **45C**

Solvent for Prep-TLC: 6.5% methanol in DCM. **36** (40 mg) was used to give **45C** (11 mg) as a white solid, yield 21%, keto form (50%),  $t_R$  7.0 min (analytical HPLC method).  $^1H$  NMR (300 MHz,  $D_2O$ ):  $\delta$  (ppm) 7.95 (s, 1H), 7.76 (d,  $J = 2.7$  Hz, 1H), 7.51 (d,  $J = 8.4$  Hz, 1H), 7.35 (dd,  $J = 8.4$  Hz, 2.7 Hz, 1H), 6.04 (d,  $J = 3.9$  Hz, 1H), 5.39 (s, 1H), 5.29 (s, 1H), 4.63 (m, 2H), 4.32 (m, 8H), 4.21 (m, 2H), 4.12 (m, 1H), 4.06 (m, 1H), 3.96 (m, 4H), 3.81 (s, 1H), 3.72 (m, 6H), 3.56 (m, 5H), 3.27-3.47 (m, 6H), 3.08 (m, 1H), 2.75 (m, 1H), 2.66 (m, 2H), 2.48 (m, 1H), 2.14 (m, 2H), 1.86 (m, 3H), 1.51 (m, 2H), 1.16 (m, 2H). HRMS (ESI)  $m/z$   $[M + H]^+$  1132.5217, calculated for  $C_{47}H_{78}N_{11}O_{19}S$  1132.5196.

#### Compound **45D**

Solvent for Prep-TLC: 7% methanol in DCM. **36** (40 mg) was used to give **45D** (9 mg) as a white solid, yield 18%, keto form (60%),  $t_R$  7.2 min (analytical HPLC method).  $^1\text{H}$  NMR (300 MHz,  $\text{D}_2\text{O}$ ):  $\delta$  (ppm) 7.94 (s, 1H), 7.76 (d,  $J = 3.0$  Hz, 1H), 7.50 (d,  $J = 8.4$  Hz, 1H), 7.36 (dd,  $J = 8.4$  Hz, 3.0 Hz, 1H), 6.04 (d,  $J = 3.9$  Hz, 1H), 5.39 (s, 1H), 5.29 (s, 1H), 4.61 (m, 2H), 4.31-4.41 (m, 8H), 4.22 (m, 2H), 4.09 (m, 1H), 4.00 (m, 1H), 3.90 (m, 4H), 3.81 (s, 1H), 3.74 (m, 4H), 3.66 (m, 6H), 3.58 (m, 2H), 3.52 (m, 1H), 3.48 (s, 2H), 3.29-3.43 (m, 6H), 3.11 (m, 1H), 2.75 (m, 1H), 2.67 (m, 2H), 2.49 (m, 1H), 2.13 (m, 2H), 1.84 (m, 3H), 1.50 (m, 2H), 1.16 (m, 2H). HRMS (ESI)  $m/z$   $[\text{M} + \text{H}]^+$  1176.5500, calculated for  $\text{C}_{49}\text{H}_{82}\text{N}_{11}\text{O}_{20}\text{S}$  1176.5458.

## Chapter 3 Design, synthesis and activity of light deactivatable miRNA inhibitor

### 3.1 Introduction

Each miRNA typically targets multiple mRNAs and its function usually depends on the local cellular context.<sup>123-126</sup> In cells, miRNAs are found to be transported to or matured/produced at different sub-cellular locations to achieve spatiotemporal specific regulation of target mRNAs.<sup>127</sup> To dissect the dynamic and context dependent function of miRNAs, spatiotemporal controllable miRNA regulators are required. Current methods for this purpose rely on the application of optical controllable probes.<sup>128</sup> By modifying synthetic antisense oligonucleotides (ASOs) with photo-removable caging groups, the hybridizations of ASOs with target RNAs are suppressed. Upon light irradiation, the caging groups can be removed and the active ASOs can be regenerated to block the function of targeted RNAs.<sup>129-131</sup> By incorporating photo-cleavable moieties between nucleotides of ASOs, these modified ASOs can be fragmented and inactivated by light.<sup>132</sup> However, using ASOs faces several limitations including poor cellular uptake efficiency and bio-distribution.<sup>70</sup> As a result, small-molecule inhibitors targeting different steps of the miRNA biogenesis have been developed.<sup>61, 102, 133-136</sup> Unfortunately, no inhibitor allowing photo control of its activity to achieve spatiotemporal regulation of miRNAs has been reported so far.

In Chapter 2, we developed a strategy to regulate miRNA biogenesis by using bifunctional small molecules inhibiting the Dicer processing of pre-miRNA.<sup>137</sup> These molecules consist of a pre-miRNA binding unit and a low affinity Dicer inhibiting unit. Neither of these 2 individual units inhibits miRNA maturation by

itself. However, when the two units are conjugated through a linker, the pre-miRNA binder can deliver the Dicer inhibiting unit to the catalytic cleavage site of Dicer in the targeted pre-miRNA/Dicer complex, which increases the effective local concentration of the weak Dicer inhibitor, thus achieving the blockage of the Dicer-mediated miRNA maturation.<sup>137</sup> Because of the bi-modular design of this strategy, we envisioned that using a photo cleavable linker to conjugate the two functional units should give a light-responsive bifunctional molecule that allow photo-induced fragmentation of the active bifunctional inhibitor into 2 separate inactive units to achieve deactivation, thus offering quick and potentially spatial controlled reversion of the inhibitory effects, which has significant importance for studying miRNA function.

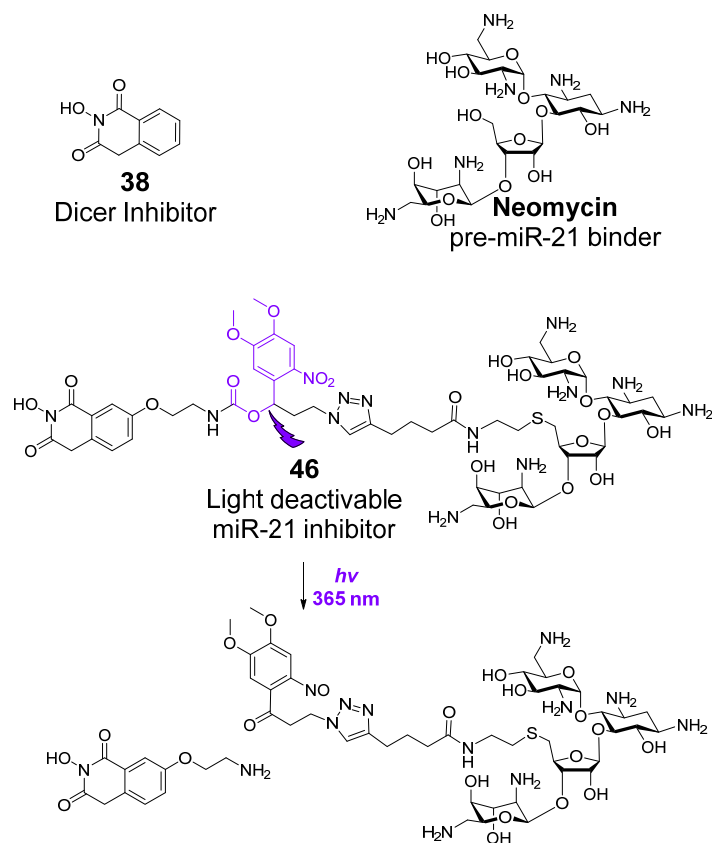


**Figure 3.1** Design of light controllable miR-21 inhibitor.

## 3.2 Results and discussion

### 3.2.1 Design and synthesis of light controllable miRNA inhibitor

We previously showed that neither compound **38**, a weak Dicer inhibitor, nor neomycin, a pre-miR-21 binder (Figure 3.1), can inhibit the Dicer-mediated maturation of miR-21 even at high  $\mu\text{M}$  or  $\text{mM}$  concentrations.<sup>137</sup> However, the conjugates of these 2 units gave bifunctional molecules that almost completely inhibit miR-21 maturation at 5  $\mu\text{M}$ .<sup>137</sup> To test the feasibility of the light deactivation approach with bifunctional molecules as proposed above, we conjugated **38** and neomycin with a photo cleavable linker with a comparable length to the linker used in previously reported active bifunctional miR-21 inhibitors. *Ortho*-nitrobenzyl (NB) derivatives are commonly used as photocleavable linkers or caging groups to offer photo-induced controls of NB-conjugated molecules.<sup>138</sup> The light irradiation condition for the cleavage of NB groups has been shown to be compatible with biological applications.<sup>130, 139-141</sup> As a result, we designed light deactivatable bifunctional miR-21 inhibitor **46** (Figure 3.1) by incorporating the photocleavable 4,5-dimethoxy-2-nitrobenzyl (DMNB) group into the linker.

The synthetic route of **46** was shown in Figure 3.2. An azide equipped NB compound **50** was synthesized from 4, 5-dimethoxy-6-nitrobenzaldehyde by multistep modifications, which was then conjugated to **53** by 1,1'-carbonyl diimidazole to generate **54**. The ester groups of **54** were hydrolyzed steadily by LiOH to give homophthalic acid derivative **55**, which was then cyclized by *O*-(tetrahydro-2*H*-pyran-2-yl)hydroxylamine following a reported method<sup>142</sup> to yield

**56.** The alkynyl modified neomycin<sup>122</sup> was conjugated to **56** through click chemistry to afford the target compound **46**.

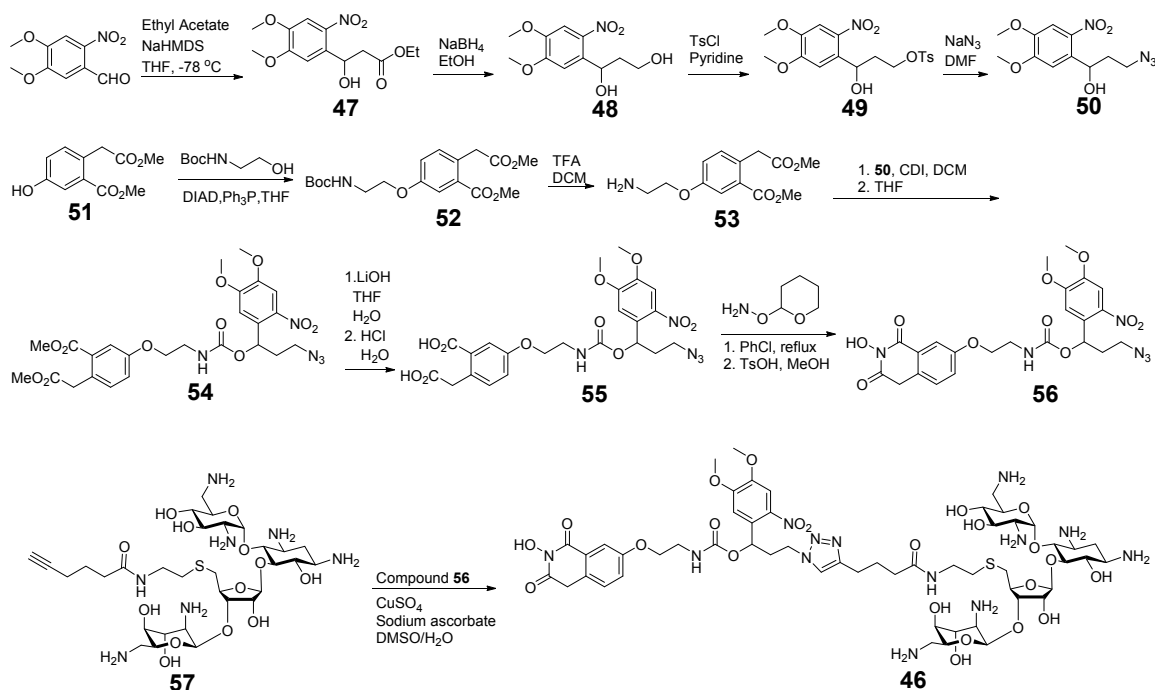


**Figure 3.2** Synthetic scheme of light deactivable miR-21 inhibitor **46**.

### 3.2.2 Photolysis study by HPLC

With the bifunctional inhibitor **46** in hand, we first checked whether the DMNB-containing linker in **46** can be cleaved by photo irradiation. Solutions of **46** (125 μM) in PBS (pH 7.4) were irradiated with 365 nm UV light under a fluorescence microscopy. Time course HPLC analysis of the photolysis reactions clearly showed that **46** rapidly disappeared upon irradiation (Figure 3.3), while two major peaks, likely corresponding to the fragmented products (Figure 3.1), were generated. These results indicated that bifunctional inhibitor **46** could be fragmented by photo irradiation. The fast reaction speed, complete within 30 s, is

desirable for biological applications that require fast stimuli response and minimal irradiation dose to avoid the phototoxicity introduced by UV irradiation.

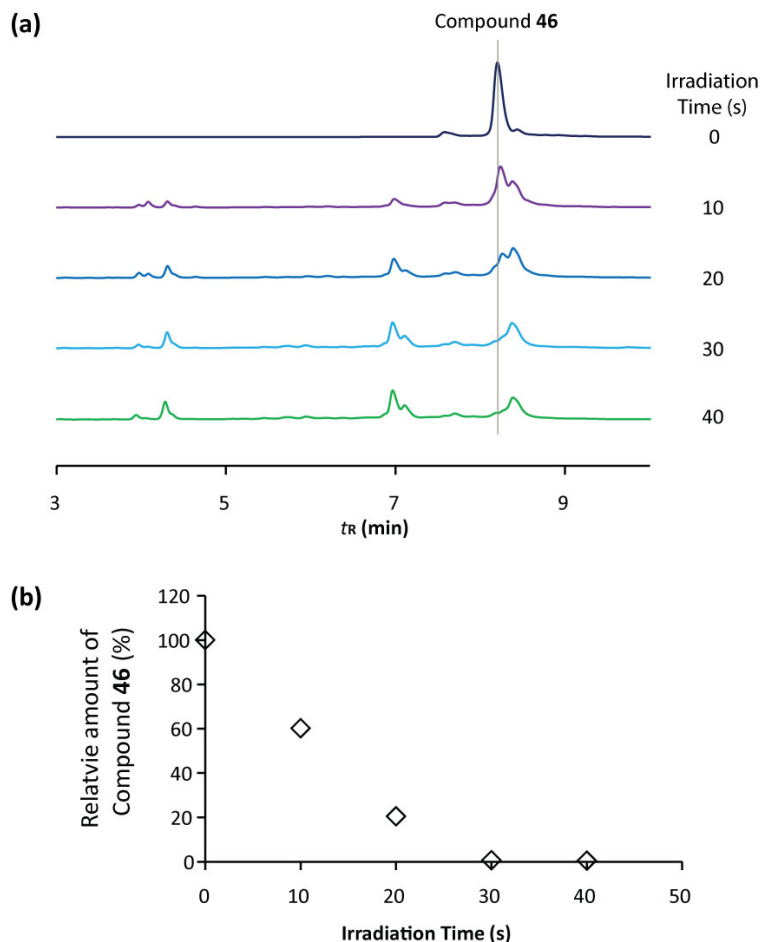


**Figure 3.3** (a) Time course HPLC analysis of the photolysis reactions of **46**. (b) Quantification of the relative amount of **46** left over in reactions as in panel (a).

### 3.2.3 *In vitro* Dicer inhibition activity

We then studied the Dicer inhibition activity of **46** before and after photo irradiation.  $^{32}\text{P}$ -labeled pre-miR-21, prepared by *in vitro* transcription, was incubated with recombinant human Dicer in the absence or presence of **46**. The processing of pre-miR-21 into mature miR-21 by Dicer was then monitored by denaturing polyacrylamide gel electrophoresis along with phosphor imaging.<sup>137</sup>

As shown in Figure 3.4, Dicer efficiently processed pre-miR-21 into mature miR-21 (Lane 2). To test if the inhibitory activity of the bifunctional inhibitor still

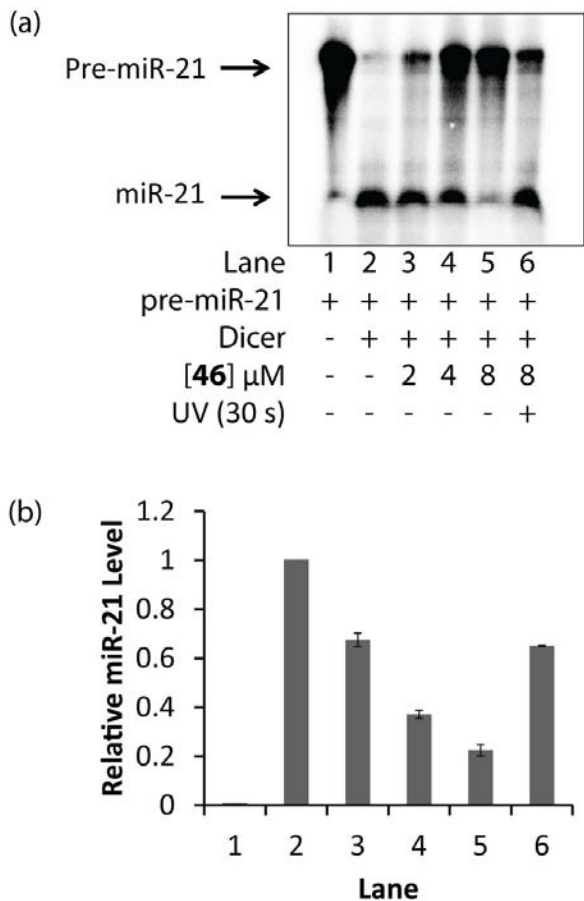


**Figure 3.4** (a) Representative image from electrophoresis analysis of Dicer-mediated pre-miR-21 cleavage in the presence of varying concentrations of **46** with or without UV (365 nm, 30 s) irradiation. (b) Densitometric quantitative analysis of miR-21 for images in panel a arising from three independent assays. Error bars represent the standard error of mean (N = 3).

remains after introducing the DMNB group into the linker, different concentrations of **3** (2 - 8  $\mu\text{M}$ ) were co-incubated with  $^{32}\text{P}$ -labeled pre-miR-21 and Dicer during the processing reaction and a dose dependent inhibition of miR-21 production was observed (Lane 3-5). These results confirm that the photo-cleavable linker does not affect the activity of the bifunctional inhibitor **46**. To test the light-

induced deactivation, **46** (8  $\mu$ M) was pre-irradiated with UV (365 nm, 30 s) before adding to the Dicer-mediated pre-miR-21 processing reaction (Lane 6). Compared to the condition treated with non-irradiated **46** at the same concentration, the production of mature miR-21 was clearly increased under the irradiated condition (Lane 5 vs 6), indicating that light irradiated **46** indeed loses its inhibitory activity. Overall, these results demonstrate that **46** could serve as a miR-21 inhibitor, and that photo irradiation could deactivate its ability to inhibit pre-miR-21 processing by Dicer.

### **3.3 Summary**

Light controllable miRNA regulators could offer an invaluable tool for studying miRNA functions through manipulating the activity or levels of miRNAs with spatiotemporal preciseness. By conjugating a Dicer inhibitor **38** and a pre-miR-21 binder (neomycin) with a photo-cleavable linker, we prepared a light deactivatable bifunctional miR-21 inhibitor **46** that inhibits pre-miR-21 processing by Dicer. The linker cleavage of **46** by photo irradiation separated the two functional units in **46** and deactivated the inhibitor. To our knowledge, this is the first reported light controllable miRNA regulator based on a small molecule instead of ASOs. By making bifunctional conjugates with RNA binders targeting other pre-miRNAs, we expect the strategy described in this work could be applied for regulating other miRNAs in a spatiotemporal manner, which would provide important chemical biology tools for miRNA studies.

### 3.4 Experimental section

#### 3.4.1 Chemistry

*Chemicals and instrumentation.* As described in 2.4.9. HPLC was performed using a Thermo Scientific UltiMate 3000 semi-preparative system coupled with a Thermo Scientific Acclaim 120 C18 column (100 mm × 4.6 mm, 3 μm). All HPLC analyses were run at RT and monitored at 260 nm. A gradient of CH<sub>3</sub>CN containing 0.1% TFA in water containing 0.1% TFA was used at a flow rate of 1 mL/min. For analytical HPLC, acetonitrile was increased from 5% to 90% in 25 min (Method A). For Prep-HPLC, acetonitrile was increased from 5% to 60% in 15 min, 60% to 95% in 0.5 min and then kept constant for 3 min (Method B).

*Ethyl 3-(4,5-dimethoxy-2-nitrophenyl)-3-hydroxypropanoate (47).*

To an argon-purged flask was added THF (25 mL) and sodium hexamethyldisilazide solution (2 M, 2.6 mL). A solution of ethyl acetate (0.463 g, 5.25 mmol) in THF (5 mL) was then added dropwise at -78 °C. The mixture was stirred for 0.5 h, after which a solution of 4, 5-dimethoxy-6-nitrobenzaldehyde (1.025 g, 4.84 mmol) in THF (20 mL) was added dropwise. The reaction was allowed to warm to room temperature and then quenched by saturated NaCl solution (50 mL). The mixture was extracted by ethyl acetate (2 × 50 mL). The combined organic phase was dried over MgSO<sub>4</sub> and concentrated by vacuum. The residue was purified by chromatography (ethyl acetate/hexane = 1:2) to give the product as a white solid (0.911 g), yield 63%. <sup>1</sup>H NMR (500 MHz, CDCl<sub>3</sub>, δ) 7.63 (s, 1H), 7.38 (s, 1H), 5.80 (dt, *J* = 9.3 Hz, 2.7 Hz, 1H), 4.22 (q, *J* = 7.2 Hz, 2H), 4.00 (s, 3H), 3.95 (s, 3H), 3.85 (d, *J* = 3.0 Hz, 1H), 2.98 (dd, *J* = 16.5 Hz, 2.7

Hz, 1H), 2.58 (dd,  $J = 16.5$  Hz, 9.3 Hz, 1H), 1.30 (t,  $J = 7.2$  Hz, 3H).  $^{13}\text{C}$  NMR (75 MHz,  $\text{CDCl}_3$ ,  $\delta$ ): 172.79, 154.00, 148.09, 139.42, 133.83, 109.13, 107.87, 66.31, 61.26, 56.60, 56.50, 42.42, 14.29. HRMS (ESI): calculated for  $\text{C}_{13}\text{H}_{17}\text{NO}_7$  [ $\text{M} + \text{Na}$ ] $^+$  322.0903, found 322.0904.

*1-(4,5-dimethoxy-2-nitrophenyl)propane-1,3-diol (48).*

To a solution of Compound **47** (900 mg, 3 mmol) in methanol (50 mL) was added  $\text{NaBH}_4$  (345 mg, 9 mmol) in small portions. The reaction was stirred at room temperature for overnight. The solvents were removed by vacuum. The residue was dissolved in a solution of HCl (0.5 M, 50 mL) and extracted with ethyl acetate (3  $\times$  30 mL). The combined organic phase was dried over  $\text{MgSO}_4$  and concentrated by vacuum. The crude product was purified by chromatography (ethyl acetate/hexane = 2:1) to give the product as a yellow solid (764 mg), yield 98%.  $^1\text{H}$  NMR (300 MHz,  $\text{CDCl}_3$ ,  $\delta$ ) 7.61 (s, 1H), 7.39 (s, 1H), 5.66 (dt,  $J = 9.0$  Hz, 2.4 Hz, 1H), 4.06 (m, 5H), 3.95 (s, 3H), 3.59 (d,  $J = 2.7$  Hz, 1H), 2.23 (t,  $J = 4.2$  Hz, 1H), 2.13 (m, 1H), 1.98 (m, 1H).  $^{13}\text{C}$  NMR (75 MHz,  $\text{CDCl}_3$ ,  $\delta$ ): 153.90, 147.82, 139.34, 135.92, 109.14, 107.80, 70.25, 62.37, 56.57, 56.47, 39.72. HRMS (ESI): calculated for  $\text{C}_{11}\text{H}_{15}\text{NO}_6$  [ $\text{M} + \text{Na}$ ] $^+$  280.0797, found 280.0783.

*3-(4,5-dimethoxy-2-nitrophenyl)-3-hydroxypropyl 4-methylbenzenesulfonate (49).*

To a solution of Compound **48** (111 mg, 0.432 mmol) in pyridine (3 mL) was added *p*-toluenesulfonyl chloride (164 mg, 0.863 mmol). The reaction was stirred at room temperature for 5 h. The solvents were removed by vacuum. The resulting residue was dissolved in ethyl acetate (30 mL) and washed with HCl (0.5 M, 20 mL) solution. The organic phase was dried over  $\text{MgSO}_4$  and

concentrated by vacuum. The residue was purified by chromatography (ethyl acetate/hexane = 1:1) to give the product as yellow oil (95 mg), yield 54%.  $^1\text{H}$  NMR (500 MHz,  $\text{CDCl}_3$ ,  $\delta$ ) 7.81 (d,  $J$  = 8.0 Hz, 2H), 7.57 (s, 1H), 7.34 (d,  $J$  = 8.0 Hz, 2H), 7.26 (s, 1H), 5.46 (dd,  $J$  = 9.0 Hz, 2.5 Hz, 1H), 4.39 (m, 1H), 4.28 (m, 1H), 3.98 (s, 3H), 3.93 (s, 3H), 2.45 (s, 3H), 2.21 (m, 1H), 1.97 (m, 1H).  $^{13}\text{C}$  NMR (125 MHz,  $\text{CDCl}_3$ ,  $\delta$ ): 153.94, 148.09, 145.06, 139.53, 134.89, 133.00, 130.03, 128.06, 109.10, 107.93, 67.80, 66.65, 56.62, 56.50, 37.17, 21.80. HRMS (ESI): calculated for  $\text{C}_{18}\text{H}_{21}\text{NO}_8\text{S}$   $[\text{M}+\text{Na}]^+$  434.0886, found 434.0886.

*3-azido-1-(4,5-dimethoxy-2-nitrophenyl)propan-1-ol (50).*

To a solution of Compound **49** (93 mg, 0.23 mmol) in DMF (3 mL) was added sodium azide (147 mg, 2.3 mmol). The reaction was stirred at 70 °C for 4 h. The mixture was partitioned between water (10 mL) and ethyl acetate (10 mL). The aqueous phase was extracted with ethyl acetate (1×10 mL). The combined organic phase was then washed with brine (3×10 mL) and dried over  $\text{MgSO}_4$ . The solvents were removed by vacuum and the residue was purified by chromatography (ethyl acetate/hexane = 1:3) to give the product as a yellow solid (46 mg), yield 72%.  $^1\text{H}$  NMR (300 MHz,  $\text{CDCl}_3$ ,  $\delta$ ) 7.55 (s, 1H), 7.29 (s, 1H), 5.47 (d,  $J$  = 8.7 Hz, 1H), 3.99 (s, 3H), 3.93 (s, 3H), 3.59 (t,  $J$  = 6.3 Hz, 2H), 3.07 (s, 1H), 2.12 (m, 1H), 1.91 (m, 1H).  $^{13}\text{C}$  NMR (75 MHz,  $\text{CDCl}_3$ ,  $\delta$ ): 153.78, 147.81, 139.22, 135.54, 108.83, 107.71, 67.56, 56.47, 56.35, 48.93, 37.03. HRMS (ESI): calculated for  $\text{C}_{11}\text{H}_{14}\text{N}_4\text{O}_5$   $[\text{M}-\text{OH}]^+$  265.0931, found 265.0906.

*Methyl 5-(2-aminoethoxy)-2-(2-methoxy-2-oxoethyl)benzoate (53).* Compound **51** was prepared as reported.<sup>109, 137</sup> To a solution of **51** (0.224 g, 1 mmol) in THF (5

mL) was added *N*-Boc-ethanolamine (0.177 g, 1.1 mmol) and triphenylphosphine (0.289 g, 1.1 mmol). The mixture was cooled down to 5 °C. Diisopropyl azodicarboxylate (0.222 g, 1.1 mmol) was then added dropwise to maintain the temperature below 5 °C and the reaction was stirred at room temperature for overnight. After removing the solvents by vacuum, the residue was purified by chromatography (Hexane:Ethyl Acetate = 3:1) to give **52** as a yellow oil. The crude product was subject to Boc removal without further purification. It was dissolved in a mixture of dichloromethane (6 mL) and trifluoroacetic acid (3 mL). The mixture was stirred at room temperature for overnight. The solvents were removed by vacuum and the residue was partitioned between saturated Na<sub>2</sub>CO<sub>3</sub> solution (15 mL) and ethyl acetate (15 mL). The aqueous phase was then extracted with ethyl acetate (3×15 mL). The combined organic phase was then washed with brine (1×15 mL) and dried with Na<sub>2</sub>SO<sub>4</sub>. After removing the solvents by vacuum, the residue was purified by chromatography (MeOH:Dichloromethane = 1:10) to give the product as an off-white solid (0.183 g), yield 69% for two steps. <sup>1</sup>H NMR (300 MHz, CDCl<sub>3</sub>, δ) 7.56 (d, *J* = 2.7 Hz, 1H), 7.16 (d, *J* = 8.4 Hz, 1H), 7.29 (dd, *J* = 8.4 Hz, 2.7 Hz, 1H), 4.03 (t, *J* = 5.1 Hz, 2H), 3.93 (s, 2H), 3.87 (s, 3H), 3.70 (s, 3H), 3.10 (t, *J* = 5.1 Hz, 2H). <sup>13</sup>C NMR (75 MHz, CDCl<sub>3</sub>, δ): 172.49, 167.45, 158.05, 133.51, 130.63, 128.39, 119.01, 116.77, 70.39, 52.22, 52.06, 41.56, 39.85. HRMS (ESI): calculated for C<sub>13</sub>H<sub>17</sub>NO<sub>5</sub> [M+H]<sup>+</sup> 268.1185, found 268.1194.

#### *Compound 54*

To a solution of compound **50** (46 mg, 0.16 mmol) in dichloromethane (3 mL) was added 1,1'-carbonyldiimidazole (79 mg, 0.49 mmol). The reaction was stirred at room temperature for 24 h. The reaction was diluted with dichloromethane (20 mL) and washed with H<sub>2</sub>O (3×20 mL). The solution was then dried with MgSO<sub>4</sub> and the solvents were removed by vacuum. The residue was dissolved in THF (3 mL). To the mixture was added compound **53** (62 mg, 0.23 mmol) and the reaction was refluxed for 8 h, after which it was diluted with dichloromethane (20 mL) and washed sequentially with HCl solution (0.1 M, 2×10 mL) and H<sub>2</sub>O (1×15 mL). The organic phase was dried with MgSO<sub>4</sub> and purified by chromatography (ethyl acetate/hexane = 1:1) to give the product as an off-white solid (80 mg), yield 85%. <sup>1</sup>H NMR (300 MHz, CDCl<sub>3</sub>, δ) 7.61 (s, 1H), 7.52 (d, *J* = 2.7 Hz, 1H), 7.17 (d, *J* = 8.7 Hz, 1H), 7.01 (d, *J* = 3.0 Hz, 1H), 6.97 (s, 1H), 6.38 (dd, *J* = 9.0 Hz, 3.0 Hz, 1H), 5.39 (t, *J* = 5.7 Hz, 1H), 4.03 (m, 2H), 3.93 (m, 5H), 3.88 (s, 3H), 3.87 (s, 3H), 3.69 (s, 3H), 3.57 (m, 2H), 3.48 (m, 2H), 2.26 (m, 1H), 2.10 (m, 1H). <sup>13</sup>C NMR (75 MHz, CDCl<sub>3</sub>, δ): 172.31, 167.13, 157.47, 155.18, 153.81, 148.24, 139.85, 133.59, 132.06, 130.70, 128.77, 118.53, 116.70, 107.96, 70.41, 67.15, 56.46, 52.22, 52.01, 48.21, 40.61, 39.73, 35.37. HRMS (ESI): calculated for C<sub>25</sub>H<sub>19</sub>N<sub>5</sub>O<sub>11</sub> [M+Na]<sup>+</sup> 598.1761, found 598.1768.

#### *Compound 55*

To a solution of **54** (80 mg, 0.14 mmol) in THF (1 mL) was added LiOH (13 mg, 0.31 mmol, in 1 mL of water) dropwise at 0 °C. The reaction was allowed to warm to room temperature and stirred for overnight. Then a solution of HCl (0.5 M, 10 mL) was added and the mixture was extracted with ethyl acetate (3×10 mL). The

combined organic phase was washed with brine (1×10 mL) and dried over MgSO<sub>4</sub>. The solid was filtered off, after which the solvents were removed under vacuum to give the product as a white solid (64 mg), yield 84%. <sup>1</sup>H NMR (500 MHz, CD<sub>3</sub>OD, δ) 7.64 (s, 1H), 7.52 (d, *J* = 2.5 Hz, 1H), 7.17 (d, *J* = 8.5 Hz, 1H), 7.10 (s, 1H), 6.99 (dd, *J* = 8.5 Hz, 2.5 Hz, 1H), 6.32 (dd, *J* = 9.5 Hz, 2.5 Hz, 1H), 4.00 (m, 2H), 3.93 (s, 2H), 3.88 (s, 3H), 3.79 (s, 3H), 3.49 (m, 4H), 2.23 (m, 1H), 2.06 (m, 1H). <sup>13</sup>C NMR (125 MHz, CD<sub>3</sub>OD, δ): 175.85, 170.07, 159.08, 157.84, 155.40, 149.64, 141.01, 134.59, 133.53, 132.45, 130.20, 119.21, 118.00, 109.53, 108.97, 70.92, 68.12, 56.79, 41.43, 40.44, 36.18. HRMS (ESI): calculated for C<sub>23</sub>H<sub>25</sub>N<sub>5</sub>O<sub>11</sub> [M+Na]<sup>+</sup> 570.1448, found 570.1457.

#### **Compound 56**

To a solution of **55** (60 mg, 0.11 mmol) in chlorobenzene was added *O*-(tetrahydro-2*H*-pyran-2-yl)hydroxylamine (19 mg, 0.16 mmol). The reaction was refluxed for overnight and the solvents were removed by vacuum. The residue was dissolved in methanol (5 mL). To the solution was then added *p*-toluenesulfonic acid (21 mg, 0.11 mmol). The mixture was stirred at room temperature for 8 h. After removing the solvents, the residue was triturated with H<sub>2</sub>O (2×5 mL) and ether (2×5 mL) sequentially and then purified by prep-HPLC (Method B) to give the product as an off-white solid (30 mg), yield 50%. <sup>1</sup>H NMR (300 MHz, DMSO, δ) 10.40 (br, 1H), 7.74 (t, *J* = 5.1 Hz, 1H), 7.60 (s, 1H), 7.43 (d, *J* = 2.4 Hz, 1H), 7.28 (d, *J* = 8.4 Hz, 1H), 7.17 (dd, *J* = 8.7 Hz, 2.7 Hz, 1H), 7.08 (s, 1H), 6.15 (dd, *J* = 8.4 Hz, 3.9 Hz, 1H), 4.18 (s, 2H), 4.02 (t, *J* = 5.1 Hz, 2H), 3.86 (s, 3H), 3.82 (s, 3H), 3.51 (m, 2H), 3.34 (m, 2H), 2.28 (m, 1H), 2.10 (m, 1H).

$^{13}\text{C}$  NMR (75 MHz, DMSO,  $\delta$ ): 166.45, 161.55, 157.42, 155.35, 153.39, 147.74, 139.41, 131.67, 129.08, 126.83, 125.98, 121.11, 111.43, 108.55, 107.63, 68.28, 66.78, 56.09, 47.34, 38.42, 36.19, 34.49. HRMS (ESI): calculated for  $\text{C}_{23}\text{H}_{24}\text{N}_6\text{O}_{10}$   $[\text{M}+\text{Na}]^+$  567.1452, found 567.1460.

### **Compound 46**

The TFA salt of Compound **57** was prepared as reported.<sup>122</sup> To a solution of **56** (4 mg, 0.007 mmol) and **57** (9 mg, 0.006 mmol) in DMSO (200  $\mu\text{L}$ ) was added  $\text{CuSO}_4$  (0.35 mg, 0.0014 mmol, in 10  $\mu\text{L}$  of water) and sodium ascorbate (0.55 mg, 0.0028 mmol, in 10  $\mu\text{L}$  of water). The mixture was protected under argon and incubated at room temperature for 8 h, after which it was purified by prep-HPLC (Method B) to give the product as an off-white solid (3.1 mg), yield 25%,  $t_{\text{R}}$  8.2 min (analytical HPLC Method A). The compound was characterized by  $^1\text{H}$  NMR (500 MHz,  $\text{D}_2\text{O}$ ) which shows the presence of both neomycin and the inhibitor moieties. HRMS (ESI): calculated for  $\text{C}_{54}\text{H}_{81}\text{N}_{13}\text{O}_{23}\text{S}$   $[\text{M}+\text{H}]^+$  1312.5367, found 1312.5396;  $[\text{M}+2\text{H}]^{2+}$  656.7723, found 656.7751.

### **3.4.2 Photolysis study**

The photolysis reaction of **46** was performed with an Axio Observer (Zeiss) microscope equipped with an HBO103 W/2 mercury arc lamp. 50  $\mu\text{L}$  of **46** (125  $\mu\text{M}$  in PBS buffer) was added in 96-well plate. The plate was irradiated using a DAPI filter, set with peak excitation at 365 nm. No objective lens was used, which created an area of illumination that completely covered one well of a 96-well plate. Light was transmitted through the polystyrene plate bottom. The reaction

was followed by HPLC (Method A). The relative amount of **46** was calculated by normalizing the peak integration to that before irradiation.

### **3.4.3 Dicer enzyme expression**

Dicer enzyme was expressed with a plasmid coding Flag tagged Dicer (Addgene plasmid # 41584)<sup>143</sup> in HEK293T cells and purified by anti-Flag M2 affinity gel (Sigma-Aldrich). HEK293T cells were cultured in DMEM medium (Gibco) without antibiotics, supplemented with 10% FBS and 2 mM GlutaMAX (Life Technologies) at 37 °C in a humidified atmosphere containing 5% CO<sub>2</sub>. The cells were plated in 15-cm dish and grown overnight to 60% confluency. Lipo3000 transfection reagent (Invitrogen) was used to transfect the cells with the plasmid DNA (9 µg) per the manufacture's protocol. After 60 h incubation, the medium was removed. The cells were then washed with PBS and lysed in 1 mL of lysis buffer (Tris 50 mM, NaCl 150 mM, Triton X-100 1%, SDS 0.1%, pH 7.5) containing Cocktail protease inhibitor (ThermoFisher). The lysate was centrifuged at 4 °C , 15000 RPM, for 10 min. The supernatant was then incubated with 60 µL of ANTI-FLAG M2 Affinity Gel at 4 °C with gentle agitation for 16 h. The gel was then washed with buffer (Tris 50 mM, NaCl 150 mM, NP-40 0.005%, pH 7.5) and suspended in H<sub>2</sub>O (25 µL) and glycerol (25 µL) for storage at -20 °C. The enzyme on gel was used directly for the following assay without cleavage.

### **3.4.4 *In vitro* Dicer inhibition assay**

<sup>32</sup>P-labeled pre-miR-21 was prepared as described before.<sup>137</sup> Right before use, the RNA was allowed to refold as follows: RNA was heated to 94 °C for 2 min and then cooled to 4 °C at a rate of 1 °C/s. A 10 µL of the reaction mixture was

made by mixing  $^{32}\text{P}$ -labeled pre-miR-21 (1  $\mu\text{L}$ , ~20 ng) with Dicer enzyme (3  $\mu\text{L}$ ) and various concentrations of **46** with or without photolysis (365 nm, 30 s) in buffer (HEPES 24 mM, NaCl 200 mM, EDTA 0.04 mM,  $\text{MgCl}_2$  2.5 mM, ATP 1 mM, pH 7.5). The reactions were incubated at 37 °C for 5 h and stopped by boiling with equal volume of Gel Loading Buffer II (ThermoFisher Scientific) for 5 min. The non-cleaved pre-miR-21 and the processed miR-21 were resolved by 18% denaturing polyacrylamide gel electrophoresis. The gel was imaged by phosphor imaging and analyzed with Quantity one software (Bio-rad).

## Chapter 4 MiRNA inhibition by macrocyclic peptidomimetics

This chapter is based on joint work with Dr. Jianfeng Cai's research group at the University of South Florida.

### 4.1 Introduction

Most of the currently developed miRNA inhibitors are comprised of polycationic scaffolds similar to those present in aminoglycosides. Unfortunately, these substances suffer from non-specific targeting and poor cell permeability.<sup>73, 82, 83</sup> Thus, despite the fact that significant progress has been made in this area, the development of small molecules that target miRNA precursors with high specificity and cell permeability remains a challenging task.

Peptidomimetics are peptides that contain unnatural polyamide backbones comprised of diverse side chains. Compared to natural peptides, these substances possess a high degree of chemical diversity, protease resistance and bioavailability.<sup>144</sup> Consequently, peptidomimetics represent a family that serves as a rich source for discovering novel binders and inhibitors for biological targets. Moreover, head to tail backbone cyclization of these substances can be utilized to improve exopeptidase resistance and enhance structural rigidity. Thus, the development and applications of cyclic peptidomimetics have become areas of increasing interest.<sup>145-148</sup>

Peptides<sup>92, 134</sup> and linear peptoids,<sup>74</sup> several of which contain polycationic side chains, have recently been found to bind and inhibit processing of pre-miRNAs. Inspired by these findings, we envisioned that cyclic peptidomimetics would serve as a new type of scaffold for targeting pre-miRNA. Moreover, we felt that a

compound library comprised of these substances would have a significantly high diversity and that screening of this library has the potential of uncovering non-polycationic inhibitors of miRNAs that could have improved specificity.

MiR-155, one of the key oncogenic miRNAs overexpressed in several human cancers,<sup>149</sup> promotes tumor formation through suppression of apoptosis and facilitation of cancer cell proliferation.<sup>150</sup> Because its downregulation has been shown to induce apoptosis of cancer cells and to block tumor growth in mice,<sup>151</sup><sup>152</sup> miR-155 is a promising anti-cancer therapeutic target. Thus, we set out to identify novel cyclic peptidomimetics for binding to pre-miR-155 and investigate their ability to antagonize miR-155 associated biological activity.

## **4.2 Results and discussion**

### **4.2.1 Screen for pre-miR-155 binder**

Oligomers of  $\gamma$ -substituted-*N*-acylated-*N*-aminoethylamino acids ( $\gamma$ -AA) were used earlier to construct one-bead-one-compound (OBOC) combinatorial libraries comprised of linear,  $\gamma$ -AA derived, peptides ( $\gamma$ -AApeptides). Members of these libraries were found to be remarkably stable and to have great functional diversity.<sup>153</sup> A new strategy for preparing cyclic  $\gamma$ -AApeptide libraries, employing a thioether-bridge approach, was recently reported.<sup>148</sup> In collaboration with Dr. Jianfeng Cai's research group at University of South Florida, we screened a library of novel macrocyclic  $\gamma$ -AApeptides against pre-miR-155. Compound **58** was identified as the hit.

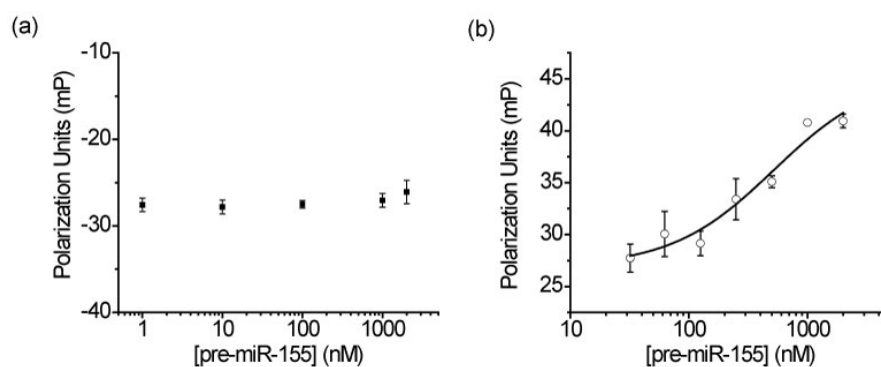
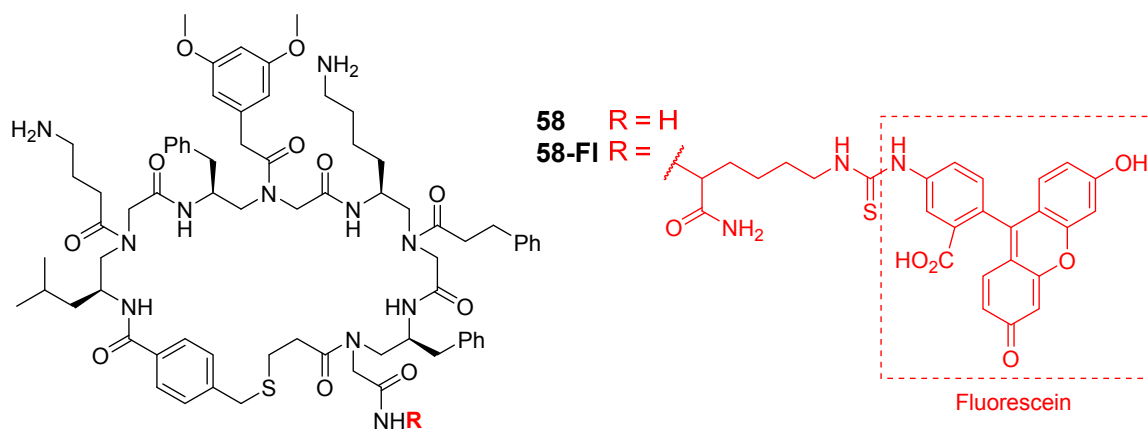


**Figure 4.1** Fluorescence polarization of fluorescein (a) and **58-FI** (b) in the presence of different concentrations of pre-miR-155. The error bars represent the standard error of the mean (N = 3).

#### 4.2.2 Binding affinity of the hit to pre-miR-155

Binding of **58** to pre-miR-155 was first demonstrated using the fluorescence polarization (FP) assay. A fluorescein-tagged derivative **58-FI** (synthesized by the Cai research group) was prepared for use in the FP assay. The results show that the fluorescence polarization of **58-FI** increases with increasing concentrations of pre-miR-155 (Figure 4.1). The data arising from the saturation binding curve was used to determine that the binding affinity ( $K_d$ ) of **58-FI** toward pre-miR-155 is 515 ( $\pm 186$ ) nM. In contrast, fluorescein alone does not have an

effect on the FP of pre-miR-155. These results indicate that the hit compound **58** binds to pre-miR-155.

Binding of **58** to pre-miR-155 was further demonstrated by using an electrophoretic mobility shift assay. The electrophoretic mobility of  $^{32}\text{P}$ -labeled pre-miR-155, prepared by using *in vitro* transcription, in the presence of various concentrations of **58** was determined by using a non-denatured polyacrylamide gel and phosphor imaging. The observation of a clear reduction in the mobility of pre-miR-155 on the gel with increasing concentrations of **58** (Figure 4.2) shows that a complex between **58** and pre-miR-155 is formed.

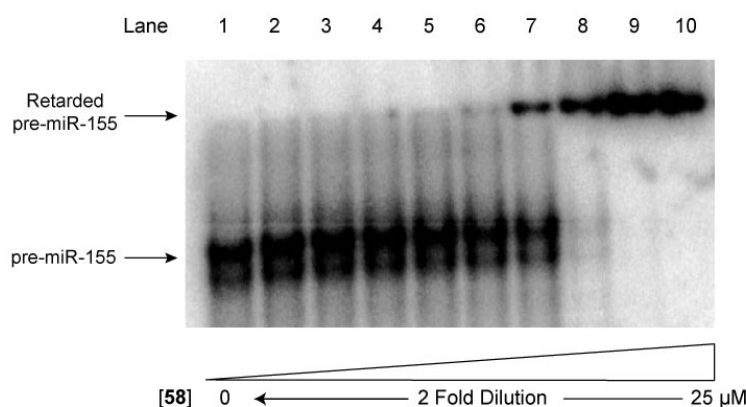


**Figure 4.2** The electrophoretic mobility of pre-miR-155 in the presence of compound **58**.

#### 4.2.3 *In vitro* Dicer blocking activity

Next we assessed whether binding of **58** to pre-miR-155 disrupts the interaction between pre-miR-155 and Dicer, and it inhibits miR-155 maturation (Credit to Umesh Bhattarai). As part of an *in vitro* pre-miR-155 processing assay,  $^{137}^{32}\text{P}$ -labeled pre-miR-155 was incubated with recombinant human Dicer in the absence or presence of **58**. The Dicer processing reaction was then monitored by using denaturing polyacrylamide gel electrophoresis along with

phosphor imaging. In the absence of **58**, Dicer efficiently cleaves pre-miR-155 to form mature miR-155. However, in the presence of increasing concentrations of **58**, Dicer-mediated miR-155 processing is disrupted (Figure 4.3), as reflected in a 63% reduction in the level of mature miR-155 formation caused by 30  $\mu$ M of **58**. This result demonstrates that **58** effectively blocks Dicer processing of pre-miR-155 *in vitro*.

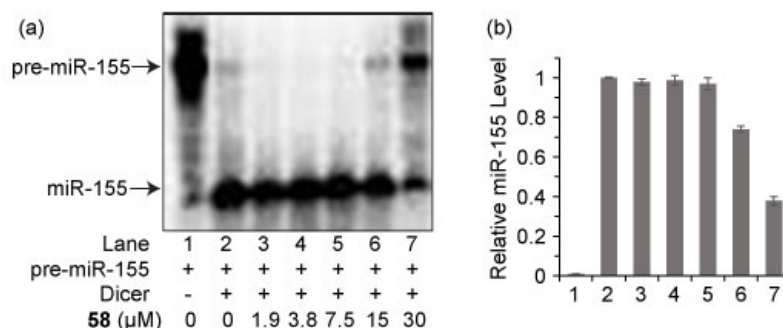


**Figure 4.3** (a) Representative image from electrophoresis analysis of Dicer-mediated pre-miR-155 cleavage in the presence of varying concentrations of **58**. (b) Densitometric quantitative analysis of miR-155 for images in panel a arising from three independent assays. Error bars represent the standard error of mean (N = 3). Figure courtesy of Umesh Bhattarai.

#### 4.2.4 MiR-155 inhibition in cell

High cell permeability is a prerequisite for the activities of miRNA inhibitors in cells. To evaluate the cellular uptake efficiency of the macrocyclic peptidomimetic **58**, HEK293T and MCF-7 cells were treated with **58-FI**. The results of fluorescent microscopy showed that after incubation for 7 h very strong fluorescence emanates from both cell lines (Figure 4.4), indicating that **58** is readily cell permeable.

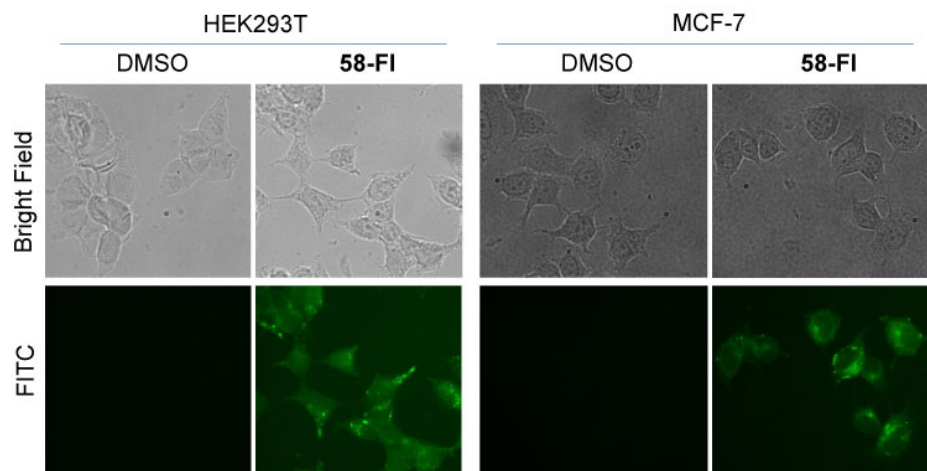


**Figure 4.4** Fluorescence microscope imaging of HEK293T and MCF-7 cells treated with DMSO or **58-FI**.

The inhibitory effect of **58** on miR-155 maturation in cells was assessed next. HEK293T cells were transiently transfected with a plasmid encoding pre-miR-155. Mature miR-155 levels were then determined as a function of the concentration of **58** using RT-qPCR. As the graph in Figure 4.5 a shows, **58** reduces the level of miR-155 in a dose dependent manner, exemplified by a 70% reduction at 30  $\mu\text{M}$  of **58**. Thus, **58** inhibits the production of miR-155 in cells.

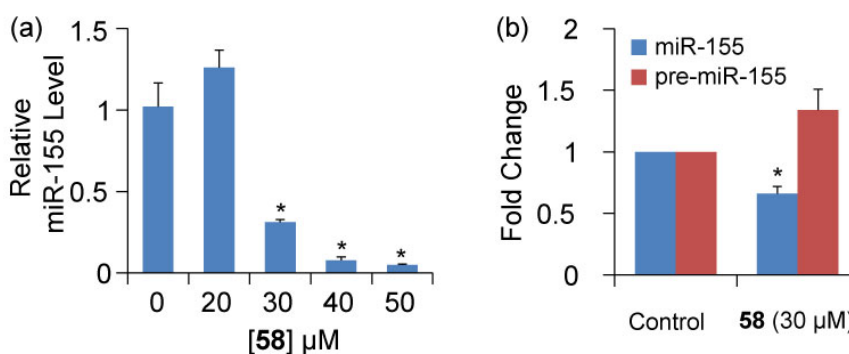


**Figure 4.5** (a) Inhibition of miR-155 production by **58** (24 h treatment) in HEK293T cells overexpressing miR-155. (b) **58** inhibits endogenous miR-155 formation after 96 h treatment of MCF-7 cells. The error bars represent the standard error of the mean (N = 3).

We next tested if **58** inhibits endogenous miR-155 production in cells. Because miR-155 is upregulated in many cancer cells, the breast cancer cell line MCF-7 was used in this study. We were aware that it might be difficult to downregulate endogenous miR-155 through blocking its biogenesis because it has a very long half-life.<sup>154</sup> Despite this, treatment of MCF-7 cells with **58** (30  $\mu$ M) for 96 h leads to a 38% decrease in miR-155 level (Figure 4.5 b), a similar reduction to that brought about by other small-molecule miRNA inhibitors.<sup>90, 113</sup> Meanwhile, miR-155 precursors were found to accumulate in the cells, indicating that the reduction in miR-155 formation is indeed caused by blocking pre-miR-155 cleavage. The combined results demonstrate that **58** inhibits endogenous miR-155 biogenesis in cancer cells by disrupting Dicer processing.

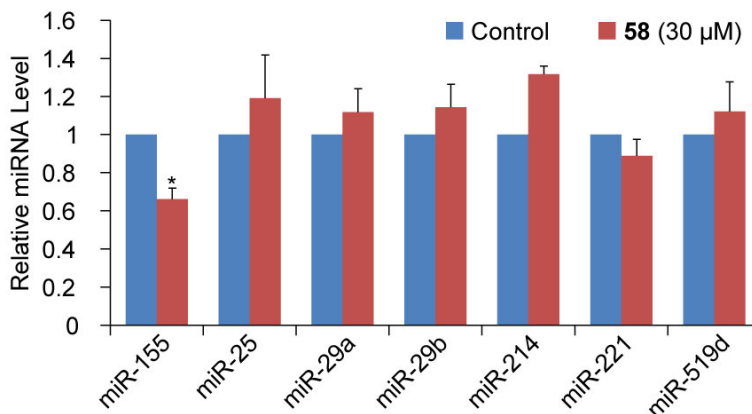


**Figure 4.6** The selectivity of **58** in inhibiting miR-155 over other miRNAs in MCF-7 cells. The error bars represent the standard error of the mean (N = 3).

#### 4.2.5 Selectivity of **58** to MiR-155 over other miRNAs

To assess whether the binding activity of **58** is selective toward miR-155, we determined if changes in the levels of several other miRNAs in MCF-7 cells are promoted by treatment with **58** for 96 h. As shown in Figure 4.6, in contrast to its

significant effect on decreasing the miR-155 level, **58** displays little or no inhibitory effects on other tested miRNAs, indicating good selectivity of **58**.

#### 4.2.6 **58** upregulates miR-155 target protein FOXO3A

Owing to its activity and selectivity in inhibiting miR-155 in cells, the macrocyclic peptidomimetic **58** serves as a model for a new family of small molecules that have potential utility in the treatment of cancers and other miR-155-associated diseases. To explore this proposal, initial experiments were carried out with tumor suppressor gene FOXO3A, a direct target of miR-155<sup>155</sup> whose loss in activity increases the resistance of cancer cells to apoptosis, which results in cell-cycle progression.<sup>156</sup> In line with expectations, we observed using RT-qPCR (Figure 4.7 a) and immunoblotting (Figure 4.7 b and c) that inhibition of miR-155 by **58** in MCF-7 cells leads to increases in the levels of FOXO3A mRNA and protein.

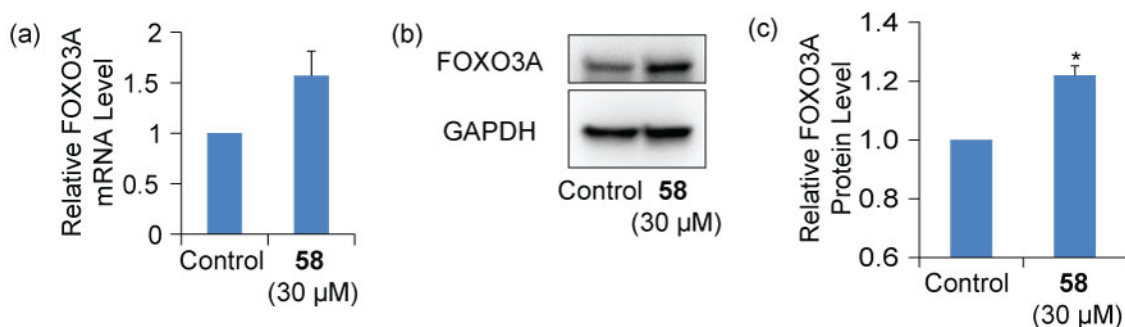


**Figure 4.7** (a) RT-qPCR analysis of mRNA and (b) Western blotting analysis of protein levels of FOXO3A in MCF-7 cells either treated or not treated with **58**. (c) Densitometric quantitative analysis of FOXO3A as shown in panel b. Error bars represent the standard error of mean (N = 3).

#### 4.2.7 58 induces cancer cell apoptosis

To assess whether **58** induces cell apoptosis, MCF-7 cells were incubated with **58** for 96 h and then stained with propidium iodide (PI) and fluorescein-labeled annexin V. Flow cytometry analysis showed that **58** promotes an increase in the population of cells undergoing both early apoptosis (Annexin+/PI-) and late apoptosis (Annexin+/PI+) (Figure 4.8 a-c). The cell apoptosis rate is increased by 12%, which is a similar level to that brought about by treatment with an anti-miR-155 oligonucleotide (Figure 4.8 d).

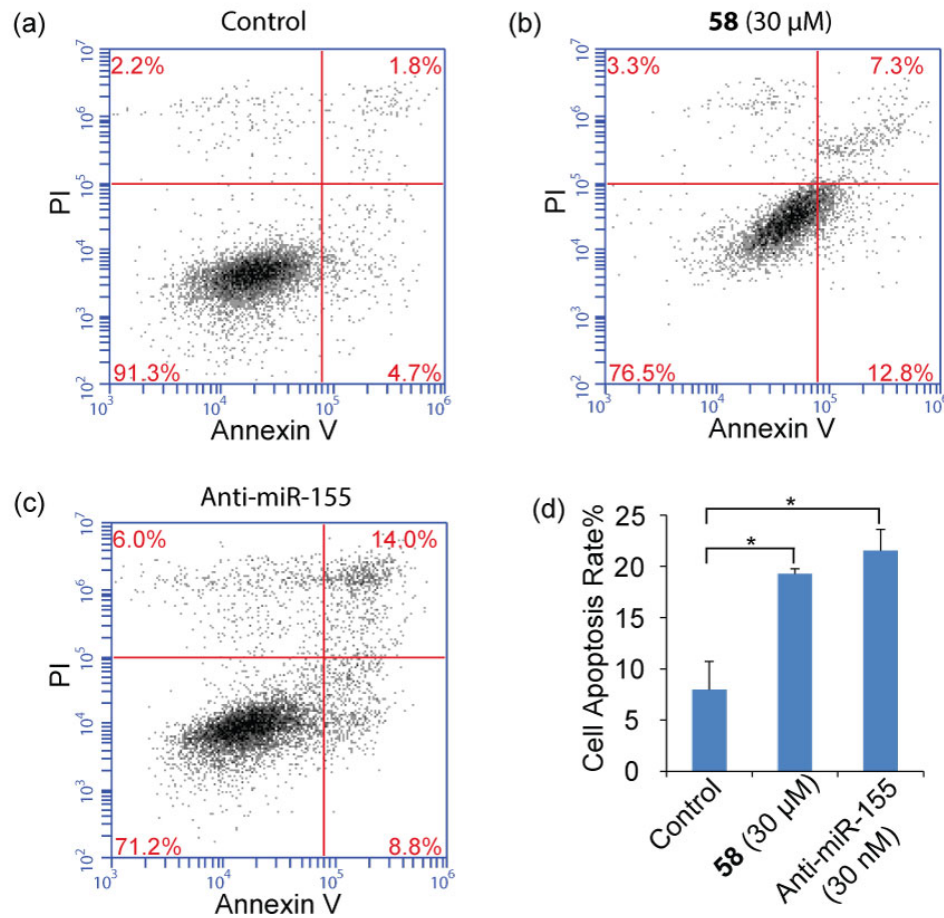


**Figure 4.8** Flow cytometry analysis of MCF-7 cell apoptosis under different conditions. (a) Control; (b) **58** (30 μM); (c) anti-miR-155 (30 nM). (d) Quantitation of cell apoptosis rate as in panel a, b and c. Error bars represent the standard error of the mean (N = 3).

Characteristic morphological changes of apoptotic cells including cell shrinkage, rounding and membrane blebbing were also observed to take place using microscopy (Figure 4.9).<sup>157</sup> These results demonstrate that **58** promotes upregulation of miR-155 target gene and induces apoptosis.

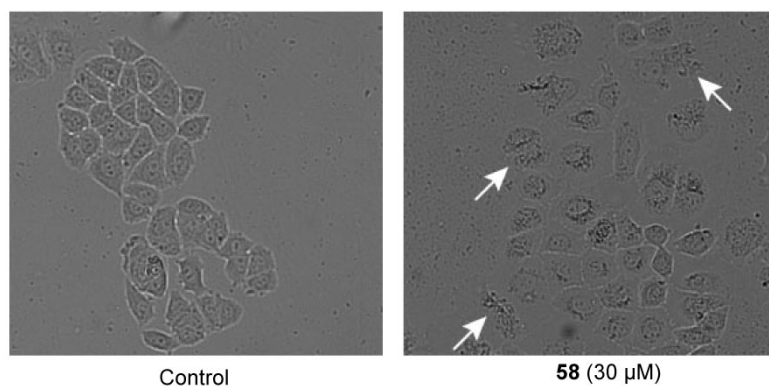


**Figure 4.9** Morphological changes of MCF-7 cells after 4 day treatment with DMSO or **58**. Arrows indicate the apoptotic cells showing blebbing.

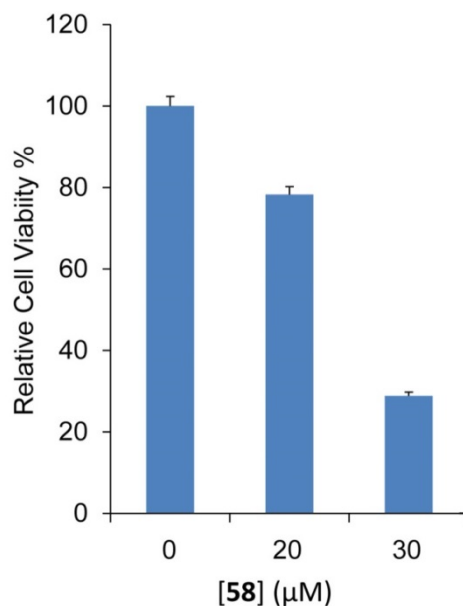


**Figure 4.10** Viability analysis for MCF-7 cells treated with **58**. The error bars represent the standard error of the mean (N = 6).

#### 4.2.8 **58** inhibits cancer cell viability

Finally, because miR-155 inhibition reduces cancer cell proliferation,<sup>151</sup> it was anticipated that **58** would cause a decrease in the viability of MCF-7 cells. To test the validity of this proposal, cell viability assays were conducted using 3-(4,5-dimethylthiazol-2-yl)-2,5-diphenyltetrazolium bromide (MTT). The observation of a 70% reduction in the viability of MCF-7 cells after incubation with **58** (30  $\mu$ M) for 96 h (Figure 4.10) demonstrates that this macrocyclic peptidomimetic strongly inhibits cancer cell viability.

#### 4.3 Summary

In summary, in the experiments described above, we designed and synthesized a novel combinatorial macrocyclic  $\gamma$ -AApeptide library. A screen of this library against pre-miR-155 led to identification of the new pre-miR-155 binder **58**. Moreover, we found that **58** inhibits Dicer-mediated pre-miR-155 processing *in vitro* and in MCF-7 cells, and, consequently, that it induces apoptosis and reduces growth of these cells. Because of their modular property along with their high propensity for side chain alteration, macrocyclic peptidomimetics should be amenable to systematic structural optimization to obtain specific miRNA binding agents. We believe that **58** is a promising lead for generating more potent miR-155 inhibitors that are designed to treat cancers and other miR-155-associated diseases. This study also demonstrates that macrocyclic peptidomimetics can serve as a new RNA targeting scaffold.

## 4.4 Experiment details

### 4.4.1 *In vitro* Transcription of pre-miR-155

Pre-miR-155 was prepared by *in vitro* transcription.<sup>111</sup> The sequence of pre-miR-155 was obtained from miRBase (<http://www.mirbase.org/>). The DNA template used for making pre-miR-155 RNA was generated by PCR primer extension. Briefly, forward primer:

5'-

GAAATTAATACGACTCACTATAGGCTGTTAATGCTAATCGTGATAGGGGTTT  
TTGCCTCCAACCTG-3'

and reverse primer:

5'-CTGTTAATGCTAATATGTAGGAGTCAGTTGGAGGCAAAAACCCCTA-3'

0.8  $\mu$ M of each were subjected to primer extension using Taq polymerase (Ambion) per the manufacturer's protocol. The extended dsDNA was purified with NucleoSpin gel and PCR clean-up kit (Macherey-Nagel). The hybrid DNA template with T7 promoter was used for *in vitro* transcription using T7 polymerase following manufacturer's instructions (New England Biolabs). The reaction mixture was treated with DNase to digest the template DNA and then extracted with phenol/chloroform/isoamyl alcohol (25:24:1) (pH 6.7). The RNA was finally precipitated by ethanol and resuspended in water for storage at -20 °C. Right before use, the RNA was allowed to refold as follows: RNA was heated to 94 °C for 2 min and then cooled to 4 °C at a rate of 1 °C/s.

#### **4.4.2 Fluorescence polarization binding assay**

The affinity of fluorescein (10 nM) or **58-FI** (10 nM) to pre-miR-155 was determined using fluorescence polarization assay as described in **2.4.2**.

#### **4.4.3 Electrophoretic mobility shift assay**

Electrophoretic mobility shift assay (EMSA) was used to study the binding of **58** to pre-miR-155. <sup>32</sup>P-labeled pre-miR-155 was prepared by *in vitro* transcription as described above except that [alpha-P32] Uridine 5'-triphosphate (UTP) (Perkinelmer) was used to take the place of regular UTP. A 10 µL of binding mixture was made by incubating <sup>32</sup>P-labeled pre-miR-155 (1 µL, 20 ng) with various concentrations of **58** in buffer (HEPES 24 mM, NaCl 200 mM, EDTA 0.04 mM, MgCl<sub>2</sub> 2.5 mM, pH 7.5) at 37 °C for 20 min. Gel loading buffer (10X, Sucrose 40%, Xylene Cyanol 0.17%, Bromophenol Blue 0.17%) was then added. The bound RNA was resolved from the free RNA using 12% non-denaturing polyacrylamide gel at 4 °C and visualized by phosphor imaging.

#### **4.4.4 Cell culture**

HEK293T and MCF-7 cells were cultured in DMEM medium (Gibco) without antibiotics, supplemented with 10% FBS and 2 mM GlutaMAX (Life Technologies) at 37 °C in a humidified atmosphere containing 5% CO<sub>2</sub>.

#### **4.4.5 Dicer enzyme expression**

The Dicer enzyme was expressed as describe in **3.4.3**.

#### **4.4.6 Dicer-mediated pre-miR-155 cleavage assay**

<sup>32</sup>P-labeled pre-miR-155 was prepared as described in EMSA assay. A 10 µL of the reaction mixture was made by incubating <sup>32</sup>P-labeled pre-miR-155 (1 µL,

~20 ng) with Dicer enzyme (3  $\mu$ L) and various concentrations of **58** in buffer (HEPES 24 mM, NaCl 200 mM, EDTA 0.04 mM, MgCl<sub>2</sub> 2.5 mM, ATP 1 mM, pH 7.5) at 37 °C for 2.5 h. The reaction was stopped by boiling with equal volume of Gel Loading Buffer II (ThermoFisher Scientific) for 5 min. The non-cleaved pre-miR-155 and the processed miR-155 were resolved by 18% denaturing polyacrylamide gel. The gel was imaged with phosphor imager and analyzed by quantity one software (Bio-rad).

#### **4.4.7 Fluorescence microscope imaging**

HEK293T or MCF-7 cells were plated into 24-well plates and grown overnight to 50%. The cells were then treated with **58-FI** (5  $\mu$ M) or DMSO (0.2% v/v) for 7 h. After removing the medium, the cells were washed with PBS and imaged by fluorescence microscope (Axio Observer, Zeiss) under the GFP channel.

#### **4.4.8 MiR-155 inhibition in cell**

HEK293T cell overexpressing miR-155 was used for evaluating the inhibition activity of **58**. MiR155 in pcDNA3.1 was a gift from Heidi Schwarzenbach (Addgene plasmid # 78126).<sup>158</sup> HEK293T cells were plated in 24-well plates (500  $\mu$ L of medium per well) and grown overnight to 60% confluency. The cells were transfected with the plasmid DNA (200 ng/well) using Lipo3000 transfection reagent (Invitrogen) per the manufacture's protocol. Briefly, DNA (200 ng/well), P3000 reagent (1  $\mu$ L/well) and Lipofectamine 3000 reagent (1  $\mu$ L/well) were incubated in 50  $\mu$ L of Opti-MEM reduced serum medium (ThermoFisher) containing appropriate amount of **58** at room temperature for 15 min. The mixture

was then added into the cell cultural medium and the cells were harvested for RNA extraction after 24 h incubation.

MCF-7 cell was used for studying the activity of **58** in inhibiting endogenous miR-155 in cell. The cells were plated in 24-well plates (500  $\mu$ L of medium per well) and grown overnight to ~60% confluency. The cells were then treated with **58** (30  $\mu$ M), DMSO (0.2% v/v) or anti-miR-155 (30 nM, transfected as described above) (Integrated DNA Technologies). The cell cultural medium was replaced with fresh one containing the corresponding small molecule every 24 h. The cells were harvested after 4-day incubation for the following RT-qPCR, Western blotting, and flow cytometry analysis.

#### **4.4.9 RNA extraction and RT-qPCR**

Total RNA was extracted using miRNeasy Mini Kit (Qiagen) per the manufacturer's protocol. MiRNA reverse transcription reactions were completed using a Taqman MicroRNA RT Kit (Applied Biosystems) per the manufacturer's protocol. Approximately 10 ng of total RNA was used for U6, miR-25, miR-29a, miR-29b and miR-221, 300 ng was used for miR-155, miR-214 and miR-519d. The qPCR was performed on 7900HT Fast Real-Time PCR System (Applied Biosystems) using Taqman Universal PCR Master Mix (Applied Biosystems) and Taqman miRNA assays (Applied Biosystems) per the manufacturer's protocol. 0.5  $\mu$ L of the RT product was used for a 10  $\mu$ L qPCR reaction. The triplicate threshold cycles (*Ct*) obtained for each treatment were used to determine the level of miRNA normalized to U6 small nuclear RNA using the  $2^{-\Delta\Delta Ct}$  method.<sup>115</sup> The results presented were based on three independent assays.

The reverse transcription reaction for mRNA (FOXO3A and GAPDH) and miR-155 precursors was completed with 300 ng of total RNA using High Capacity cDNA Reverse Transcription Kit (Applied Biosystems) per the manufacturer's protocol. 0.5  $\mu$ L of the reaction mixture was used for qPCR assay (10  $\mu$ L) with PowerUp SYBR Green Master Mix (Applied Biosystems) per the manufacturer's protocol. Following are the sequences of primers used for qPCR:

Target	Forward primer	Reverse primer
FOXO3A	5'-TGACACAGTCGGACCCCTTG-3'	5'-GTTCTGATTGACCAAACCTCCCT-3'
GAPDH	5'-GGTGGTCTCCTCTGACTTCAACA-3'	5'-GTTGCTGTAGCCAAATTCGTTGT-3'
miR-155 precursors	5'-CTGTTAATGCTAATCGTGATAGGG-3'	5'-TGTAGGAGTCAGTTGGAGGC-3'

The triplicate threshold cycles ( $C_t$ ) obtained for each treatment were used to determine the level of target RNA normalized to GAPDH mRNA using the  $2^{-\Delta\Delta C_t}$  method.<sup>115</sup> The results presented were based on three independent assays.

#### 4.4.10 Western Blotting

Western blotting assays were carried out following 2.4.6. FOXO3A primary antibody (Cell Signaling Technology, FoxO3a (D19A7) Rabbit mAb) and GAPDH primary antibody (Cell Signaling Technology, GAPDH (D16H11) XP® Rabbit mAb) were used.

#### 4.4.11 Flow Cytometry Assay

MCF-7 cells were treated with different compounds as described above for 4 days. After washing with PBS twice, the cells were collected by trypsinizing and centrifugation. The cells were then stained with a mixture of fluorescein-annexin V and propidium iodide (PI) using an apoptosis kit (Invitrogen, eBioscience Annexin V-FITC Apop Kit) per the manufacture's protocol. Flow cytometry was

performed using a BD Accuri C6 Plus flow cytometer (BD Biosciences). The quantification data provided were based on three independent assays.

#### **4.4.12 Cell viability assay**

The effect of **58** on MCF-7 cell proliferation were tested by MTT assay (MTT = 3-(4, 5-dimethylthiazol-2-yl)-2, 5-diphenyltetrazolium bromide). MCF-7 cells were seeded in 96-well plates and grown overnight to around 60% confluency. The cells were then treated with appropriate amount of **58** or DMSO (0.2% v/v). The cell cultural medium was replaced with fresh one containing corresponding compound. After 4 day treatment, the medium was removed and 10  $\mu$ L of MTT stock solution (12 mM) was added to wells along with 100  $\mu$ L of phenol free DMEM. The cells were incubated at 37 °C for 4 h. The MTT containing medium was replaced with 50  $\mu$ L of DMSO. The solution was mixed thoroughly by pipetting and incubated at 37 °C for 10 min. The absorbance at 540 nm was recorded with a plate reader (SpectraMax i3X, Molecular Devices). The relative viability of the cells was calculated based on 6 parallel tests by comparing to the controls. The result presented was based on three independent assays.

#### **Statistical analysis**

Data are presented as the mean  $\pm$  SEM of three independent experiments. Student's t-test for significance was carried out using Microsoft Excel 2010 software. \* $p < 0.03$  verses control sample were considered significant.

## Reference

1. Ambros, V. (2004) The functions of animal microRNAs, *Nature* 431, 350-355.
2. Alvarez-Garcia, I., and Miska, E. A. (2005) MicroRNA functions in animal development and human disease, *Development* 132, 4653-4662.
3. Bushati, N., and Cohen, S. M. (2007) MicroRNA functions, In *Annu. Rev. Cell Dev. Biol.*, pp 175-205.
4. Shenoy, A., and Blelloch, R. H. (2014) Regulation of microRNA function in somatic stem cell proliferation and differentiation, *Nat. Rev. Mol. Cell Biol.* 15, 565-576.
5. Ameres, S. L., and Zamore, P. D. (2013) Diversifying microRNA sequence and function, *Nat. Rev. Mol. Cell Biol.* 14, 475-488.
6. Dong, H., Lei, J., Ding, L., Wen, Y., Ju, H., and Zhang, X. (2013) MicroRNA: Function, Detection, and Bioanalysis, *Chem. Rev.* 113, 6207-6233.
7. Garzon, R., Fabbri, M., Cimmino, A., Calin, G. A., and Croce, C. M. (2006) MicroRNA expression and function in cancer, *Trends Mol. Med.* 12, 580-587.
8. Kloosterman, W. P., and Plasterk, R. H. A. (2006) The diverse functions of MicroRNAs in animal development and disease, *Dev. Cell* 11, 441-450.
9. Piva, R., Spandidos, D. A., and Gambari, R. (2013) From microRNA functions to microRNA therapeutics: Novel targets and novel drugs in breast cancer research and treatment, *Int. J. Oncol.* 43, 985-994.
10. Jiang, Q., Wang, Y., Hao, Y., Juan, L., Teng, M., Zhang, X., Li, M., Wang, G., and Liu, Y. (2009) miR2Disease: a manually curated database for microRNA deregulation in human disease, *Nucleic Acids Res.* 37, D98-D104.
11. Lee, R. C., Feinbaum, R. L., and Ambros, V. (1993) The *C. elegans* heterochronic gene *lin-4* encodes small RNAs with antisense complementarity to *lin-14*, *Cell* 75, 843-854.
12. Wightman, B., Ha, I., and Ruvkun, G. (1993) Posttranscriptional regulation of the heterochronic gene *lin-14* by *lin-4* mediates temporal pattern formation in *C. elegans*, *Cell* 75, 855-862.
13. Kozomara, A., and Griffiths-Jones, S. (2014) miRBase: annotating high confidence microRNAs using deep sequencing data, *Nucleic Acids Res.* 42, D68-D73.
14. Rodriguez, A., Griffiths-Jones, S., Ashurst, J. L., and Bradley, A. (2004) Identification of mammalian microRNA host genes and transcription units, *Genome Res.* 14, 1902-1910.
15. Stenvang, J., Petri, A., Lindow, M., Obad, S., and Kauppinen, S. (2012) Inhibition of microRNA function by antimiR oligonucleotides, *Silence* 3, 1-1.
16. Friedman, R. C., Farh, K. K.-H., Burge, C. B., and Bartel, D. P. (2009) Most mammalian mRNAs are conserved targets of microRNAs, *Genome Res.* 19, 92-105.
17. Vasudevan, S., Tong, Y., and Steitz, J. A. (2007) Switching from repression to activation: MicroRNAs can up-regulate translation, *Science* 318, 1931-1934.

18. Place, R. F., Li, L.-C., Pookot, D., Noonan, E. J., and Dahiya, R. (2008) MicroRNA-373 induces expression of genes with complementary promoter sequences, *Proc. Natl. Acad. Sci. U. S. A.* *105*, 1608-1613.
19. Eiring, A. M., Harb, J. G., Neviani, P., Garton, C., Oaks, J. J., Spizzo, R., Liu, S., Schwind, S., Santhanam, R., Hickey, C. J., Becker, H., Chandler, J. C., Andino, R., Cortes, J., Hokland, P., Huettner, C. S., Bhatia, R., Roy, D. C., Liebhaber, S. A., Caligiuri, M. A., Marcucci, G., Garzon, R., Croce, C. M., Calin, G. A., and Perrotti, D. (2010) miR-328 Functions as an RNA Decoy to Modulate hnRNP E2 Regulation of mRNA Translation in Leukemic Blasts, *Cell* *140*, 652-665.
20. Fabbri, M., Paone, A., Calore, F., Galli, R., Gaudio, E., Santhanam, R., Lovat, F., Fadda, P., Mao, C., Nuovo, G. J., Zanesi, N., Crawford, M., Ozer, G. H., Wernicke, D., Alder, H., Caligiuri, M. A., Nana-Sinkam, P., Perrotti, D., and Croce, C. M. (2012) MicroRNAs bind to Toll-like receptors to induce prometastatic inflammatory response, *Proc. Natl. Acad. Sci. U. S. A.* *109*, E2110-E2116.
21. Bernstein, E., Kim, S. Y., Carmell, M. A., Murchison, E. P., Alcorn, H., Li, M. Z., Mills, A. A., Elledge, S. J., Anderson, K. V., and Hannon, G. J. (2003) Dicer is essential for mouse development, *Nat. Genet.* *35*, 215-217.
22. Bhaskaran, M., and Mohan, M. (2014) MicroRNAs: History, Biogenesis, and Their Evolving Role in Animal Development and Disease, *Vet. Pathol.* *51*, 759-774.
23. Melton, C., Judson, R. L., and Blelloch, R. (2010) Opposing microRNA families regulate self-renewal in mouse embryonic stem cells, *Nature* *463*, 621-U645.
24. Tu, J., Ng, S. H., Luk, A. C. S., Liao, J., Jiang, X., Feng, B., Mak, K. K. L., Rennert, O. M., Chan, W.-Y., and Lee, T.-L. (2015) MicroRNA-29b/Tet1 regulatory axis epigenetically modulates mesendoderm differentiation in mouse embryonic stem cells, *Nucleic Acids Res.* *43*, 7805-7822.
25. Wang, Y., Baskerville, S., Shenoy, A., Babiarz, J. E., Baehner, L., and Blelloch, R. (2008) Embryonic stem cell-specific microRNAs regulate the G1-S transition and promote rapid proliferation, *Nat. Genet.* *40*, 1478-1483.
26. Shaham, L., Binder, V., Gefen, N., Borkhardt, A., and Izraeli, S. (2012) MiR-125 in normal and malignant hematopoiesis, *Leukemia* *26*, 2011-2018.
27. Chen, Y., Liu, W., Chao, T., Zhang, Y., Yan, X., Gong, Y., Qiang, B., Yuan, J., Sun, M., and Peng, X. (2008) MicroRNA-21 down-regulates the expression of tumor suppressor PDCD4 in human glioblastoma cell T98G, *Cancer Lett.* *272*, 197-205.
28. Papagiannakopoulos, T., Shapiro, A., and Kosik, K. S. (2008) MicroRNA-21 targets a network of key tumor-suppressive pathways in glioblastoma cells, *Cancer Res.* *68*, 8164-8172.
29. Reinhart, B. J., Slack, F. J., Basson, M., Pasquinelli, A. E., Bettinger, J. C., Rougvie, A. E., Horvitz, H. R., and Ruvkun, G. (2000) The 21-nucleotide let-7 RNA regulates developmental timing in *Caenorhabditis elegans*, *Nature* *403*, 901-906.
30. Gao, F.-B. (2010) Context-dependent functions of specific microRNAs in neuronal development, *Neural Dev.* *5*, 25.

31. Zhao, Y., Ransom, J. F., Li, A., Vedantham, V., von Drehle, M., Muth, A. N., Tsuchihashi, T., McManus, M. T., Schwartz, R. J., and Srivastava, D. (2007) Dysregulation of cardiogenesis, cardiac conduction, and cell cycle in mice lacking miRNA-1-2, *Cell* 129, 303-317.
32. Small, E. M., and Olson, E. N. (2011) Pervasive roles of microRNAs in cardiovascular biology, *Nature* 469, 336-342.
33. Esau, C., Davis, S., Murray, S. F., Yu, X. X., Pandey, S. K., Pear, M., Watts, L., Booten, S. L., Graham, M., McKay, R., Subramaniam, A., Propp, S., Lollo, B. A., Freier, S., Bennett, C. F., Bhanot, S., and Monia, B. P. (2006) miR-122 regulation of lipid metabolism revealed by in vivo antisense targeting, *Cell Metab.* 3, 87-98.
34. Najafi-Shoushtari, S. H., Kristo, F., Li, Y., Shioda, T., Cohen, D. E., Gerszten, R. E., and Naeaeer, A. M. (2010) MicroRNA-33 and the SREBP Host Genes Cooperate to Control Cholesterol Homeostasis, *Science* 328, 1566-1569.
35. O'Connell, R. M., Taganov, K. D., Boldin, M. P., Cheng, G., and Baltimore, D. (2007) MicroRNA-155 is induced during the macrophage inflammatory response, *Proc. Natl. Acad. Sci. U. S. A.* 104, 1604-1609.
36. Baltimore, D., Boldin, M. P., O'Connell, R. M., Rao, D. S., and Taganov, K. D. (2008) MicroRNAs: new regulators of immune cell development and function, *Nat. Immunol.* 9, 839-845.
37. Calin, G. A., Dumitru, C. D., Shimizu, M., Bichi, R., Zupo, S., Noch, E., Aldler, H., Rattan, S., Keating, M., Rai, K., Rassenti, L., Kipps, T., Negrini, M., Bullrich, F., and Croce, C. M. (2002) Frequent deletions and down-regulation of micro-RNA genes miR15 and miR16 at 13q14 in chronic lymphocytic leukemia, *Proc. Natl. Acad. Sci. U. S. A.* 99, 15524-15529.
38. Calin, G. A., Sevignani, C., Dan Dumitru, C., Hyslop, T., Noch, E., Yendamuri, S., Shimizu, M., Rattan, S., Bullrich, F., Negrini, M., and Croce, C. M. (2004) Human microRNA genes are frequently located at fragile sites and genomic regions involved in cancers, *Proc. Natl. Acad. Sci. U. S. A.* 101, 2999-3004.
39. Cimmino, A., Calin, G. A., Fabbri, M., Iorio, M. V., Ferracin, M., Shimizu, M., Wojcik, S. E., Aqeilan, R. I., Zupo, S., Dono, M., Rassenti, L., Alder, H., Volinia, S., Liu, C. G., Kipps, T. J., Negrini, M., and Croce, C. M. (2005) miR-15 and miR-16 induce apoptosis by targeting BCL2, *Proc. Natl. Acad. Sci. U. S. A.* 102, 13944-13949.
40. Johnson, S. M., Grosshans, H., Shingara, J., Byrom, M., Jarvis, R., Cheng, A., Labourier, E., Reinert, K. L., Brown, D., and Slack, F. J. (2005) RAS is regulated by the let-7 MicroRNA family, *Cell* 120, 635-647.
41. He, L., Thomson, J. M., Hemann, M. T., Hernando-Monge, E., Mu, D., Goodson, S., Powers, S., Cordon-Cardo, C., Lowe, S. W., Hannon, G. J., and Hammond, S. M. (2005) A microRNA polycistron as a potential human oncogene, *Nature* 435, 828-833.
42. Medina, P. P., Nolde, M., and Slack, F. J. (2010) OncomiR addiction in an in vivo model of microRNA-21-induced pre-B-cell lymphoma, *Nature* 467, 86-U119.

43. Costinean, S., Zanesi, N., Pekarsky, Y., Tili, E., Volinia, S., Heerema, N., and Croce, C. M. (2006) Pre-B cell proliferation and lymphoblastic leukemia/high-grade lymphoma in E mu-miR155 transgenic mice, *Proc. Natl. Acad. Sci. U. S. A.* 103, 7024-7029.
44. Almeida, M. I., Reis, R. M., and Calin, G. A. (2011) MicroRNA history: Discovery, recent applications, and next frontiers, *Mutat. Res.* 717, 1-8.
45. Maegdefessel, L. (2014) The emerging role of microRNAs in cardiovascular disease, *J. Intern. Med.* 276, 633-644.
46. Zhao, Y., Samal, E., and Srivastava, D. (2005) Serum response factor regulates a muscle-specific microRNA that targets Hand2 during cardiogenesis, *Nature* 436, 214-220.
47. Chen, J. F., Mandel, E. M., Thomson, J. M., Wu, Q. L., Callis, T. E., Hammond, S. M., Conlon, F. L., and Wang, D. Z. (2006) The role of microRNA-1 and microRNA-133 in skeletal muscle proliferation and differentiation, *Nat. Genet.* 38, 228-233.
48. van Rooij, E., Sutherland, L. B., Liu, N., Williams, A. H., McAnally, J., Gerard, R. D., Richardson, J. A., and Olson, E. N. (2006) A signature pattern of stress-responsive microRNAs that can evoke cardiac hypertrophy and heart failure, *Proc. Natl. Acad. Sci. U. S. A.* 103, 18255-18260.
49. Jazbutyte, V., and Thum, T. (2010) MicroRNA-21: From Cancer to Cardiovascular Disease, *Curr. Drug Targets* 11, 926-935.
50. Schaefer, A., O'Carroll, D., Tan, C. L., Hillman, D., Sugimori, M., Llinas, R., and Greengard, P. (2007) Cerebellar neuro degeneration in the absence of microRNAs, *J. Exp. Med.* 204, 1553-1558.
51. Lukiw, W. J. (2007) Micro-RNA speciation in fetal, adult and Alzheimer's disease hippocampus, *Neuroreport* 18, 297-300.
52. Sonkoly, E., Stahle, M., and Pivarcsi, A. (2008) MicroRNAs and immunity: Novel players in the regulation of normal immune function and inflammation, *Semin. Cancer Biol.* 18, 131-140.
53. Xiao, J., Luo, X., Lin, H., Zhang, Y., Lu, Y., Wang, N., Zhang, Y., Yang, B., and Wang, Z. (2007) MicroRNA miR-133 represses HERG K<sup>+</sup> channel expression contributing to QT prolongation in diabetic hearts, *J. Biol. Chem.* 282, 12363-12367.
54. Price, N. L., Ramirez, C. M., and Fernandez-Hernando, C. (2014) Relevance of microRNA in metabolic diseases, *Crit. Rev. Clin. Lab. Sci.* 51, 305-320.
55. Umbach, J. L., and Cullen, B. R. (2009) The role of RNAi and microRNAs in animal virus replication and antiviral immunity, *Genes Dev.* 23, 1151-1164.
56. Ura, S., Honda, M., Yamashita, T., Ueda, T., Takatori, H., Nishino, R., Sunakozaka, H., Sakai, Y., Horimoto, K., and Kaneko, S. (2009) Differential MicroRNA Expression Between Hepatitis B and Hepatitis C Leading Disease Progression to Hepatocellular Carcinoma, *Hepatology* 49, 1098-1112.
57. Abbott, A. L., Alvarez-Saavedra, E., Miska, E. A., Lau, N. C., Bartel, D. P., Horvitz, H. R., and Ambros, V. (2005) The let-7 microRNA family members mir-48, mir-84, and mir-241 function together to regulate developmental timing in *Caenorhabditis elegans*, *Dev. Cell* 9, 403-414.

58. Sokol, N. S., and Ambros, V. (2005) Mesodermally expressed *Drosophila* microRNA-1 is regulated by Twist and is required in muscles during larval growth, *Genes Dev.* **19**, 2343-2354.
59. Du, C., Liu, C., Kang, J., Zhao, G., Ye, Z., Huang, S., Li, Z., Wu, Z., and Pei, G. (2009) MicroRNA miR-326 regulates T-H-17 differentiation and is associated with the pathogenesis of multiple sclerosis, *Nat. Immunol.* **10**, 1252-U1254.
60. Boutla, A., Delidakis, C., and Tabler, M. (2003) Developmental defects by antisense-mediated inactivation of micro-RNAs 2 and 13 in *Drosophila* and the identification of putative target genes, *Nucleic Acids Res.* **31**, 4973-4980.
61. Jayaraj, G. G., Nahar, S., and Maiti, S. (2015) Nonconventional chemical inhibitors of microRNA: therapeutic scope, *Chem. Commun.* **51**, 820-831.
62. Catuogno, S., Rienzo, A., Di Vito, A., Esposito, C. L., and de Franciscis, V. (2015) Selective delivery of therapeutic single strand antimiRs by aptamer-based conjugates, *J. Control. Release* **210**, 147-159.
63. Cheng, C. J., Bahal, R., Babar, I. A., Pincus, Z., Barrera, F., Liu, C., Svoronos, A., Braddock, D. T., Glazer, P. M., Engelman, D. M., Saltzman, W. M., and Slack, F. J. (2015) MicroRNA silencing for cancer therapy targeted to the tumour microenvironment, *Nature* **518**, 107-110.
64. Devulapally, R., Sekar, N. M., Sekar, T. V., Foygel, K., Massoud, T. F., Willmann, J. K., and Paulmurugan, R. (2015) Polymer Nanoparticles Mediated Codelivery of AntimiR-10b and AntimiR-21 for Achieving Triple Negative Breast Cancer Therapy, *ACS Nano* **9**, 2290-2302.
65. Obad, S., dos Santos, C. O., Petri, A., Heidenblad, M., Broom, O., Ruse, C., Fu, C., Lindow, M., Stenvang, J., Straarup, E. M., Hansen, H. F., Koch, T., Pappin, D., Hannon, G. J., and Kauppinen, S. (2011) Silencing of microRNA families by seed-targeting tiny LNAs, *Nat. Genet.* **43**, 371-U160.
66. Janssen, H. L. A., Reesink, H. W., Lawitz, E. J., Zeuzem, S., Rodriguez-Torres, M., Patel, K., van der Meer, A. J., Patick, A. K., Chen, A., Zhou, Y., Persson, R., King, B. D., Kauppinen, S., Levin, A. A., and Hodges, M. R. (2013) Treatment of HCV Infection by Targeting MicroRNA, *N. Engl. J. Med.* **368**, 1685-1694.
67. van Zandwijk, N., Pavlakis, N., Kao, S., Clarke, S., Lee, A., Brahmabhatt, H., Macdiarmid, J., Pattison, S., Leslie, F., Huynh, Y., Linton, A., and Reid, G. (2015) P1.02MesomiR 1: A Phase I study of TargomiRs in patients with refractory malignant pleural mesothelioma (MPM) and lung cancer (NSCLC), *Ann. Oncol.* **26**, ii16-ii16.
68. Cheng, C. J., Saltzman, W. M., and Slack, F. J. (2013) Canonical and Non-Canonical Barriers Facing AntimiR Cancer Therapeutics, *Curr. Med. Chem.* **20**, 3582-3593.
69. Juliano, R. L., Ming, X., and Nakagawa, O. (2012) The Chemistry and Biology of Oligonucleotide Conjugates, *Acc. Chem. Res.* **45**, 1067-1076.
70. Juliano, R., Bauman, J., Kang, H., and Ming, X. (2009) Biological Barriers to Therapy with Antisense and siRNA Oligonucleotides, *Mol. Pharmaceutics* **6**, 686-695.

71. Gumireddy, K., Young, D. D., Xiong, X., Hogenesch, J. B., Huang, Q. H., and Deiters, A. (2008) Small-molecule inhibitors of microRNA miR-21 function, *Angew. Chem. Int. Ed.* **47**, 7482-7484.
72. Young, D. D., Connelly, C. M., Grohmann, C., and Deiters, A. (2010) Small Molecule Modifiers of MicroRNA miR-122 Function for the Treatment of Hepatitis C Virus Infection and Hepatocellular Carcinoma, *J. Am. Chem. Soc.* **132**, 7976-7981.
73. Thomas, J. R., and Hergenrother, P. J. (2008) Targeting RNA with small molecules, *Chem. Rev.* **108**, 1171-1224.
74. Diaz, J. P., Chirayil, R., Chirayil, S., Tom, M., Head, K. J., and Luebke, K. J. (2014) Association of a peptoid ligand with the apical loop of pri-miR-21 inhibits cleavage by Drosha, *RNA* **20**, 528-539.
75. Velagapudi, S. P., Gallo, S. M., and Disney, M. D. (2014) Sequence-based design of bioactive small molecules that target precursor microRNAs, *Nat. Chem. Biol.* **10**, 291-297.
76. Disney, M. D., Labuda, L. P., Paul, D. J., Poplawski, S. G., Pushechnikov, A., Tran, T., Velagapudi, S. P., Wu, M., and Childs-Disney, J. L. (2008) Two-dimensional combinatorial screening identifies specific aminoglycoside - RNA internal loop partners, *J. Am. Chem. Soc.* **130**, 11185-11194.
77. Velagapudi, S. P., Seedhouse, S. J., and Disney, M. D. (2010) Structure-Activity Relationships through Sequencing (StARTS) Defines Optimal and Suboptimal RNA Motif Targets for Small Molecules, *Angew. Chem. Int. Ed.* **49**, 3816-3818.
78. Velagapudi, S. P., and Disney, M. D. (2014) Two-dimensional combinatorial screening enables the bottom-up design of a microRNA-10b inhibitor, *Chem. Commun.* **50**, 3027-3029.
79. Childs-Disney, J. L., and Disney, M. D. (2015) Small Molecule Targeting of a MicroRNA Associated with Hepatocellular Carcinoma, *ACS Chem. Biol.*
80. Haga, C. L., Velagapudi, S. P., Strivelli, J. R., Yang, W.-Y., Disney, M. D., and Phinney, D. G. (2015) Small Molecule Inhibition of miR-544 Biogenesis Disrupts Adaptive Responses to Hypoxia by Modulating ATM-mTOR Signaling, *ACS Chem. Biol.* **10**, 2267-2276.
81. Mingeot-Leclercq, M. P., Glupczynski, Y., and Tulkens, P. M. (1999) Aminoglycosides: Activity and resistance, *Antimicrob. Agents Chemother.* **43**, 727-737.
82. Luedtke, N. W., Carmichael, P., and Tor, Y. (2003) Cellular uptake of aminoglycosides, guanidinoglycosides, and poly-arginine, *J. Am. Chem. Soc.* **125**, 12374-12375.
83. Tor, Y. (2003) Targeting RNA with small molecules, *ChemBiochem* **4**, 998-1007.
84. Liang, F. S., Wang, S. K., Nakatani, T., and Wong, C. H. (2004) Targeting RNAs with tobramycin analogues, *Angew. Chem. Int. Ed.* **43**, 6496-6500.
85. Bose, D., Jayaraj, G., Suryawanshi, H., Agarwala, P., Pore, S. K., Banerjee, R., and Maiti, S. (2012) The Tuberculosis Drug Streptomycin as a Potential Cancer Therapeutic: Inhibition of miR-21 Function by Directly Targeting Its Precursor, *Angew. Chem. Int. Ed.* **51**, 1019-1023.

86. Maiti, M., Nauwelaerts, K., and Herdewijn, P. (2012) Pre-microRNA binding aminoglycosides and antitumor drugs as inhibitors of Dicer catalyzed microRNA processing, *Bioorg. Med. Chem. Lett.* **22**, 1709-1711.
87. Thi Phuong Anh, T., Duc Duy, V., Di Giorgio, A., and Duca, M. (2015) Ribosome-targeting antibiotics as inhibitors of oncogenic microRNAs biogenesis: Old scaffolds for new perspectives in RNA targeting, *Bioorg. Med. Chem.* **23**, 5334-5344.
88. Bose, D., Jayaraj, G. G., Kumar, S., and Maiti, S. (2013) A Molecular-Beacon-Based Screen for Small Molecule Inhibitors of miRNA Maturation, *ACS Chem. Biol.* **8**, 930-938.
89. Nahar, S., Ranjan, N., Ray, A., Arya, D. P., and Maiti, S. (2015) Potent inhibition of miR-27a by neomycin-bisbenzimidazole conjugates, *Chem. Sci.* **6**, 5837-5846.
90. Vo, D. D., Staedel, C., Zehnacker, L., Benhida, R., Darfeuille, F., and Duca, M. (2014) Targeting the Production of Oncogenic MicroRNAs with Multimodal Synthetic Small Molecules, *ACS Chem. Biol.* **9**, 711-721.
91. Murata, A., Otabe, T., Zhang, J., and Nakatani, K. (2016) BzDANP, a Small-Molecule Modulator of Pre-miR-29a Maturation by Dicer, *ACS Chem. Biol.* **11**, 2790-2796.
92. Pai, J., Hyun, S., Hyun, J. Y., Park, S. H., Kim, W. J., Bae, S. H., Kim, N. K., Yu, J., and Shin, I. (2016) Screening of Pre-miRNA-155 Binding Peptides for Apoptosis inducing Activity Using Peptide Microarrays, *J. Am. Chem. Soc.* **138**, 857-867.
93. Pande, J., Szewczyk, M. M., and Grover, A. K. (2010) Phage display: Concept, innovations, applications and future, *Biotechnol. Adv.* **28**, 849-858.
94. Lamichhane, T. N., Abeydeera, N. D., Duc, A.-C. E., Cunningham, P. R., and Chow, C. S. (2011) Selection of Peptides Targeting Helix 31 of Bacterial 16S Ribosomal RNA by Screening M13 Phage-Display Libraries, *Molecules* **16**, 1211-1239.
95. Bose, D., Nahar, S., Rai, M. K., Ray, A., Chakraborty, K., and Maiti, S. (2015) Selective inhibition of miR-21 by phage display screened peptide, *Nucleic Acids Res.* **43**, 4342-4352.
96. Sliwoski, G., Kothiwale, S., Meiler, J., and Lowe, E. W., Jr. (2014) Computational Methods in Drug Discovery, *Pharmacol. Rev.* **66**, 334-395.
97. Shi, Z., Zhang, J., Qian, X., Han, L., Zhang, K., Chen, L., Liu, J., Ren, Y., Yang, M., Zhang, A., Pu, P., and Kang, C. (2013) AC1MMYR2, an Inhibitor of Dicer-Mediated Biogenesis of Oncomir miR-21, Reverses Epithelial-Mesenchymal Transition and Suppresses Tumor Growth and Progression, *Cancer Res.* **73**, 5519-5531.
98. Watashi, K., Yeung, M. L., Starost, M. F., Hosmane, R. S., and Jeang, K. T. (2010) Identification of Small Molecules That Suppress MicroRNA Function and Reverse Tumorigenesis, *J. Biol. Chem.* **285**, 24707-24716.
99. Tan, G. S., Chiu, C.-H., Garchow, B. G., Metzler, D., Diamond, S. L., and Kiriakidou, M. (2012) Small Molecule Inhibition of RISC Loading, *ACS Chem. Biol.* **7**, 402-409.

100. Naro, Y., Thomas, M., Stephens, M. D., Connelly, C. M., and Deiters, A. (2015) Aryl amide small-molecule inhibitors of microRNA miR-21 function, *Bioorg. Med. Chem. Lett.* **25**, 4793-4796.
101. Wickramasinghe, N. S., Manavalan, T. T., Dougherty, S. M., Riggs, K. A., Li, Y., and Klinge, C. M. (2009) Estradiol downregulates miR-21 expression and increases miR-21 target gene expression in MCF-7 breast cancer cells, *Nucleic Acids Res.* **37**, 2584-2595.
102. Vo, D. D., Tran, T. P. A., Staedel, C., Benhida, R., Darfeuille, F., Di Giorgio, A., and Duca, M. (2016) Oncogenic MicroRNAs Biogenesis as a Drug Target: Structure-Activity Relationship Studies on New Aminoglycoside Conjugates, *Chem. Eur. J.* **22**, 5350-5362.
103. Kirk, S. R., Luedtke, N. W., and Tor, Y. (2000) Neomycin-acridine conjugate: A potent inhibitor of Rev-RRE binding, *J. Am. Chem. Soc.* **122**, 980-981.
104. Michael, K., Wang, H., and Tor, Y. (1999) Enhanced RNA binding of dimerized aminoglycosides, *Bioorg. Med. Chem.* **7**, 1361-1371.
105. Tok, J. B. H., Cho, J. H., and Rando, R. R. (1999) Aminoglycoside antibiotics are able to specifically bind the 5'-untranslated region of thymidylate synthase messenger RNA, *Biochemistry* **38**, 199-206.
106. Sucheck, S. J., Greenberg, W. A., Tolbert, T. J., and Wong, C. H. (2000) Design of small molecules that recognize RNA: Development of aminoglycosides as potential antitumor agents that target oncogenic RNA sequences, *Angew. Chem. Int. Ed.* **39**, 1080-+.
107. Zhao, F., Zhao, Q., Blount, K. F., Han, Q., Tor, Y., and Hermann, T. (2005) Molecular recognition of RNA by neomycin and a restricted neomycin derivative, *Angew. Chem. Int. Ed.* **44**, 5329-5334.
108. MacRae, I. J., Zhou, K. H., Li, F., Repic, A., Brooks, A. N., Cande, W. Z., Adams, P. D., and Doudna, J. A. (2006) Structural basis for double-stranded RNA processing by dicer, *Science* **311**, 195-198.
109. Parkes, K. E. B., Ermert, P., Fassler, J., Ives, J., Martin, J. A., Merrett, J. H., Obrecht, D., Williams, G., and Klumpp, K. (2003) Use of a pharmacophore model to discover a new class of influenza endonuclease inhibitors, *J. Med. Chem.* **46**, 1153-1164.
110. Billamboz, M., Bailly, F., Barreca, M. L., De Luca, L., Mouscadet, J. F., Calmels, C., Andreola, M. L., Witvrouw, M., Christ, F., Debyser, Z., and Cotellet, P. (2008) Design, Synthesis, and Biological Evaluation of a Series of 2-Hydroxyisoquinoline-1,3(2H,4H)-diones as Dual Inhibitors of Human Immunodeficiency Virus Type 1 Integrase and the Reverse Transcriptase RNase H Domain, *J. Med. Chem.* **51**, 7717-7730.
111. Huang, C., and Yu, Y.-T. (2013) Synthesis and Labeling of RNA In Vitro, In *Curr. Protoc. Mol. Biol.*, John Wiley & Sons, Inc., Hoboken, New Jersey.
112. Asangani, I. A., Rasheed, S. A. K., Nikolova, D. A., Leupold, J. H., Colburn, N. H., Post, S., and Allgayer, H. (2008) MicroRNA-21 (miR-21) post-transcriptionally downregulates tumor suppressor Pcd4 and stimulates invasion, intravasation and metastasis in colorectal cancer, *Oncogene* **27**, 2128-2136.

113. Childs-Disney, J. L., and Disney, M. D. (2016) Small Molecule Targeting of a MicroRNA Associated with Hepatocellular Carcinoma, *ACS Chem. Biol.* **11**, 375-380.
114. Disney, M. D., and Angelbello, A. J. (2016) Rational Design of Small Molecules Targeting Oncogenic Noncoding RNAs from Sequence, *Acc. Chem. Res.* **49**, 2698-2704.
115. Livak, K. J., and Schmittgen, T. D. (2001) Analysis of relative gene expression data using real-time quantitative PCR and the  $2^{-\Delta\Delta Ct}$  method, *Methods* **25**, 402-408.
116. Wu, J. I., Lessard, J., Olave, I. A., Qiu, Z., Ghosh, A., Graef, I. A., and Crabtree, G. R. (2007) Regulation of dendritic development by Neuron Specific chromatin remodeling complexes, *Neuron* **56**, 94-108.
117. Fulmer, G. R., Miller, A. J. M., Sherden, N. H., Gottlieb, H. E., Nudelman, A., Stoltz, B. M., Bercaw, J. E., and Goldberg, K. I. (2010) NMR Chemical Shifts of Trace Impurities: Common Laboratory Solvents, Organics, and Gases in Deuterated Solvents Relevant to the Organometallic Chemist, *Organometallics* **29**, 2176-2179.
118. Yang, Y.-Y., Ascano, J. M., and Hang, H. C. (2010) Bioorthogonal Chemical Reporters for Monitoring Protein Acetylation, *J. Am. Chem. Soc.* **132**, 3640-3641.
119. Gao, F., Yan, X. X., Baettig, O. M., Berghuis, A. M., and Auclair, K. (2005) Regio- and chemoselective 6'-N-derivatization of aminoglycosides: Bisubstrate inhibitors as probes to study aminoglycoside 6'-N-acetyltransferases, *Angew. Chem. Int. Ed.* **44**, 6859-6862.
120. Roestamadji, J., Grapsas, I., and Mobashery, S. (1995) Loss of individual electrostatic interactions between aminoglycoside antibiotics and resistance enzymes as an effective means to overcoming bacterial drug-resistance, *J. Am. Chem. Soc.* **117**, 11060-11069.
121. Liu, B., and Tian, H. (2005) A selective fluorescent ratiometric chemodosimeter for mercury ion, *Chem. Commun.*, 3156-3158.
122. Esko, J. D., and Tor, Y. (2011) Assisted enzyme replacement therapy, WO2011034951 A2, The University of California, USA.
123. Lim, L. P., Lau, N. C., Garrett-Engele, P., Grimson, A., Schelter, J. M., Castle, J., Bartel, D. P., Linsley, P. S., and Johnson, J. M. (2005) Microarray analysis shows that some microRNAs downregulate large numbers of target mRNAs, *Nature* **433**, 769.
124. Agarwal, V., Bell, G. W., Nam, J.-W., and Bartel, D. P. (2015) Predicting effective microRNA target sites in mammalian mRNAs, *eLife* **4**, e05005.
125. Preusse, M., Theis, F. J., and Mueller, N. S. (2016) miTALOS v2: Analyzing Tissue Specific microRNA Function, *PLOS ONE* **11**, e0151771.
126. Lagos-Quintana, M., Rauhut, R., Yalcin, A., Meyer, J., Lendeckel, W., and Tuschl, T. (2002) Identification of Tissue-Specific MicroRNAs from Mouse, *Current Biology* **12**, 735-739.
127. Sambandan, S., Akbalik, G., Kochen, L., Rinne, J., Kahlstatt, J., Glock, C., Tushev, G., Alvarez-Castelao, B., Heckel, A., and Schuman, E. M. (2017)

Activity-dependent spatially localized miRNA maturation in neuronal dendrites, *Science* 355, 634.

128. Kowalik, L., and Chen, J. K. (2017) Illuminating developmental biology through photochemistry, *Nat. Chem. Biol.* 13, 587.

129. Shestopalov, I. A., Sinha, S., and Chen, J. K. (2007) Light-controlled gene silencing in zebrafish embryos, *Nat. Chem. Biol.* 3, 650.

130. Deiters, A., Garner, R. A., Lusic, H., Govan, J. M., Dush, M., Nascone-Yoder, N. M., and Yoder, J. A. (2010) Photocaged Morpholino Oligomers for the Light-Regulation of Gene Function in Zebrafish and Xenopus Embryos, *J. Am. Chem. Soc.* 132, 15644-15650.

131. Yamazoe, S., Shestopalov Ilya, A., Provost, E., Leach Steven, D., and Chen James, K. (2012) Cyclic Caged Morpholinos: Conformationally Gated Probes of Embryonic Gene Function, *Angew. Chem. Int. Ed.* 51, 6908-6911.

132. Li, Y.-F. (2016) Functionalizing Morpholino Oligos for Antisense Drug Research and Development, *J. Drug Discov. Develop. and Deliv.* 3, 1021.

133. Velagapudi, S. P., Vummidi, B. R., and Disney, M. D. (2015) Small molecule chemical probes of microRNA function, *Curr. Opin. Chem. Biol.* 24, 97-103.

134. Shortridge, M. D., Walker, M. J., Pavelitz, T., Chen, Y., Yang, W., and Varani, G. (2017) A Macrocyclic Peptide Ligand Binds the Oncogenic MicroRNA-21 Precursor and Suppresses Dicer Processing, *ACS Chem. Biol.* 12, 1611-1620.

135. Connelly, C. M., Boer, R. E., Moon, M. H., Gareiss, P., and Schneekloth, J. S. (2017) Discovery of Inhibitors of MicroRNA-21 Processing Using Small Molecule Microarrays, *ACS Chem. Biol.* 12, 435-443.

136. Angelbello, A. J., Chen, J. L., Childs-Disney, J. L., Zhang, P., Wang, Z.-F., and Disney, M. D. (2018) Using Genome Sequence to Enable the Design of Medicines and Chemical Probes, *Chem. Rev.* 118, 1599-1663.

137. Yan, H., Bhattarai, U., Guo, Z.-F., and Liang, F.-S. (2017) Regulating miRNA-21 Biogenesis By Bifunctional Small Molecules, *J. Am. Chem. Soc.* 139, 4987-4990.

138. Klán, P., Šolomek, T., Bochet, C. G., Blanc, A., Givens, R., Rubina, M., Popik, V., Kostikov, A., and Wirz, J. (2013) Photoremovable Protecting Groups in Chemistry and Biology: Reaction Mechanisms and Efficacy, *Chem. Rev.* 113, 119-191.

139. Zhang, H., Aonbangkhen, C., Tarasovetc, E. V., Ballister, E. R., Chenoweth, D. M., and Lampson, M. A. (2017) Optogenetic control of kinetochore function, *Nat. Chem. Biol.* 13, 1096.

140. Wright Catherine, W., Guo, Z. F., and Liang, F. S. (2014) Light Control of Cellular Processes by Using Photocaged Abscisic Acid, *ChemBioChem* 16, 254-261.

141. Leriche, G., Chisholm, L., and Wagner, A. (2012) Cleavable linkers in chemical biology, *Bioorg. Med. Chem.* 20, 571-582.

142. Tang, J., Vernekar, S. K. V., Chen, Y.-L., Miller, L., Huber, A. D., Myshakina, N., Sarafianos, S. G., Parniak, M. A., and Wang, Z. (2017) Synthesis, biological evaluation and molecular modeling of 2-Hydroxyisoquinoline-1,3-dione

analogues as inhibitors of HIV reverse transcriptase associated ribonuclease H and polymerase, *European Journal of Medicinal Chemistry* 133, 85-96.

143. Gurtan, A. M., Lu, V., Bhutkar, A., and Sharp, P. A. (2012) In vivo structure–function analysis of human Dicer reveals directional processing of precursor miRNAs, *RNA* 18, 1116-1122.

144. Vagner, J., Qu, H., and Hruby, V. J. (2008) Peptidomimetics, a synthetic tool of drug discovery, *Curr. Opin. Chem. Biol.* 12, 292-296.

145. Simpson, L. S., and Kodadek, T. (2012) A cleavable scaffold strategy for the synthesis of one-bead one-compound cyclic peptoid libraries that can be sequenced by tandem mass spectrometry, *Tetrahedron Lett.* 53, 2341-2344.

146. Lee, J. H., Kim, H.-S., and Lim, H.-S. (2011) Design and Facile Solid-Phase Synthesis of Conformationally Constrained Bicyclic Peptoids, *Org. Lett.* 13, 5012-5015.

147. Oh, M., Lee, J. H., Moon, H., Hyun, Y. J., and Lim, H. S. (2016) A Chemical Inhibitor of the Skp2/p300 Interaction that Promotes p53-Mediated Apoptosis, *Angew. Chem. Int. Ed.* 55, 602-606.

148. Shi, Y., Challa, S., Sang, P., She, F., Li, C., Gray, G. M., Nimmagadda, A., Teng, P., Odom, T., Wang, Y., van der Vaart, A., Li, Q., and Cai, J. (2017) One-Bead–Two-Compound Thioether Bridged Macrocyclic  $\gamma$ -AApeptide Screening Library against EphA2, *J. Med. Chem.* 60, 9290-9298.

149. Higgs, G., and Slack, F. (2013) The multiple roles of microRNA-155 in oncogenesis, *J. Clin. Bioinforma.* 3, 17.

150. Zhang, C.-M., Zhao, J., and Deng, H.-Y. (2013) MiR-155 promotes proliferation of human breast cancer MCF-7 cells through targeting tumor protein 53-induced nuclear protein 1, *J. Biomed. Sci.* 20, 79.

151. Chen, J., Wang, B. C., and Tang, J. H. (2012) Clinical significance of MicoRNA-155 expression in human breast cancer, *J. Surg. Oncol.* 106, 260-266.

152. Cheng, C. J., Bahal, R., Babar, I. A., Pincus, Z., Barrera, F., Liu, C., Svoronos, A., Braddock, D. T., Glazer, P. M., Engelman, D. M., Saltzman, W. M., and Slack, F. J. (2015) MicroRNA silencing for cancer therapy targeted to the tumor microenvironment, *Nature* 518, 107-110.

153. Shi, Y., Teng, P., Sang, P., She, F., Wei, L., and Cai, J. (2016)  $\gamma$ -AApeptides: Design, Structure, and Applications, *Acc. Chem. Res.* 49, 428-441.

154. Gantier, M. P., McCoy, C. E., Rusinova, I., Saulep, D., Wang, D., Xu, D., Irving, A. T., Behlke, M. A., Hertzog, P. J., Mackay, F., and Williams, B. R. G. (2011) Analysis of microRNA turnover in mammalian cells following Dicer1 ablation, *Nucleic Acids Res.* 39, 5692-5703.

155. Yamamoto, M., Kondo, E., Takeuchi, M., Harashima, A., Otani, T., Tsuji-Takayama, K., Yamasaki, F., Kumon, H., Kibata, M., and Nakamura, S. (2011) miR-155, a Modulator of FOXO3a Protein Expression, Is Underexpressed and Cannot Be Upregulated by Stimulation of HOZOT, a Line of Multifunctional Treg, *PLOS ONE* 6, e16841.

156. Myatt, S. S., and Lam, E. W. F. (2007) The emerging roles of forkhead box (Fox) proteins in cancer, *Nat. Rev. Cancer* 7, 847.

157. Elmore, S. (2007) Apoptosis: A Review of Programmed Cell Death, *Toxicol. Pathol.* 35, 495-516.

158. Eichelser, C., Stückrath, I., Müller, V., Milde-Langosch, K., Wikman, H., Pantel, K., and Schwarzenbach, H. (2014) Increased serum levels of circulating exosomal microRNA-373 in receptor-negative breast cancer patients, *Oncotarget* 5, 9650-9663.